Strain Hardening UHPFRC

Optimization for Tensile Loading Behaviour using High Modulus Polyethylene Fibres

Isa Eijs

TU Delft

Strain Hardening UHPFRC

Optimization for Tensile Loading Behaviour using High Modulus Polyethylene Fibres

by

Isa Eijs

to obtain the degree of Master of Science

at the Delft University of Technology,

to be defended publicly on Thursday June 23, 2022 at 4:00 PM.

Student number:	4590333	
Project duration:	February 2021 – June 2022	
Thesis committee:	Dr. ir. M. Luković,	TU Delft, supervisor
	Dr. ir. S. Grünewald,	TU Delft
	Dr. ir. B. Šavija,	TU Delft
	ir. Y. Huang	TU Delft

An electronic version of this thesis is available at http://repository.tudelft.nl/.

TU Delft

Preface

This thesis would not have ended up the way it does without the help of several people. Starting with my main supervisor dr. ir. Mladena Luković, who not only provided me with this topic but also guided me throughout the process and kept me on track when I would try to do a little bit of everything rather than staying focused on the main goal, for which I am very grateful. I would also like to thank dr. ir. Steffen Grünewald for teaching me things concerning the optimization of a mix design and material properties, much of the shared knowledge has found an easy way into this thesis. Despite only joining the committee near the end of this research, dr. ir. Branko Šavija provided some nice questions and sharp comments, contributing to improving the thesis in these final stages. Ir. Yitao Huang regularly helped me out in the lab and was always there to provide me with quick advice whenever needed. I have appreciated your approachability and helpfullness a lot during our many meetings. Despite the situation in 2021/22 not being the easiest to graduate, you all have guided me through it all and provided me with many good insights, ideas and plans.

Besides those in my assessment committee, I would also like to thank the lab staff, who helped me out with experiments whenever needed but also made it very enjoyable to be in the lab, even before 8 AM on some days. Especially Ton Blom and Maiko van Leeuwen deserve my gratitude as they spent much of their time helping me out with all things I could not, or was not allowed to, do by myself.

Of course the support from people not directly involved can be just as important as those who are. My family and friends have regularly taken the time to revive my energy and encouraged me to keep going when things got tough. My busy lab schedule, sometimes very bad moods and endless not-always-so-interesting stories about concrete were all accepted and I am very grateful for that.

Isa Eijs
Delft, May 2022

Abstract

Combining the high strength of Ultra High Performance Concrete (UHPC) and the strain capacity of Strain Hardening Cementitious Composites (SHCC), Strain Hardening Ultra High Performance Fibre Reinforced Concrete (SH-UHPFRC) could be a promising material for the application of strengthening RC elements. This research describes the development of an SH-UHPFRC mixture, using Ultra High Molecular Weight Polyethylene (UHMWPE) fibres. The benefits of using this material as a strengthening material were analysed using a numerical model and the environmental impact of the SH-UHPFRC was evaluated.

During the material development the effects of different material types and the applied ratios were considered. The flowability of the mixture, compressive strength and tensile response were tested to determine the mixture design. The effect of different cement types and amount of superplasticizer played a significant role in the increasing of the workability of the mixture. The effect of using UHMWPE fibres over steel fibres was investigated, as well as the effect the amount of UHMWPE fibres had on different properties. The material properties of the material research were implemented in a numerical model using ATENA software, representing a strengthened reinforced concrete (RC) beam subjected to a three-point bending test. In addition to the modelling of a RC beam strengthened with SH-UHPFRC, a parameter study was executed to determine the effect of increased strain capacity in the strengthening material. This was done by adjusting the tensile stress-strain relation in the material model. Three levels of strain were tested and the capacity and cracking behaviour of the strengthened beam were compared. The environmental impact was evaluated using the CUR Groen Beton calculation tool. The mixture design of SH-UHPFRC was compared to that of relevant concrete types. The environmental impact per volume is high for SH-UHPFRC, but the mechanical properties are superior which leads to a lower required volume to achieve similar mechanical results. Comparing a strengthened beam to a RC beam demonstrated the contribution of SH-UHPFRC, proving that, including the environmental impact, SH-UHPFRC could outperform NC as a strengthening material.

The developed mixture granted a compressive strength of nearly 120 MPa, a tensile strength of 8.9 MPa and a tensile strain capacity over 2%. The use of this material for the strengthening of a RC beam lead to an increase in shear capacity of 78%, following from the numerical model. Evaluating the environmental impact, the use of SH-UHPFRC overcomes the use of NC to strengthen a shear-deficient beam. It is recommended to conduct further research on specific aspects of the material optimization of SH-UHPFRC. For the numerical modal the resemblance to practice could be improved and the range of parameters expanded. The environmental impact of a beam strengthened with SH-UHPFRC proved to be lower compared to an RC beam with equal shear capacity, showing the benefit of this superior material. An analysis of the full life cycle of an element strengthened with SH-UHPFRC could be done to get a better estimation of the environmental effect of using this material for strengthening purposes over NC.

Contents

Nomenclature

Abbreviations

A&A curve	Andreasen and Andersen curve
AVG	Average
CH	Calcium Hydroxyde
CSH	Calcium Silicate Hydrate
DIC	Digital Image Correlation
E-modulus	Young's modulus of elasticity, Elastic modulus
ECC	Engineered Cementitious Composites
ECI	Environmental Cost Indicator
FA	Fly Ash
FEM	Finite Element Method
FRC	Fibre Reinforced Concrete
GGBFS	Ground Granulated Blast Furnace Slag
GWP	Global Warming Potential
HMPE	High Modulus Polyethylene
HS-SHCC	High Strength Strain Hardening Cementitious Composite
LCA	Life Cycle Analysis
LP	Limestone Powder
NC	Normal Concrete
PE	Polyethylene
PSD	Particle Size Distribution
PVA	Polyvinyl Alcohol
RC	Reinforced Concrete
RH	Relative Humidity
RI	Reinforcement index
SCM	Supplementary Cementitious Material
SF	Silica Fume
SH-UHPFRC	Strain Hardening Ultra High Performance Fibre Reinforced Concrete
SHCC	Strain Hardening Cementitious Composite

SP	Superplasticizer
STDV	Standard Deviation
UHMWPE	Ultra High Molecular Weight Polyethylene
UHP-SHCC	Ultra High Performance Strain Hardening Cementitious Composite
UHPC	Ultra High Performance Concrete
UHPFRC	Ultra High Performance Fibre Reinforced Concrete
W/B-ratio	Water-binder ratio
W/C-ratio	Water-cement ratio

Symbols

δ	Deflection
ϵ	Strain
σ	Stress
b	Beam width
D	Particle diameter
d_f	Fibre diameter
h	Beam height
l	Beam span
l_f	Fibre length
q	Particle size distribution modulus
V_f	Fibre volume content

List of Figures

List of Tables

1 Introduction

1.1. Background and Motivation

Ultra High Performance Concrete (UHPC) has been developed to fulfil a need for stronger concrete. With a minimum compressive strength requirement of 150 MPa it is significantly stronger than other concrete types. This high strength is obtained by reducing the water-to-binder ratio (W/B), using a large binder content and optimizing the packing density by using only fine materials which leads to a reduced porosity [1]. This low porosity reduces the penetration of harmful fluids and gases and therefore increases the durability of the material. Ultra High Performance Fibre Reinforced Concrete (UHPFRC) behaves much more ductile compared to normal concrete. Very fine (steel or synthetic) fibres are incorporated in the mixture and once micro cracks occur, these fibres are activated and the growth of the cracks is counteracted. Both Bajaber and Hakeem [2] and Schmidt and Fehling [1] mention how adding a small amount of fibres to a mixture can significantly increase the tensile strength while barely affecting the compressive strength. Because of the improved mechanical properties of UHPFRC compared to normal reinforced concrete (RC) or fibre reinforced concrete (FRC), more slender or more aesthetically designed structures can be obtained [3].

Because of the large amounts of cement required to produce this material (leading to a larger environmental impact compared to traditional concrete) and the high costs, it is not always viable to use UHPFRC construction elements instead of normal reinforced concrete ones. Nowadays, a lot of research is performed on using UHPFRC in hybrid structures and strengthening or repairing of existing structures. The material has already been used in realized applications as mentioned by Bajaber and Hakeem [2] and Walraven [4]. This way the advantages of UHPFRC can be used while limiting the construction costs and environmental impact. Figure 1.1 shows how the use of UHPFRC as a strengthening material compares to the use of NC to rehabilitate a structural element. Because the superior properties of UHPFRC enable a longer service life, less maintenance is required [5]. This also reduces the costs compared to a maintenance strategy including multiple rehabilitations using NC [6].

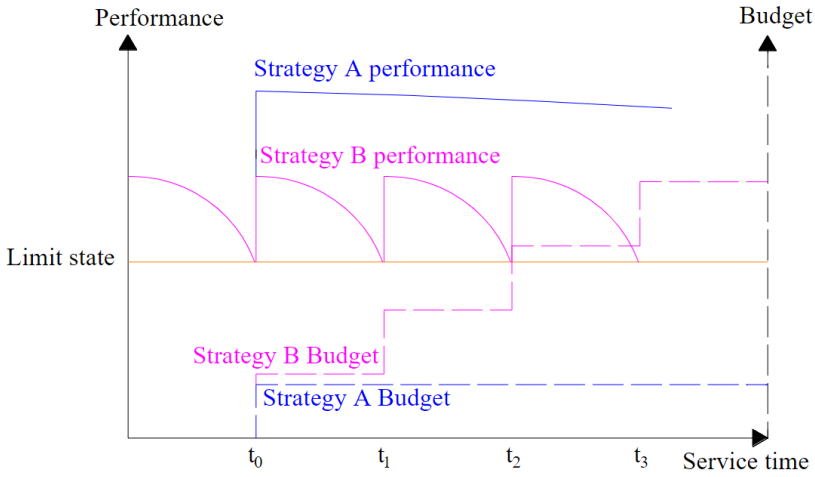

Figure 1.1: Comparison of different strengthening strategies: strengthening using UHPFRC (Strategy A) or using NC (Strategy B), based on performance and costs [6, 7]

When using a cementitious material to strengthen or repair a RC structural element, a high deformation capacity, high energy absorption and good durability are beneficial [8]. These properties can be found in Strain-Hardening Cementitious Composites (SHCC), also known as Engineered Cementitious Composites (ECC). The development of this material is based on micro-mechanics. Naaman [9] describes the tensile behaviour of strain hardening FRC, which equals SHCC, using three stages as shown in Figure 1.2: elastic behaviour, hardening and softening. After a linear elastic behaviour up to the cracking strength (part I), multiple small cracks will occur in which small fibres transfer the tensile stresses, causing the stresses in the element to keep increasing with the increase of strain (hardening behaviour) and because of this behaviour a large strain can be achieved (part II). Softening behaviour follows, cracks localize and the tensile stress quickly drops with increasing strain (part III) [9]. The fibres used in SHCC are usually made of polymers like polyvinyl alcohol (PVA) or polyethylene (PE), while in UHPFRC steel fibres are more common. The mechanical interactions between the fibres and matrix are governing in the material design. The strength of the matrix, fibres and matrix-fibre interface must all be proportional to prevent early failure [10]. Chen et al. [8] looked into a simple cost analysis to compare using a high strength strain hardening material and the use of conventional repair mortar. The relatively high unit material costs of this material are compensated by the lower amount of material required and fewer labour required because a smaller patch of repair material can be used, making this an economically beneficial method of repairing RC structures.

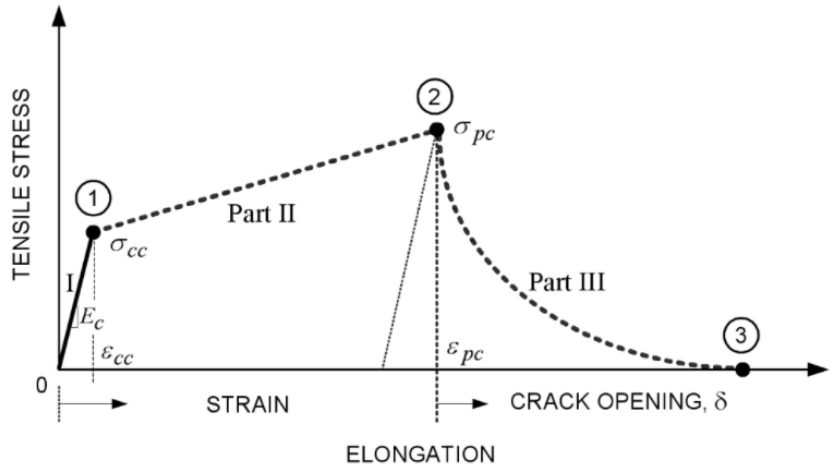

Figure 1.2: Idealized stress-elongation response in tension of a strain hardening FRC composite for modelling [11]

Although UHPFRC can show some hardening (when enough fibres are used), the softening behaviour sets in quickly after reaching the stress at which cracking starts. Compared to UHPFRC, SHCC shows a lower cracking and ultimate strength but a much higher strain capacity due to the long hardening phase. Figure 1.3 schematically shows the differences in constitutive behaviour of UHPFRC, SHCC and FRC. Combining the beforementioned characteristics of UHPFRC and SHCC into one material, a material with a high compressive and tensile strength (due to optimized packing and low W/B-ratio), large strain capacity (due to multiple cracking and hardening behaviour) and high durability (due to low porosity) can be developed, which can be of great advantage for strengthening and repair of existing and future concrete structures. The behaviour wished to obtain for Strain hardening Ultra High Performance Concrete (SH-UHPFRC) is also schematically presented in Figure 1.3.

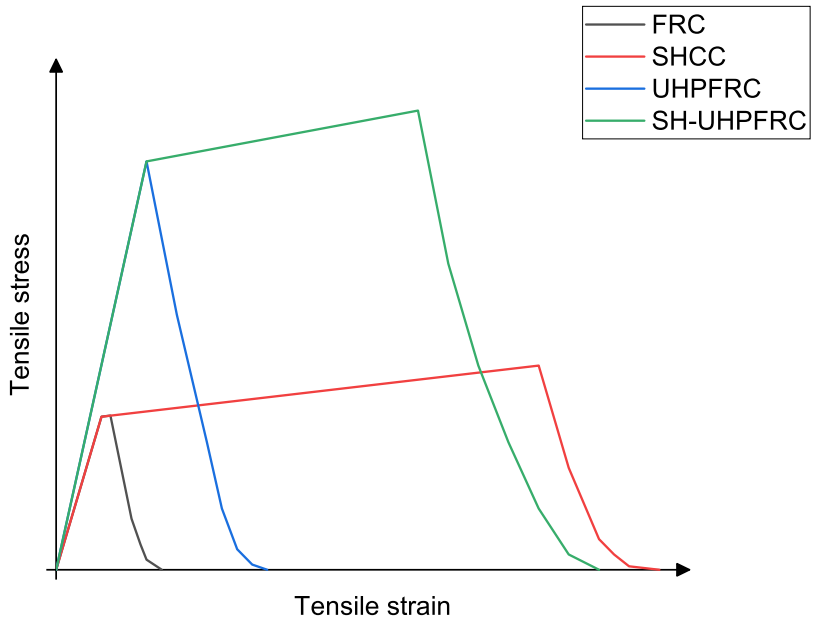

Figure 1.3: Schematic tensile constitutive behaviour of different concrete types

1.2. Research Objectives and Scope

This thesis is part of a PhD project investigating different aspects of strengthening RC elements using UHPFRC. The main objective of this MSc research was to develop a mixture design for SH-UHPFRC, using locally commonly available components and Ultra High Molecular Weight Polyethylene (UHMWPE) fibres, that reach a tensile strain capacity of at least 1.5% and a tensile strength of 7 MPa. The effect these synthetic fibres have on the behaviour under tensile load was an important focus point in this research. The mixture not only had to meet the requirements in tensile behaviour. The compressive strength had to be at least 120 MPa and the mixture had to be be sufficiently workable so thin elements can be cast for a strengthening application. Self consolidation was not a requirement. It can be noted that this compressive strength requirement is lower than most definitions suggest for UHPC. This value was set because this left room to focus on the tensile behaviour of the material while still significantly exceeding the strength requirement of High Strength Concrete (HSC).

To take the information gathered throughout the material research to the structural level, a numerical model was built to investigate the effect of strengthening a structural element with the developed material. The input for this model was based on experimentally gathered data for all necessary material properties. Multiple material models were used and the resulting shear capacity of the beam was compared. The scope of this numerical study included only using different material models, differences in bonding parameters and dimensions were not included.

Finally, the environmental impact of the SH-UHPFRC mixture as a strengthening material was determined. First the environmental impact of the developed mixture was compared to that of NC and related concrete types, based on impact per volume. This was followed by a comparison between a RC beam and a SH-UHPFRC strengthened beam considering the difference in performance. For this purpose, the results from the numerical study were used.

1.3. Research Questions and Methodology

The research questions of this thesis were the following:

1. What ratios of material components can lead to a mixture for SH-UHPFRC with a minimum compressive strength of 120 MPa, tensile strength of 7 MPa and tensile strain capacity of 1.5%?
   (a) What ratios of components should be altered when trying to achieve strain hardening?
   (b) What is the effect of using different quantities of UHMWPE fibres on the material's behaviour under compressive and tensile loading and how does the fibre content affect the flowability of the mixture?
   (c) How does the use of UHMWPE fibres compare to using steel fibres considering mechanical behaviour and flowability?
2. What does the use of SH-UHPFRC as a strengthening material contribute to the shear capacity of a beam element compared to a conventional RC element? And what contribution does an increase in strain capacity make to the shear capacity of a strengthened beam?
3. What effect on the environmental impact does the use of SH-UHPFRC as a strengthening material for a structural element have?
   (a) How does the environmental impact of SH-UHPFRC compare to relevant other concrete types?
   (b) How does the strengthening of a RC beam using SH-UHPFRC affect the environmental impact of the element, considering the mechanical performance?

To answer these questions, the research was divided into four parts: literature review, material development, numerical analysis and environmental analysis. The starting point for the material development was an UHPFRC mixture. For every step in the material development a material ratio was adapted to benefit the compressive strength, workability and/or tensile response of the mixture. After determining the final mixture, the properties of this mixture are determined and summarized. This data was used as the input for a numerical model in the subsequent part of the research. This model represents a setup used by TU Delft to determine the shear capacity of strengthened beams. The reference beam was validated against previous experimental outcome to assure a proper model, after which the strengthening laminates are included. The shear capacity, ductility and cracking behaviour of the strengthened beam was analysed. Additionally, a parametric study on the effect of increased strain capacity of the strengthening material was done. In the last step of the research, the environmental impact of the developed mixture was evaluated. The environmental impact was compared to that of other concrete types for reference. To regard the contribution of SH-UHPFRC to the mechanical properties of a structural element, the beam modelled in the numerical part of the thesis is used to make a performance-based comparison.

1.4. Thesis Overview

After a literature study in Chapter 2, the material research done is extensively discussed in Chapter 3. The numerical analysis and the outcomes following from this can be found in Chapter 4. Chapter 5 discusses the analysis of the environmental impact of the developed material. This thesis is wrapped up with conclusions and recommendations in Chapter 6.

2

Literature Study

2.1. Development of (SH-)UHPFRC

After the development of High Strength Concrete (HSC) in the 1980's with a compressive strength of 100-110 N/mm^2, it was thought the practical maximum was reached since the maximal capacity of the aggregates was met [4]. Later, a method arose to prevent the development of micocracks by increasing the density of the concrete by using fine particles, which was called Reactive Powder Concrete (RPC) because of the use of reactive mineral additions [1]. Considering Fibre reinforced Concrete (FRC), the limits were also found due to the reduced workability with increasing fibre contents [1]. To solve these problems, SIFCON [12] and SIMCON [13] were developed, both firstly fixing the placement of the steel fibres, using compressed loose fibres and a fibre mat respectively, after which a cement-based slurry is cast over it.

These developments have led to what is now known as UHPC, characterized by small particles, a high particle packing density, a low W/C-ratio and, in case of UHPFRC, fine fibres [4]. Figure 2.1 by Mishra and Singh [14] graphically shows the difference in use of particles between NC and UHPC. Exact definitions concerning the strength of UHPC differ throughout literature, but often a compressive strength in the range of 150-200 N/mm^2 is used as a characteristic value [3, 15, 16]. Using heat or pressure curing, the strength of the material can increase significantly above these values but this is not a practical curing method for large-scale application [17, 18, 19]. Besides the superior compressive strength of this material, it also has an increased durability compared to other concrete types since harmful substances can hardly penetrate the material due to the material's low porosity. Graybeal and Tanesi [20] have shown the inviolability of UHPC to different types of deterioration and chloride penetration compared to other concrete types. Though the method of curing can slightly increase or decrease the extent in which this resistance is present, the difference with other concrete types is significant.

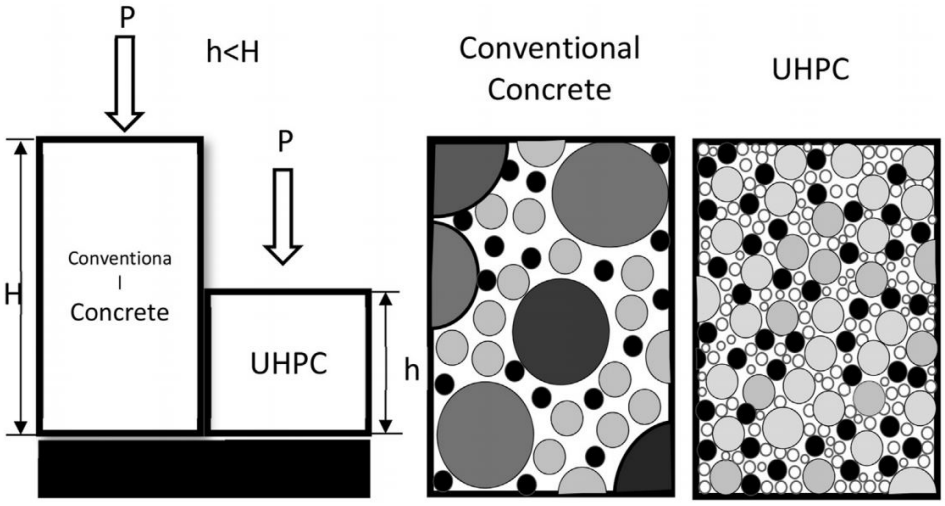

Figure 2.1: Conventional concrete (NC) versus UHPC [14]

To be able to achieve larger deformations on top of the beforementioned properties, Strain Hardening UHP(FR)C (SH-UHPFRC) has been developed. A material is considered strain hardening if after cracking, the tensile stress can still increase with increasing elongation, meaning the peak stress is higher than the stress at first cracking ($\sigma_{pc} \geq \sigma_{cc}$) [21]. This behaviour can be seen in SHCC, which has a lower cracking strength compared to UHP(FR)C but a significantly larger strain capacity due to a long strain hardening trajectory. A typical stress-strain curve for a strain hardening material including fibres as described by Naaman [9] starts with a steep linear elastic part up to the point at which the first crack occurs after which the strain hardening branch with multiple cracking starts. At the peak point, crack localization sets off and the stress decreases with persistent strain. This behaviour can be seen in Figure 2.2. This behaviour makes the material suitable for repair and strengthening of structures where high loads, harsh environmental conditions or large deformations play a role [10, 22, 23, 24]. A more elaborate discussion on this strain hardening behaviour can be found in Section 2.3.2.

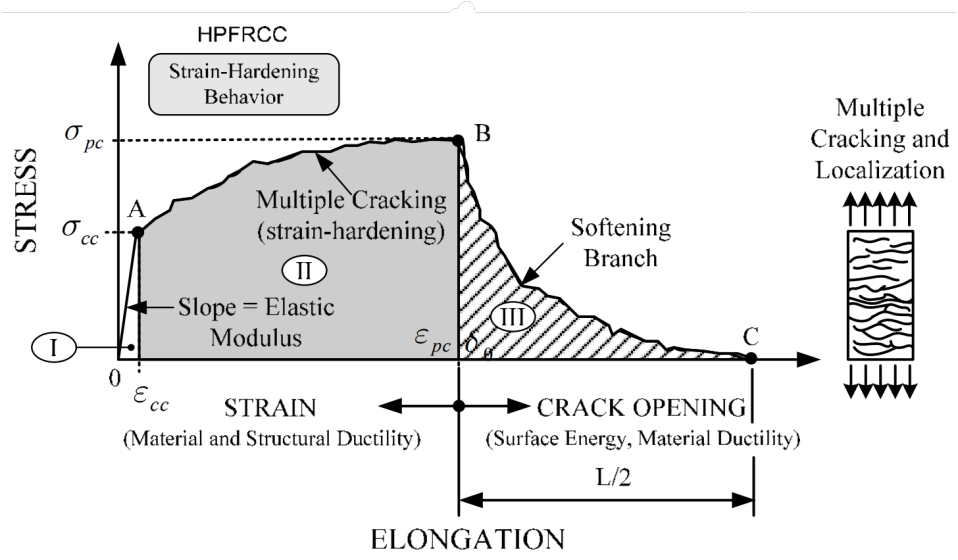

Figure 2.2: Typical stress-strain curve in tension up to complete separation of strain-hardening FRC or HPFRCC [9]

2.2. Influence of Mixture Components

The standard ingredients in a UHPC mixture are cement, silica fume, sand, water, superplasticizer and, when considering UHPFRC, fibres. These materials must be proportioned well to lead to the properties desired in UHPC. Optionally, other materials like alternative binders, fillers or chemical admixtures can be added to the mixture to alter properties of the final material.

2.2.1. Cement

In UHPC, a higher cement content is needed compared to NC. This is due to the finer particles in the mixture, leading to a larger surface area that needs to be covered by the paste to bind all components together. When the cement reacts with water, Calcium Silicate Hydrate (CSH), which is the main binder in concrete, is formed alongside Calcium Hydroxide (CH). The amount of water in this type of concrete is very limited, causing part of the cement to stay unhydrated. Instead, these particles will act as fillers [2, 25].

When choosing a cement type some aspects must be considered. Because of the high strength requirements, CEM I 52.5 is used most. A very fine cement can cause problems because of its larger surface area, since it has a high water demand and will reduce the flowability of the mixture in the fresh state [26]. A slightly coarser cement is thus recommended, leading to a lower water demand but also a slower strength development. The particle size of the cement used can also influence the setting time of the mixture. With a larger surface area, a finer cement has a higher hydration rate but it also must create more 'bridges' between particles, counteracting the quick hydration [27]. The use of a cement with a low C_3A content is also recommended, since a larger content speeds up the hydration process [18], reducing the workability. A lower C_3A content corresponds with a lower early strength, but does not influence the later strength and reduces the required amount of water and superplasticizer [28, 29].

2.2.2. Silica Fume

Silica fume (SF) is a byproduct from the production of silicon and ferrosilicon alloys. It is used in UHPC for multiple reasons. The very fine particles of this material fill the pores between larger cement particles, leading to a better durability and higher strength. Another advantage of this material is the pozzolanic reaction of the silica with a byproduct from the cement hydration. SF is rich in silicon dioxide (SiO_2), which reacts with the CH from the hydrated cement to form additional CSH, which increases the strength of the mixture [26]. The addition of SF increases the packing density of the mixture, leading to a higher compressive strength, and makes it more flowable, leading to less air entrapment [17, 30]. Compared to other pozzolanic materials, SF has a high surface area, making it highly reactive and therefore giving a lot of early strength to the concrete [31, 32]. A ratio of SF to cement of 0.2-0.3 is recommended for an optimum compressive strength [33].

2.2.3. Sand

Sands maintain the stability of the concrete by carrying loads. In UHPC, only very fine particles are used. The use of finer aggregates generates a higher compressive strength, because fewer stress concentrations and flaws occur due to a more uniform distribution of loads [17]. For the rheology of the mixture, rounded grains are preferred over angular ones [34]. Considering strain hardening properties, smooth and small grains contribute to the strain hardening behaviour of the material by facilitating the slip of fibres. Contrary, using larger grains will lead to a higher fracture toughness and retain fibre slippage, leading to less strain hardening behaviour [35]. Initially refined quartz sands were used to produce UHPC, but after finding natural sands can bring the same mechanical properties with much lower costs, this changed [36].

The amount of sand in a mixture can highly affect the mechanical properties of the material. In UHPC or UHPFRC the amount of sand is usually around 1000 kg/m^3 or slightly above [3, 37, 38], although many deviations from this amount can be found in literature. In SHCC, this amount is usually between 450-700 kg/m^3 [35, 39, 40, 41] but can go as low as 150 kg/m^3 [42, 43] when aiming for certain material properties. When increasing the amount of sand, the viscosity of the mix also increases [34], which may cause an increase in the entrapped air volume. To reduce the viscosity, the water content must then be increased, which is to be avoided in UHPC mixtures.

2.2.4. Water

The amount of water used in the mixture influences many of the concrete's characteristics. The amount of water should be enough to enable hydration of the cement particles as described in Section 2.2.1 and to ensure a workable mixture. With UHPC a smaller amount of water is used since an increase W/C-ratio leads to a lower compressive strength [44]. This occurs due to excess water creating pores in the concrete matrix, leading to a higher permeability and lower strength [2]. A positive effect of a slightly higher W/C-ratio is that the tensile strain capacity increases without significant decrease in tensile strength [45]. Adopting a lower W/C-ratio leads to a higher viscosity which will increase the amount of entrapped air in the fresh mixture [34], leading to problems after hardening regarding both the mechanical properties and the durability. In literature one will not only find a value for the W/C-ratio but also for the W/B-ratio or the W/CM-ratio (water-cementitious materials ratio), which also include additional materials like SF. Wille et al. [18] uses a W/CM-ratio in the range 0.15-0.25 for UHPC with a compressive strength above 150 MPa, which is a common range considering other literature [14, 36].

2.2.5. Superplasticizer

Superplasticizer (SP) is used to enhance the workability of a mixture without increasing the amount of water. SP prevents cement particles from agglomerating and creates a water film around the particles, causing the water to be available for a longer time, increasing the workability [25]. Compared to regular concrete, the total surface area of UHPC using only small particles is very large, leading to a higher demand for SP to keep the workability sufficient without increasing the water content. Because of the chemical composition, it is recommended to use no more than 2% SP in a mixture [2]. This can prevent problems like bleeding [45].

2.2.6. Fibres

The addition of fibres to the mixture increases the ductility of the material. Concrete itself is a very brittle material so reinforcement is necessary to resist tensile forces. Once tensile stresses become too large for the concrete matrix and a micro crack occurs, fibres will provide resistance to prevent the crack from widening. Besides a better performance under tensile loading, the addition of fibres also increases the shear strength of the concrete [17]. With the increase (up to a certain point) of the fibre content, the tensile strength and tensile strain capacity increase [46]. Literature shows that the maximum fibre content should be around 2.5% when considering the contribution to mechanical properties and costs [2, 46]. When the fibre volume gets too high, this can lead to interlocking of fibres because a uniform distribution gets harder to achieve [47]. Interlocking fibres can create a network, reducing the homogeneity of the mixture and affecting structural properties negatively. Due to their high surface area and elongated shape, fibres decrease the workability. Especially long and stiff fibres can cause problems, since these can push particles in the mixture apart, increasing the porosity while short and flexible fibres can reduce porosity by filling spaces between particles [48]. The exact shape of the fibres also influences the properties of the mixture. Twisted fibres or those with hooked end can lead to higher tensile strengths and a higher ductility [21]. Rossi [49] describes how different sizes of crack require different types of fibre. To act on microcracks, a large number of very thin fibres is required, having a very large surface area. For macrocracks, the length of individual fibres is of higher significance to create sufficient bond and to maintain a certain workability these must be present in lower dosages.

Besides the shape and size of the fibres, the material is important to consider. Conventionally, steel fibres are used in UHPFRC but many other materials like polymer and textile have been researched. In the past, asbestos fibres have been used. However, because of the associated health risks, this is nowadays not considered an option [2]. Curosu et al. [42] explored the effects of different synthetic fibres on the tensile behaviour of high strength strain hardening cement-based composites (HS-SHCC). They found that compared to PVA (polyvinyl alcohol) fibres, High Density Polyethylene (HDPE) fibres have a higher modulus of elasticity and tensile strength, but also the fact that HDPE fibres are hydrophobic, making them highly suitable for the use in very dense matrices. These properties make that the HDPE is suitable for strain hardening behaviour in high strength materials, as sudden fibre rupture will not easily occur because of the fibre's material properties and limited bond between the tough fibre and concrete matrix [42, 50]. A larger aspect ratio (l_f/d_f) of the fibre will increase the bond between fibre and matrix [51]. The proportions in bond strength and fibre strength highly influence the

strain hardening properties of the material [21]. The failure mechanisms that can occur are shown in Figure 2.3. The Young's modulus (elastic modulus, E-modulus) is lower than that of the concrete matrix, in contrast to steel fibres that have a higher Young's modulus, leading to a tougher behaviour after cracking [52]. After the first crack, the slip bond strength between the materials causes the stress to be transferred through the fibre into the concrete, causing another crack at an other location and thus leading to multiple cracking [53]. Improving the packing density of the concrete leads to an increase in bond strength [17]. Ultra High Molecular Weight Polyethylene (UHMWPE) (often also called High Modulus Polyethylene (HMPE)) is similar to HDPE but has longer molecular chains and has a much higher molecular weight. These properties make this material the best polymer for sliding wear and impact resistance according to Kanamoto et al. [54].

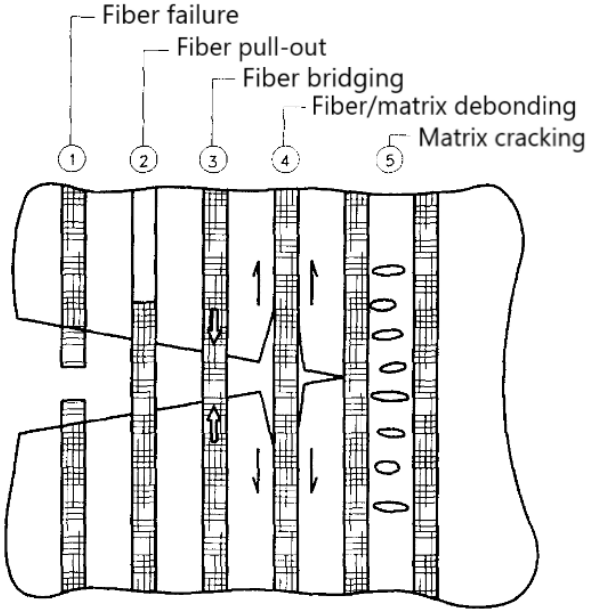

Figure 2.3: Fiber-matrix failure mechanisms [55]

The volume of fibres used in a mixture has a significant influence on the material properties. To achieve strain hardening, a sufficient amount of fibres is needed. Said and Razak [46] show how the reinforcement index (RI) can be linearly related to the cracking strength and ultimate tensile strength for a certain mixture, see Figure 2.4a. The reinforcement index is the product of the fibre volume content and aspect ratio ($RI = V_f \cdot l_f/d_f$). The amount of fibres needed depends on multiple aspects of the material. In SHCC, the achieved strain hardening behaviour does not depend on special ingredients or very large volumes of fibres. Instead, the properties are obtained by tailoring different attributes: fibre properties (length, diameter, strength, elastic modulus), interface properties (bond and slip behaviour) and cementitious matrix properties (fracture toughness, elastic modulus, flaw size) [56]. Finding a good combination of these attributes can produce strain hardening behaviour while using $\leq$2% fibres. In SH-UHP(FR)C mixtures, PE fibre contents between 1.5% and 2.0% are usually observed [50].

In addition to the positive influence a switch from steel to PE fibre types can have, a possible negative influence must be considered. The review written by Zhou et al. [57] includes many references [46, 51, 58, 59] stating the negative influence an increase in volume of PE fibres can have on the compressive strength of cementitious materials. The contrary is proven for steel fibres, as the addition of these improves the compressive strength of the concrete mix [58]. The fibres bridge cracks that form during the compression of concrete, delaying the propagation of large cracks which lead to the failure of the material and therefore increasing the compressive strength of the material. Despite also bridging cracks in the concrete matrix this same effect is not observed for PE fibres. This is thought to occur due to the difficulty in dispersing these fibers properly and the entrapping of air bubbles when using PE fibres [17]. Besides the found relation between the reinforcement index and the tensile strength, Said and Razak [46] also relate the reinforcement index to a decrease in compressive strength as can be seen

in Figure 2.4b. Dai et al. [50] describe the difference in compressive strength between 'ordinary' and strain hardening UHPC. Where for 'ordinary' UHPC the *minimum* compressive strength requirement equals 150 MPa, the gathered research results on SH-UHPC show compressive strengths ranging from 110 to 211 MPa, only *averaging* around 150 MPa. When using (UHMW)PE fibres to improve the tensile behaviour, the negative influence on the compressive strength must be taken into account.

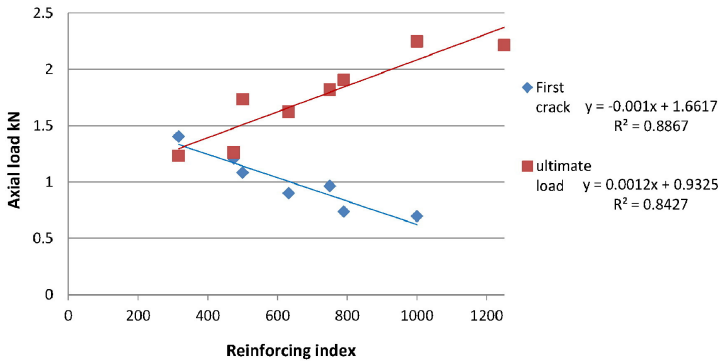

(a) Relation between the reinforcing index and tensile cracking and peak strength [46]

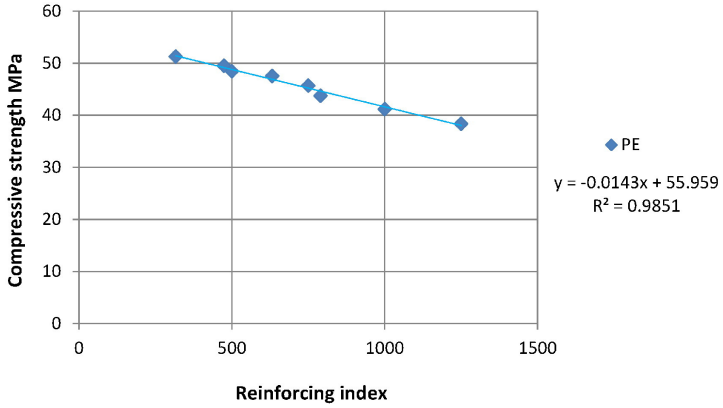

(b) Relation between the reinforcing index and compressive strength [46]

Figure 2.4: Relation between reinforcing index and mechanical properties as found by Said and Razak [46]

2.2.7. Other Components

Besides the standard components used in UHP(FR)C, other materials can be used. These materials can have different effects on the properties of a mixture. An important class of materials are Supplementary Cementitious Materials (SCMs). These materials are often used when attempting to lower the cement content of a mixture to reduce the environmental impact. Looking into literature one can come across many different materials, of which the most common are discussed below.

Fly Ash

Fly Ash (FA) is a byproduct from coal combustion that must be captured to prevent air pollution. It is a pozzolanic material that, like SF, reacts with CH to form CSH. According to Khan et al. [35] the addition of FA controls the fracture toughness of the matrix to match the toughness of fibres and can improve the rheological properties of the matrix, increase fibre dispersion and reduce the demand for other admixtures. In strain hardening materials it can be used, partially replacing cement, to reduce the interfacial bond strength between matrix and fibres improving slip of the fibre and preventing fibre breakage [24, 42].

Ground Granulated Blast Furnace Slag

Ground Granulated Blast Furnace Slag (GGBFS) is a by-product from the iron and steel industry, where it accumulates on top of the molten iron. This reactive material can be used to replace part of the cement, reducing the environmental impact and reducing the required amounts of water and SP while

leaving the compressive strength unaffected [60]. The use of GGBFS also retards the setting time of the mixture [2]. When used in a mixture including fibres, an increase in the amount of GGBFS is said to improve the workability and fibre dispersion while also increasing the slippage between fibres and matrix, leading to fibre pull-out rather than fibre rupture [61].

Limestone Powder
Limestone powder (LP) is made by grinding limestone rocks, which are high in calcium carbonate ($CaCO_3$). Limestone powder is not a pozzolanic material, but the calcium carbonate accelerates the hydration of C_3S [62]. Huang et al. [63] did a research on the effect of partly replacing the cement in a UHPC mixture by limestone. They found the partial replacement lead to increased workability, increased mechanical properties, a higher hydration degree and better microstructural development. Considering Portland Limestone Cement (PLC) concretes, a replacement of cement by LP up to 10% can decrease the water demand and decrease the permeability of the material without affecting the mechanical properties significantly [62].

Quartz Powder / Silica Flour
Quartz powder and silica flour are mineral fillers. These materials can appear in many different particle sizes and size distributions. Being much smaller than normal silica sands and larger than silica fume, these in-between fillers can be used to get to perfect the particle size distribution (PSD) curve of the mixture. The silica in these materials can react with CH, similar to what silica fume does, but does so at a much lower rate. Rashad and Zeedan [64] showed that the inclusion of quartz powder can increase the resistance of concrete at elevated temperatures.

2.2.8. Packing

By increasing the particle packing density, the properties of the UHPC are improved. A denser structure not only leads to a higher compressive strength and more durable material [2], it also influences the anchoring of the fibres [42]. To achieve a dense packing, several models can be used that have evolved over time. Stovall et al. [65] proposed the Linear Packing Density Model of grain mixtures, a discrete packing model based on a theory by Mooney [66]. Larrard and Sedran [34] improved this model by correcting for the angular points in the curves generated due to its linear nature and created the Solid Suspension Model. Beside discrete models, continuous models can be used to determine the packing of mixtures. The fundamental work for this way of determining how to get to an ideal packing was done by Feret [67] and Fuller and Thompson [68]. They found that a proper packing of particles can improve the mechanical properties of concrete mixtures when considering these continuous particle size distributions (PSDs). Andreasen [69] did a research on the space between particles and compared packing curves for different values of the distribution modulus (q) to that of Fuller and Thompson [68]. The equation found to determine the fraction $P(D)$ of particles with a size up to D is shown in equation 2.1.

$$P(D) = \frac{D^q}{D_{max}^q} \tag{2.1}$$

Funk and Dinger [70] modified this method by introducing the minimum particle size to the equation to eliminate non-appearing particle sizes. This Modified Andreasen and Andersen (A&A) method (also called the Dinger-Funk Particle Size Distribution Equation) is shown in equation 2.2.

$$P(D) = \frac{D^q - D_{min}^q}{D_{max}^q - D_{min}^q} \tag{2.2}$$

This equation was used to determine a proper packing for the concrete mixtures in this thesis. Combining the PSDs of different materials, the distribution as described by the equation was approached. The closer this combined PSD comes to the A&A curve, the better. The value of the distribution modulus determines the exact curvature of this distribution curve. For a lower q, more fine aggregates will be present in the mixture, while a high q will lead to a relatively large amount of coarse particles. For an UHPC mixture a lower q is used since this material consists of mostly fine particles. According to Sbia et al. [71] a 'traditional' UHPC has a value $q = 0.25$ when using particles with a maximum particle size of 1 mm. In literature, it is seen that values close to this (often 0.23) are used for UHPC mixtures and show a very high compressive strength [38, 72, 73, 74]. Values above 0.3 are usually not considered

for UHPC. The fine particle distribution associated with a low q corresponds with the definition of UHPC. Decreasing the value of q decreases the fracture toughness of the material [75], so choosing a value too low must be prevented.

2.3. Material Behaviour and Properties

2.3.1. Compressive Strength

The compressive strength of SH-UHPFRC must meet the requirements of UHPC. An exact definition for this requirement is missing. HSC is considered to go up to a cubic compressive strength of around 100-115 MPa [76]. For UHPC, a strength of 150-200 MPa is often considered [2, 76]. The effect of fibres on the compressive strength of UHPC is discussed in Section 2.2.6. Compared to concrete types without fibres, a notable difference can be observed when testing for compressive strength. The fibres will make that the shape of an UHPFRC sample remains mostly intact, whereas fibre-less samples will split into multiple pieces, showing a very brittle behaviour [77].

2.3.2. Tensile Response

UHPFRC already has limited strain hardening behaviour as can be seen in Figure 2.5. For SH-UHPFRC, a longer strain hardening trajectory must be present. Such strain hardening can be seen in SHCC, of which the development was based on micro-mechanics. Mechtcherine [10] describes how from materials like Textile Reinforced Concrete (TRC) and SHCC one can see that materials that have an overcritical fibre content show tensile strain-hardening behaviour characterized by the formation of many fine cracks and relatively large deformations. Compared to these other strain hardening materials the tensile strength requirement of UHPFRC is higher. This can cause complications since some steps in the development of SHCC are contradictory to that of UHP(FR)C. Curosu et al. [42] describe that, to avoid fibre rupture in SHCC during cracking, which negatively affects the strain hardening behaviour, the bond between fibre and matrix must be limited. Therefore often part of the cement is replaced by FA and the W/C-ratio is chosen relatively high, leading to reduced mechanical properties and a higher permeability. This is opposite to what defines a UHPC. Wille et al. [21] described the following goals to achieve strain hardening in UHPFRC: (1) a relatively high tensile strength by achieving a high bond strength between fibres and matrix and (2) a high ductility by using a sufficient amount of fibres and assuring enough bond strength.

The behaviour of a specimen under tension can be described in a few steps [78]: once a micro crack occurs, leading to a drop in the stress-strain diagram, this crack is bridged by the fibres, which will slip-harden and thereby transfer the load through the crack. The stress in the specimen can then increase again as the load in the crack is now carried by the fibres. At another point in the specimen, the matrix will crack again and this process is repeated for multiple cracks. When the specimen reaches a point where it becomes saturated with micro cracks, fibre pull-out starts occurring and the bridging strength of the fibres will decrease until one of the cracks starts to widen. All strain localizes at this crack until the fibres' bridging capacity goes to zero. Besides fibre pull-out, the rupture of fibres is also a possible failure mechanism. This occurs when the cracking strength of the matrix is higher than the bridging strength of the fibres and would lead to fibres breaking in the first crack before the next crack would occur. Therefore the cracking strength of the concrete matrix must be determined keeping in mind the maximum it can reach concerning the fibre strength. The bond between fibres and matrix can be either chemical, frictional or mechanical [79]. Steel (deformed) fibres can have mechanical bonding, while for soft synthetic fibres as considered in this thesis, chemical and frictional bond play a role. Using coatings and treatments, these bonds can be increased or decreased [80, 81, 82]. See Figure 2.3 for a visualization of different fibre failure mechanisms.

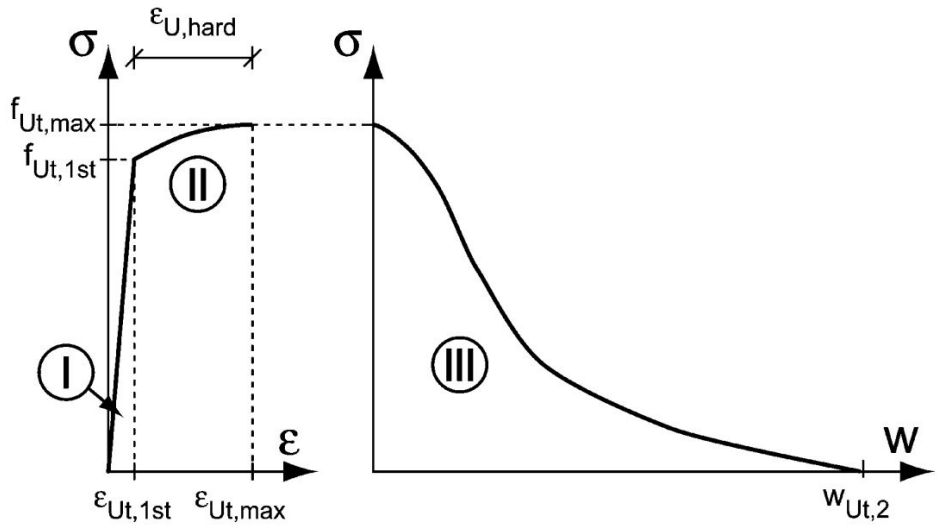

Figure 2.5: Schematic description of the tensile behaviour of UHPFRC: I) linear-elastic stress rise, II) domain of strain hardening and distributed macrocracking, III) softening behaviour and crack localization [83]

2.3.3. Modulus of Elasticity

For UHPC an elastic modulus (E-modulus) of 40-60 GPa is considered normal [77, 84], where for normal concrete classes the modulus normally ranges around 30-40 GPa. Ouyang et al. [84] related the E-modulus to several material contents in UHPC and found an increase in elastic modulus with the increase of cement and sand content and the decrease of the w/b-ratio. The properties of the used component are of large influence on the E-modulus [85].

2.3.4. Shrinkage

The characteristic low W/C-ratio of UHPC and high binder content have a large effect on shrinking behaviour of the material. Because of the limited amount of water, not all cement particles fully hydrate. This can lead to an increased amount of autogenous shrinkage, while having only very limited drying shrinkage [86]. This is also increased by the addition of SCMs, as the hydration and pozzolanic reactions increase the water consumption at early ages [87]. A large amount of autogenous shrinkage can cause problems as this can lead to early-age cracking, resulting in reduced strength and durability [88]. The severity of this issue depends on the rate of cracking and present stresses and restraints [88, 89].

2.4. Structural Applications

Wille et al. [17] have shown that high strength and ductility can be achieved without special curing methods including heat, pressure or vibration, by using a proper packing density, strong fibres and good fibre-matrix interaction. Without complicated production techniques, the material becomes more interesting for full-scale applications. Besides the use of this material to create elements with smaller dimensions and larger structural capacities as described by Bajaber and Hakeem [2] and Walraven [4], the possibilities of using it for the strengthening and repair of concrete elements is examined. Considering the high environmental impact and costs of this material, these applications where smaller volumes of the material are used, appear to be worth researching.

2.4.1. Repair of NC/RC Structural Elements

The possibilities for the use of UHPFRC for the repair of old and/or damaged NC structures have been studied. Having proven to provide a good mechanical bond and a positive effect on the permeability (and thus on the durability), UHPFRC has been found an appropriate material for the repair of NC structures [90]. For this application, the bond between the original deteriorated surface and that of the repair material is very important. Valikhani et al. [91] found that using UHPC over NC can double the strength of the NC substrate when testing in shear. An increase of surface roughness increases the shear bond strength, while the use of a bonding agent actually reduced the bond strength at the interface

[91]. SHCC has been mentioned as a decent flexural repair material for elements with corroded steel bars, requiring a relatively short bond length compared to conservative methods [8]. Because of their superior distributed cracking, strain hardening materials are considered good protective materials for damaged structural elements, both because of their crack-bridging abilities and the protection against harmful substances [10]. For this application, it is also important to consider the effect of shrinkage, as this can be very different for the concrete and repair material [92]. Besides possibly having different shrinkage behaviour, the age of the material is also different, leading to a larger shrinkage in the repair material. Depending on the bond strength, two types of failure can be caused by this shrinkage behaviour: the repair layer can debond due to the bond strength being too low compared to the material's strength; or the bond strength is high enough to prevent debonding, causing a restraint at the interface for the repair material which then becomes more prone to cracking [93].

2.4.2. Strengthening of NC/RC Structural Elements

Azad and Hakeem [94, 95] studied different ways of reinforcing NC elements with UHPC, using either faces or bars of the UHPC to strengthen the normal concrete and create hybrid elements. Both researches show that the inclusion of UHPC benefits the flexural behaviour, creating softening behaviour after the peak load and even enabling the exclusion of traditional steel reinforcement in the concrete elements. Other research showed using a layer of UHPC on a NC bridge deck can significantly improve the service life of the deck, given there is enough roughness to the material to attain sufficient bonding [96]. Multiple researches have shown that besides flexural strengthening, shear strengthening using UHP(FR)C is beneficial [6]. Using different methods like gluing multiple thin plates to a RC beam [97], gluing a plate over the full length of a RC beam [98] or casting UHPC directly against NC elements [99], all resulting in an increase in the shear capacity of a concrete element. An interesting research on the shear strengthening of corroded RC elements shows how not only the shear capacity but also the crack control behaviour can be improved by the addition of a layer of UHPC [100].

With the development of high strength strain hardening materials come additional strengthening possibilities. Khalil et al. [101] tested RC beams reinforced with a bottom layer of UHP-SHCC (Ultra High Performance Strain Hardening Cementitious Composite) and compared both cracking behaviour and flexural strength. The addition of a layer of the strain hardening material lead to a large increase in both the cracking and ultimate load. This research also includes the investigation of the effect of reinforcement in the UHP-SHCC layer. It shows that the addition of reinforcement leads to a better distributed cracking pattern, with more and narrower cracks compared to the samples without reinforcement [101]. A similar research was carried out by Hussein et al. [102], also including the comparison between strengthening using reinforced mortar and (reinforced) UHP-SHCC, in which the UHP-SHCC layer proved to be superior. Wei et al. [103] did a research on the shear strengthening of RC beams with a 10 mm thick layer of HS-SHCC on each side. A significant increase in shear strength depending on the span-to-depth ratio was found, but also the failure behaviour improved, showing a less brittle behaviour with smaller cracks, opposed to the spontaneous spalling normally observed with shear failure [103].

2.4.3. Numerical Modelling of Strengthened Structures

For the numerical modelling of strain hardening materials, the tensile stress-strain relationship is an important input aspect. The results from direct tensile tests can be simplified and used for this purpose. Lampropoulos et al. [99] reduced the tensile results of direct tensile tests using dogbone specimen to four linear segments, of which the first part represents the elastic regime, followed by strain hardening and strain softening. The results of the numerical simulation were in agreement with the experimental outcomes, showing the assumed description of the tensile behaviour was acceptable.

Considering a numerical model for a shear strengthened structure, the modelling of the interface between NC and the strengthening material is an important factor. The relation between bond stress and slip is the most important property for the bonding materials, but has also been found to be one of the hardest things to describe [104]. In the ATENA software used in this thesis, the interface material model used was based on the Mohr-Coulomb criterion with a tension cut-off, see Figure 2.6 [105]. This shows the failure surface, indicating the maximum resistible shear stress depending on the occurring normal stress. The values for the coefficient of friction ϕ, cohesion c and tensile bond strength f_t are based on the properties of the connected materials. The assumption of a perfect bond between the concrete

and the strengthening material indicates delamination is not considered in the numerical model. This could simplify the modelling of structures for which it has been experimentally proven that delamination has a limited or negligible effect on the capacity of the structure [106].

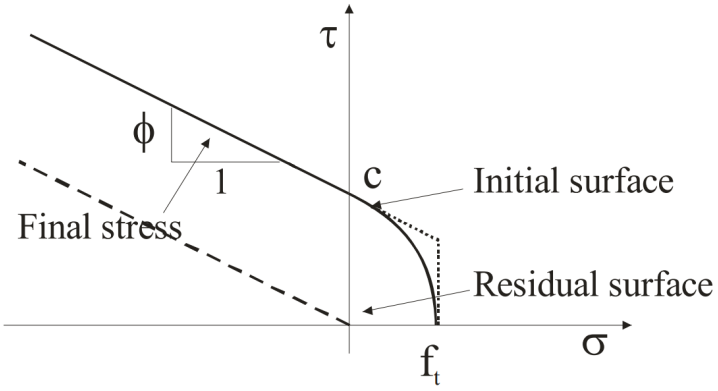

Figure 2.6: Failure surface for interface elements [105]

2.5. Environmental Impact

Besides the mechanical properties, the environmental impact of building materials has become another important aspect over the past decades. The high cement content in UHPC increases the environmental impact per cubic meter significantly [107]. This is (partially) compensated by the reduced dimensions of UHPC elements needed. Because of the superior mechanical properties, the cross section can be reduced and with that, the mass of elements. With lower mass and possible longer spans compared to ordinary concrete solutions, the sustainable potential of UHPC is interesting for structural elements [108]. Replacing part of the cement by SCMs can also be a good way to reduce the material's environmental impact, although this requires consideration regarding the strength development, as this might be affected by SCMs [107, 109, 110].

The production of the fine steel fibres used in most UHPCs is responsible for half of the Global Warming Potential (GWP) for a mean UHPC mixture [111]. Because of the significant environmental impact of these fibres in UHPFRC, it is interesting to investigate the possibilities to lower this impact caused by the fibres. Multiple studies focused on the reduction or replacement of fibres in UHPC mixtures [80, 112]. Hajiesmaeili and Denarié [113] investigated the effect of replacing steel fibres by UHMWPE fibres. While drastically reducing the environmental impact, this replacement did not lead to a notable difference in the strength values measured, even with a decreased cement content. Their research showed that in flexural testing, the material with UHMWPE fibres and low cement content can reach similar forces but with a much higher deflection capacity, making this an interesting material for multiple applications[113].

A life cycle analysis (LCA) on different methods to strengthen a bridge deck was done by Hajiesmaeili et al. [114], comparing the use of post-tensioned RC, UHPRFC with steel fibres and PE-UHPFRC. The results of this study are shown in Figure 2.7. This shows a large improvement using UHPFRC over RC and an even larger difference when using PE fibres. This research again showed that among the different material components, the influence of steel (fibres and reinforcement) and cement was largest.

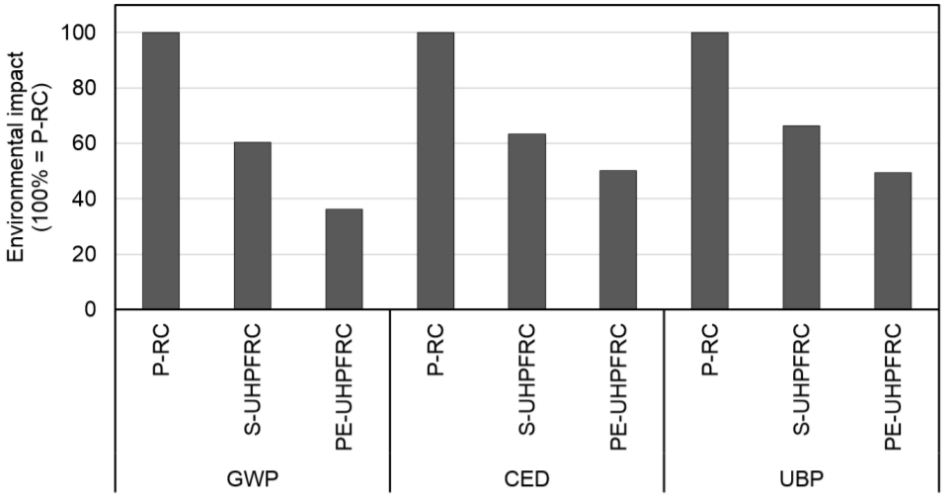

Figure 2.7: Normalized environmental impact over a life cycle of 100 years for different strengthening methods for a bridge deck. Calculated for three environmental impact factors:global warming potential (GWP), cumulative energy demand (CED) and ecological scarcity (UBP) [114]

3

Mix Design Development

This chapter describes the first phase of the research. In this first phase the mixture design of the material was developed using knowledge described in Chapter 2 and many experimental trials. First an overview is given on the methodology and components used in this research. After this, every step taken in the mixture development is discussed, including a study on mixtures from literature. Different component ratios are modified and the effect of this on the material properties was measured. Also the difference between different material components was investigated. In the final section the properties of the final mixture are determined.

3.1. Experimental Procedure and Component Properties

A consistent approach throughout the research is of great importance. The procedure followed is described in this section. This was used for all experimental steps unless mentioned otherwise in the concerning paragraph.

3.1.1. Mix Design Starting Point and Key Points of Attention

Mixtures from literature and those currently used at TU Delft are used as references. The starting point is a UHPFRC mixture developed by Awasthy [115] at TU Delft. This mixture is chosen for its promising compressive strength, good workability and the fact no direct revision of the mixture is required as the materials used in this mixture are the same as those used for this research. From this base mixture the best possible mixture will be designed by altering proportions of the mixtures, comparing testing data and linking results to literature.

For every step one proportion is changed, the effect on the material properties is measured and a choice is made to continue with this new mix design or to go back to the previous version. Because the material development is not the only objective in this research and because of the large amount of time necessary for each individual step, not every component ratio and design aspect can be tested. This means that some ratios are not changed over the process and others are only changed to one or two different values instead of using a range of values. Some design aspects are kept in mind throughout the process but not changed as individual attributes: minimum and maximum proportions following literature, low W/C-ratio and good particle packing following the A&A-method. The interaction between fibres and matrix is not studied in this thesis. Despite the fibre-matrix interaction being a significant parameter, especially regarding tensile material properties, this is not within the scope of this research. Some changes will have a positive effect on one material property while negatively affecting another, here a balance must be found. Especially between good workability and high compressive strength values compromises must be made as these properties often experience opposite effects from a change in the concrete mix design. The last aspect to keep in mind is the environmental impact. As some components have a larger environmental impact, the included amount of these must be limited when possible.

3.1.2. Component properties

Cement

For this research CEM I 52.5 was used, having a minimum of 95% OPC and a high strength. The standard available type at TU Delft was CEM I 52.5 R HSR, having a quick strength development (R) and a high sulfate resistance (HSR). To achieve a quick strength development, the surface area of the material must be very large, which is accomplished by having very fine particles. To improve the workability, halfway through the material research the possibility to use an other cement type was explored. CEM I 52.5 N SR3 LA was selected for this purpose. This cement type has the same minimum amount of OPC and strength class, is resistant against sulphate (SR3) and has a low alkali content (LA). The important difference lies in the larger grain size of this material. Because this material is designed for normal strength development (N), the distribution of particle sizes is coarser compared to the originally used cement type. The difference in particle size distribution can be seen in Figure 3.1. In further sections these cement types are referred to as CEM I 52.5 R and CEM I 52.5 N as this indicates the differences between the two.

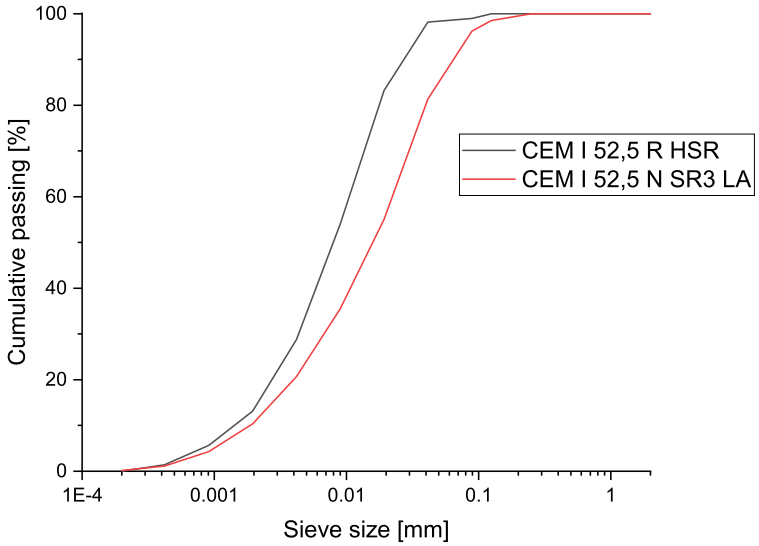

Figure 3.1: Particle Size Distribution curves of all dry materials used in research

Other Granular Materials

Besides cement, silica fume and blast furnace slag were used as binders. Sands in three size ranges were included in this research, the largest being 0.5-1 mm. As an additional filler, M4 silica powder was used. Multiple size ranges of this material were available, the M4 powder has an average diameter of 32 µm and maximum diameter of 125 µm. This material was (among other reasons) selected to fill the 'gap' in the PSD curves around 0.1 mm. All materials used are listed in Table 3.1 with their densities. The PSD curves of all materials are shown in Figure 3.2.

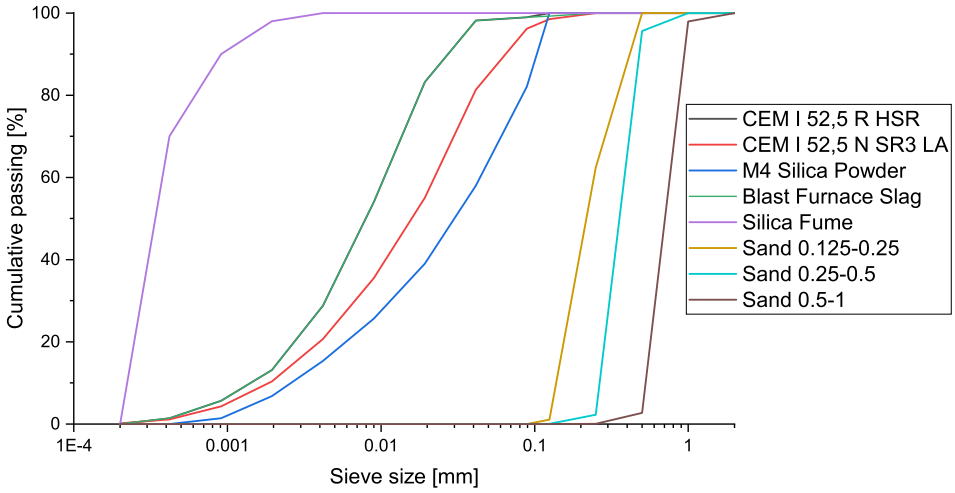

Figure 3.2: Particle size distribution curves of all granular materials used in research

Table 3.1: Density of all granular materials used in research

Material	Density kg/L
CEM I 52,5 R HSR	3.13
CEM I 52,5 N SR3 LA	3.16
M4 Silica Powder	2.65
Blast Furnace Slag	2.89
Silica Fume	2.36
0.125-0.25	2.61
0.25-0.5	2.61
0.5-1.0	2.61

Superplasticizer

Two types of superplasticizer (SP) have been used in this research. Both were based on polycarboxylic ether (PCE) polymers. MasterGlenium 51 con. 35% NL was the originally used SP for UHPC mixtures and can be used in mixtures with very low w/c-ratios, increases early and late strength and improves durability properties [116]. Sika® ViscoCrete®-20 HE was developed for mixtures requiring high (early) strength, high water reduction and improved flowability [117]. Because of the limited workability - caused by a low w/b-ratio and the high aspect-ratio PE fibres - the type of SP can be of great significance. As both materials have promising features, an experimental comparison was performed to select the one best to use in research. Table 3.2 includes characteristics of both SP types. No further admixtures were included in this research.

Table 3.2: Characteristics of SP types [116, 117]

Characteristic	MasterGlenium 51 con. 35% NL	Sika® ViscoCrete®- 20 HE
SP base	PCE	PCE
Density [kg/L]	1.075	1.09
pH-value	7.0	4.5
Dry material content [wt%]	35	40
Max chloride content [wt%]	0.1	0.1
Recommended max. dosage	1.25% wt. binder	2% wt. cement

Fibres
For previous UHPFRC mixtures, steel fibres with a diameter of 0.16 mm and a length of 6 or 13 mm were used. In this research, Ultra High Molecular Weight Polyethylene (UHMWPE) fibres were used. DSM Dyneema® SK99 fibres were used, similar to the fibres used in the research by Hajiesmaeili and Denarié [113]. Besides the different material, these fibres are also much thinner (12 µm) compared to the previously mentioned steel fibres. An overview of the UHMWPE fibre properties is shown in Table 3.3.

Table 3.3: Properties DSM Dyneema® SK99 [118]

Density [kg/m^3]	975
Diameter [µm]	12
Length [mm]	6
Tensile strength [GPa]	4.1
Compressive strength [GPa]	0.1
Young's modulus [GPa]	155
Elongation at break [%]	3-4

3.1.3. Casting and Curing
The mixture was prepared in a Hobart mixer according to the following procedure:

1. Place all dry materials except for the fibres (sand, cement, silica fume and other binders) in the bowl with the coarsest material on the bottom and the finest material on top. Mix this for 30 seconds at low speed.
2. Pour about 90% of the water in the bowl and mix this for 45 seconds at low speed.
3. Pour the remaining 10% of the water into the SP and together pour this into the mixer. First mix for 45 seconds at low speed, then increase to medium high speed for 3 minutes and 30 seconds.
4. As the mixture becomes one whole, increase the speed to high and continue mixing for 1 minute and 30 seconds.
5. When the mixture is flowable and well-combined, add the fibres continuously in small portions while mixing at low speed to avoid the drift of fibres.
6. After all fibres are included, set the mixer to high speed and mix for another 2 minutes. At this point no agglomerations of fibre should be perceptible.

The mixture was poured into the moulds, vibrated for 10-15 seconds and covered to harden for 24 hours before demoulding. After one day the samples were demoulded and, if necessary, cut. After this the samples were cured in a fog room with a temperature of 22°C and a relative humidity (RH) of 99%, in accordance with EN 12390-2. The specimens were kept here until the day they were tested. This standard curing procedure was used for all samples unless mentioned otherwise.

3.1.4. Testing Procedures
Compressive Strength Testing
In the first phase of the research the main focus was on compressive strength and flowability of each mixture, both for paste mixtures and total mix designs. For the compressive strength test, three 40 mm cubes were cut from a 40×40×160 mm^3 beam. These were compressed under a constant rate until failure after which the maximum load was recorded. This test was executed for every mixture after 1, 3, 7, 14, 21 and 28 days of hardening. The setup for this was shown in Figure 3.3. The recorded maximum load was divided by the area of the cube (1600 mm^2) to determine the compressive strength. For every age, three cubes were tested and the mean value and standard deviation were used to compare different mixtures.

Flow Table Test
The flowability was measured using a flow table test, see Figure 3.4 for the setup. This procedure was executed according to NEN-EN 1015-3, using a cone of 60 mm height with a width ranging from 100 mm at the bottom to 70 mm at the top. After lifting the cone, the mortar sample was vibrated 15 times before the diameter was measured in two orthogonal directions. These values were averaged to determine the flow.

Figure 3.3: Setup compressive strength test 40 mm cubes

Figure 3.4: Setup flow table test

Direct Tensile Test

For promising mixtures the tensile behaviour was determined. Because this tensile testing was a time consuming process and required the availability of both specific machinery and the assistance of a supervisor, this property was not tested for every mixture. For the determination of the tensile behaviour, a direct tensile test was done using an Instron testing system or the Hordijk setup. Dogbone specimens with dimensions as shown in Figure 3.5a were used on which strain gauges were attached. Figures 3.5b and 3.5c show the setups for these measurements for both testing systems. In both setups, the sample was glued to the top and bottom plate using metal plates on the sides of the specimen to increase the glued contact area. The application of strain gauges was different for both methods. In case of the Instron setup, the gauges were installed on the sides of clamps attached to the specimen. For the Hordijk setup holders were glued to the sample's front and back side. For both setups the strain gauges were located at the end of the narrow part of the specimen, as indicated in Figure 3.5a.

The strain over a measured length over the narrow part of the sample was measured alongside the force the device exerts and the total displacement. The strain was calculated by dividing the averaged measured displacement from both gauges over the gauges' span. The stress was calculated by dividing the measured force over the area of the narrow part of the sample. The stress and strain measurements were used to determine the cracking strength and strain, peak strength and maximum strain. From the graph that followed from these measurements, the tensile behaviour including strain hardening and/or softening could be observed.

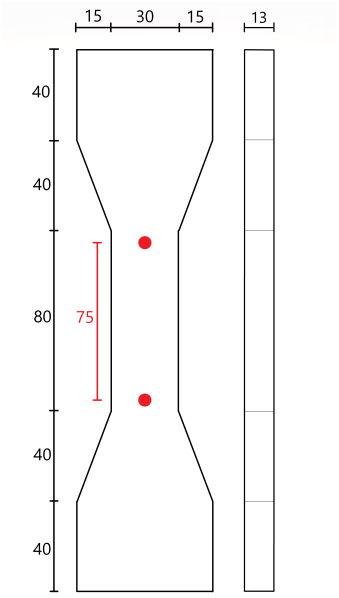

(a) Dimensions dogbone specimen (mm)

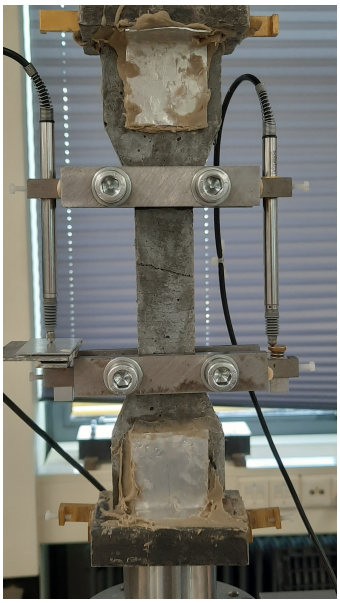

(b) Setup direct tensile test Instron

(c) Setup direct tensile test Hordijk

Figure 3.5: Direct tensile testing setup. Dimensions of dogbone specimen displayed in mm. The red dots indicate the location of attachment for strain gauges.

DIC

To be able to analyse the cracking pattern formed during a direct tensile test, Digital Image Correlation (DIC) was used. The specimen had to be prepared with a high-contrast pattern to capture displacements between pictures. To do this, one side of the specimen was painted white, after which a pattern was created using black spray paint, see Figure 3.6a. The specimen was glued into the setup similar to a regular direct tensile test. Both strain gauges were now glued on one side of the specimen, opposite of the painted surface, see Figure 3.6b. During the test, every five seconds a picture was taken. A flash was used to prevent changes in light and shadow forming, which could lead to a disturbed pattern between pictures. A picture of the camera setup is shown in Figure 3.6c. After testing, GOM Correlate was used to determine displacements and strains relative to the reference picture (taken before the start of the direct tensile test).

(a) DIC pattern

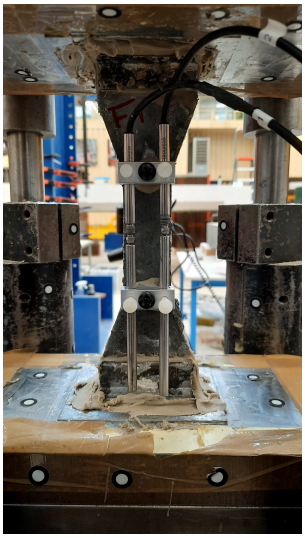

(b) Strain gauge placement for DIC

(c) Camera setup DIC

Figure 3.6: DIC direct tensile testing setup

E-modulus Test

For the determination of the E-modulus of the final mixture, two samples of 100×100×400 mm^3 were cast. Holders for strain gauges were glued to all long sides and the sample was placed in the TONI bank. This setup is shown in Figure 3.7. The bank was brought into position such that contact was made with the sample. The sample was compressed up to 30% of the compressive strength corresponding to the sample's age and then lowered to 10% of the compressive strength. This procedure was repeated three times. The load was divided by the sample area and the measured displacement was divided by the distance between the holders to determine the stress and strain curve. The E-modulus was calculated following EN 12390-13.

Figure 3.7: Setup for E-modulus measurement using TONI bank

Shrinkage Test

Both drying and autogenous shrinkage were determined for the final mixture using 40×40×160 mm^3 samples with measuring tips encasted in the ends of the sample. A total of six specimens was cast of which three were wrapped using bitumen tape which was secured using regular tape. The length and weight of these samples was measured over a span of 90 days to determine the shrinkage behaviour. The first measurement was done a little over one day after casting, as soon as the samples were set. Figure 3.8 shows the two types of samples and the measuring device for the change in length. The change in weight and length of the bare sample indicated the total shrinkage of the mixture, whereas the wrapped sample only showed results for autogenous shrinkage. The difference between these results equal the drying shrinkage. The shrinkage was measured two times per day in the first week of age, once a day in the second and third week and every three days after that.

(a) Sample for total shrinkage (b) Sample for autogenous shrinkage

Figure 3.8: Setup for length measurement for shrinkage

Setting Time Determination

A Vicat device was used to determine the initial and final setting time of the final mixture. This device used a needle to penetrate fresh mortar at a predetermined time interval. The setup can be seen in Figure 3.9. This test was executed following NEN-EN 480-2. This setup is normally executed for pastes only but in this research, the final mixture including sand and fibres was tested. A cone with a height of 40 mm and internal diameter ranging from 80 mm at the bottom to 70 mm at the top was placed on a glass base plate, secured with a plastic ring and filled with mortar. The top of the sample was covered to prevent the surface from drying. Time intervals were selected and the test was started. The sample was penetrated 44 times, preserving a distance of at least 1 cm between measuring points, following a pattern as shown in Figure 3.9c. The reached distance penetrated into the sample was recorded along with the exact time of penetration. The initial setting time was considered to correspond with a penetration depth of 36.5 mm and the final setting time to 2.5 mm. Using different time intervals, the initial and final setting times could be estimated more accurately.

(a) Vicat setup (b) Vicat sample (c) Penetration pattern

Figure 3.9: Vicat setup for setting time determination

3.2. The Effect of Material Components on Material Properties

In this section, the development of the mixture design is discussed. Preceded by an evaluation of mixtures from literature, the effects different material components have on the properties of the mixture were analysed. After changing one mixture ratio or component in every step, the mechanical properties were studied and the mix design adapted. This was repeated until the final mixture is determined. A flow scheme of all mixtures in the design process can be seen in Figure 3.10. This shows each step taken in the development of the SH-UHPFRC mixture.

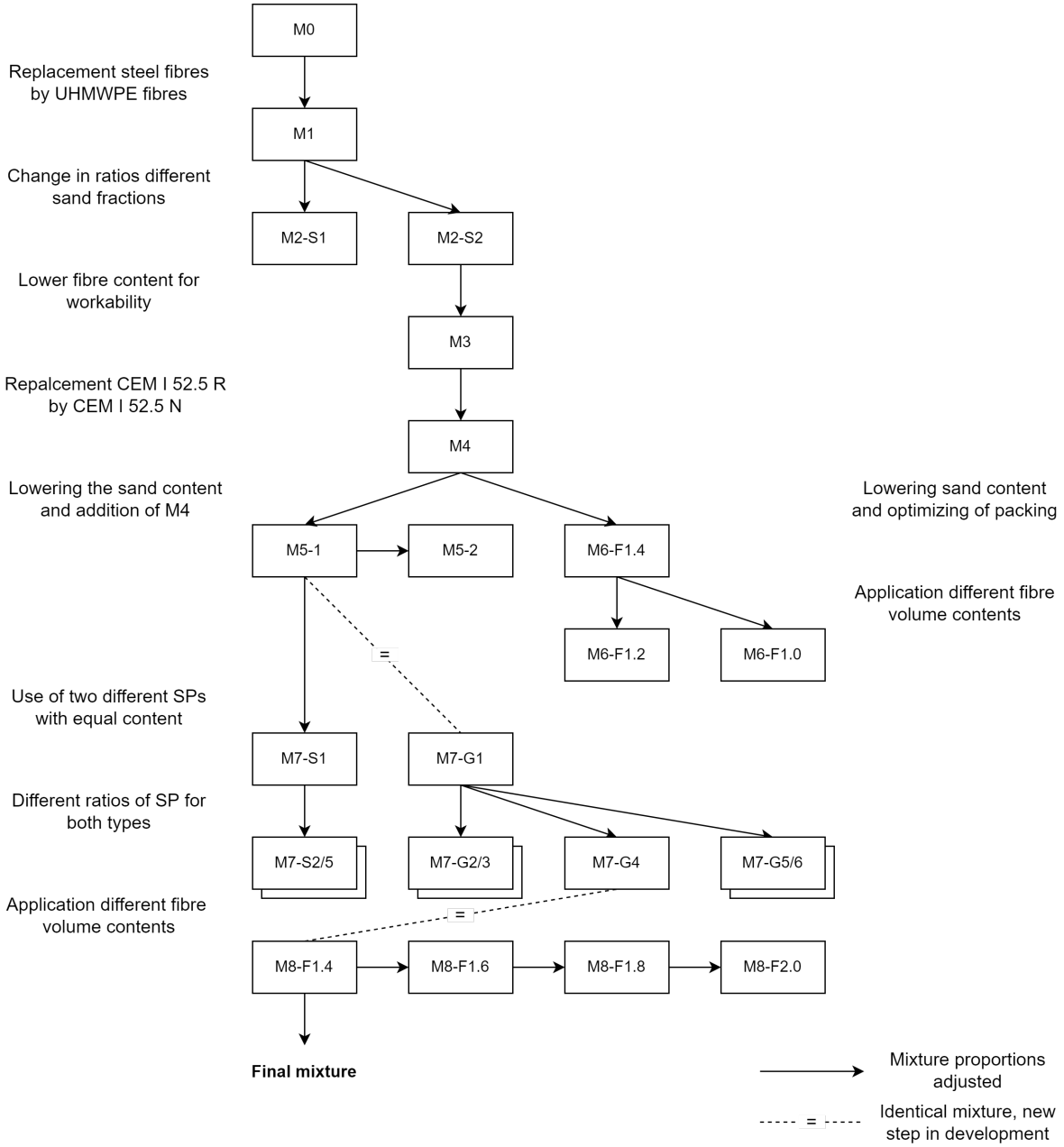

Figure 3.10: Flow scheme mixture development

3.2.1. Preliminary Research based on Literature

Several relevant mixtures from literature have been studied. A collection of some of these mixtures can be seen in Table 3.4, including the mechanical properties as stated in the corresponding literature. The starting point mixture is also included in this table for comparison. Part of these mixtures were adapted to the available materials for this research and compared based on compressive strength and workability to make a comparison excluding the effect of components' specific material properties. The most remarkable properties of these mixtures were taken into consideration in the composing of the design mixture.

A clear difference between the base mixture and the other mixtures from literature was the sand content. This value being much higher can lead to a difference in mechanical properties. Besides the sand content, the type of sand used in the base mixture also seemed to be coarser. As discussed in Section 2.2.3, finer sands can have a beneficial effect on the strain hardening behaviour of a material. As a consequence of the large amount of sand, the binder content in the starting mixture is relatively low. The combined weight of binders was significantly higher in the strain-hardening materials compared to the base mixture. For all mixtures, a variety of different binders was used.

Using the standard available materials in the laboratory, some of these mixtures were imitated and tested. Because the materials were not exactly the same, slight deviations were to be expected. For the substitution of components, all available information from the paper corresponding to the mixture was consulted, trying to stay as close to the original as possible. Despite the mixtures originally containing different fibre types, all imitated mixtures were made using UHMWPE fibres since these were used throughout the whole research. The compressive strength development of these mixtures is shown in Figure 3.11. The mixture imitating that of Ranade [39] did not include fibres, as the workability did not allow the addition of fibres with the components used in this research; this would have abolished the workability of the mixture. This can influence the compressive strength of the mixture and must therefore be considered when comparing the results of different mixtures. Figure 3.11 shows that the mixture by He et al. [80] clearly had the highest strength of the imitated mixtures. The base mixture for this research (Awasthy [115]) showed a 28-day compressive strength 10 MPa lower than that of He et al. [80], yet slightly higher than the other mixtures.

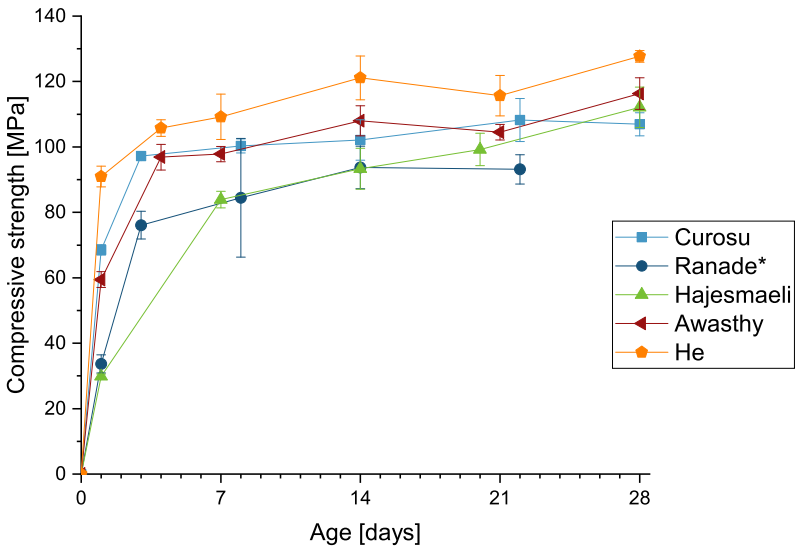

Figure 3.11: Compressive strength development of literature mixtures [39, 42, 80, 113, 115]. *The mixture by Ranade does not include fibres.

Because of the superior strength the imitated mixture by He et al. [80] showed, the tensile properties of this mixture were also examined. The results of this test are shown in Figure 3.12. It can be seen that

the peak strength ranged approximately between 6 and 7.5 MPa and the strain the strain capacity was 2% or higher. These results deviating from the results in the original research was to be expected as the used material components were not identical. Although not perfectly matching these original results, this result looked promising and the characteristic ratios of this mix design could motivate changes in later mix development.

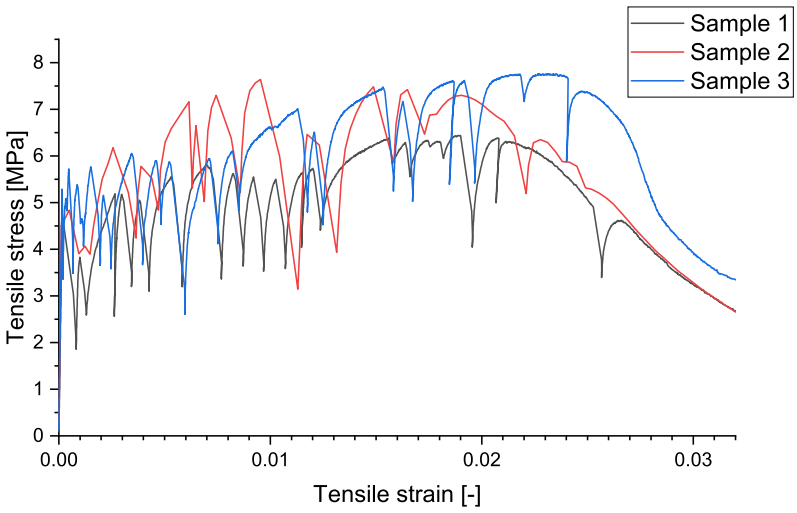

Figure 3.12: Direct tensile test results replicated mixture He et al. [80]

Table 3.4: Literature mixture designs, quantities in kg/m^3. Between brackets the ratios for all components relative to cement are displayed. *Mix design by Wille et al. [16] was converted from ratios to kg/m^3 using assumed material densities to compare all mix designs.

	Wille[16] *	Hajiesmaeli[113]	He[80]	Curosu[42]	Ranade[39]	Awasthy[115]
Concrete type	SH-UHPFRC	(SH) PE-UHPFRC	SH-UHPC	HS SHCC	HSHDC	UHPFRC
Cement	855.3 (1)	508 (1)	1289 (1)	1460 (1)	907 (1)	870 (1)
Silica fume	213.8 (0.25)	178 (0.13)	143 (0.11)	292 (0.2)	353 (0.38)	43 (0.05)
Silica flour	-	-	430 (0.33)	-	251 (0.27)	-
Blast furnace slag	-	-	-	-	-	104 (0.12)
Glass powder	213.8 (0.25)	-	-	-	-	-
Limestone fillers	-	559 (0.43)	-	-	-	-
Quartz powder	-	223 (0.17)	-	-	-	-
Calcium Nitrate	-	11 (0)	-	-	-	-
Water	162.5 (0.19)	165 (0.12)	284 (0.22)	315 (0.21)	189 (0.2)	204 (0.23)
Superplasticizer	9.4 (0.011)	27 (0.02)	22 (0.01)	35 (0.023)	16 (0.017)	26 (0.03)
Sand	786.8 (0.91)	525 (0.4)	143 (0.11)	145 (0.09)	635 (0.7)	1061 (1.21)
Fibres	230.9 (0.27)	19 (0.01)	14 (0.01)	20 (0.01)	19 (0.02)	125 (0.14)
Cement type	-	CEM I 52.5 HTS	CEM I 52.5 N	CEM I 52.5 R-SR3/NA	Class H	CEM I 92% 52.5 R HSR, 8% 42.5 N
Superplasticizer type	-	-	Polycarboxy-late-based	Glenium ACE 460	-	Glenium 51
Sand type	30% <0.2 mm, 70% <0.8 mm	”Fine sand” (d50 = 250 µm)	Micro sand (d50=150µm)	Quartz sand 0.06-0.2 mm	100 - 600 µm	50% 0.5-1, 30% 0.25-0.5, 20% 0.125-0.25
Fibre type	HS steel, 13mm/ 0.20mm	UHMWPE (Dyneema SK99)	HSHM PE, 19mm/ 23µm	HDPE, 6mm/20µm	UHMWPE, 12.7mm/ 28µm	Steel, 13mm
Fibre volume [%]	3	2	1.5	2	2	1.6
Density [kg/m^3]	2505	2216	2325	2134	2371	2439
Compr. strength [MPa]	250	120	144	134	166	132
Tens. cracking strength [MPa]	-	-	7.6	3.8	-	-
Tens. peak strength [MPa]	18.0	11.7	13.1	7.6	14.5	-
Tens. peak strain [%]	0.5	3.5	-	-	-	-
Tens. ultimate strain [%]	-	-	1.9	3.9	3.4	-

3.2.2. Sand Particle Size

Starting from the base mixture, different ratios in sand size fractions were compared based on their effect on the workability and compressive strength. The largest size fraction was excluded in the new versions of the mixture as from references it was clear that the use of only very fine materials is beneficial. One variant with only the finest sand fraction and one variant with a combination of the finest and second finest fraction were compared to the original base mixture (M1), see Table 3.5. Figure 3.13 shows the particle size distributions of these mixtures compared to A&A-curves using maximum particle sizes of 0.5 and 1.0 mm. The corresponding compressive strength at 28 days and the standard deviation for this value are also included in Table 3.5. Having a very limited difference in compressive strength, the workability became the more decisive factor. The poor workability of M2-S1 containing only the finest sand particles ensured that no further consideration was needed. With the increased surface area compared to M1, the workability did not reach a sufficient level. For the remaining two mixtures, the workability was similar and the difference in compressive strength almost negligible. The decision was made to continue the process using M2-S2 as the use of larger sand particles in M1 might have a negative influence on the tensile behaviour as described in section 2.2.3.

Table 3.5: Mixtures used to compare the effect of different sand particle size fractions followed by compressive strength and flow diameter test results. Mixture ratios in kg/m^3

	M1	M2-S1	M2-S2
Cement I 52.5 R	800.4	800.4	800.4
Cement I 42.5	69.6	69.6	69.6
Blast furnace slag	104.4	104.4	104.4
Silica fume	43.8	43.8	43.8
Water	204.6	204.6	204.6
Superplasticizer	26.6	26.6	26.6
Sand 0.125-0.25	213.3	1061.1	707.4
Sand 0.25-0.5	318.7	0	353.7
Sand 0.5-1.0	529.1	0	0
PE fibres	15.6	15.6	15.6
28-day compr. strength [MPa]	116.28	115.62	113.01
STD compr. strength [MPa]	4.84	1.48	2.74
Flow diameter [mm]	12.25	11.00	12.25

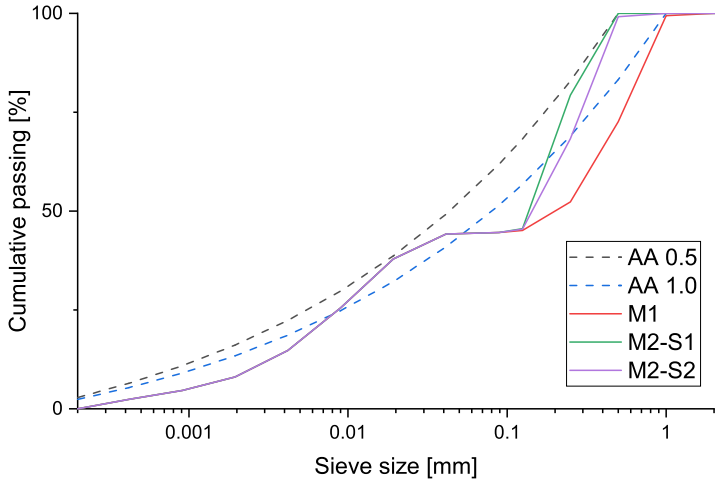

Figure 3.13: PSDs of mixtures for determination of the effect of different sand fractions on mechanical properties

3.2.3. Cement Type

A very low w/b-ratio is associated with a limited workability. To increase this workability without increasing the amount of water in the mixture, the effect of a coarser cement type was examined. The details on the used cement types and their PSDs can be seen in Section 3.1.2. Both cement types (52.5 R and 42.5) in the previous mixture were replaced by the new CEM I 52.5 N. The mixtures used for this comparison are shown in Table 3.6, accompanied by their measured flowability and compressive strength at 28 days. The compressive strength development over time can be seen in Figure 3.14. Here the difference in strength development using different cement types can be seen. The change to the N-type cement decreased the early strength compared to that of the mixture using CEM I 52.5 R and decreased the 28-day strength by about 10 MPa. A steeper slope was visible with the N cement compared to the R cement, showing a more pronounced development over a longer period of time.

Table 3.6: Mixtures using different cement types, component quantities in kg/m^3

	M3	M4
Cement I 52.5 R	800.4	-
Cement I 42.5	69.6	-
Cement I 52.5 N	-	870
Blast furnace slag	104.4	104.4
Silica fume	43.8	43.8
Water	204.6	204.6
Superplasticizer	26.6	26.6
Sand 0.125-0.25	707.4	707.4
Sand 0.25-0.5	353.7	353.7
PE fibres	13.7	13.7
Compressive strength [MPa]	116.6	106.9
Standard deviation [MPa]	0.7	1.9
Flow diameter [mm]	13.5	14.5

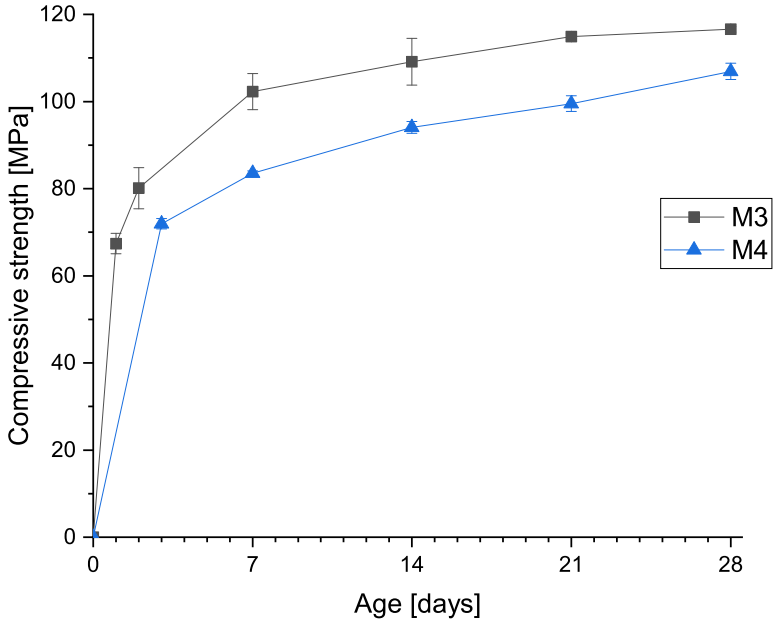

Figure 3.14: Compressive strength development over time of mixtures using different cement types

The visual difference in workability can be seen in Figure 3.15. This showed the fresh state of the same two mixtures, right after lifting the small cone, before applying compaction energy. A clear dif-

ference was visible in the consistency of the mixtures. While the first specimen preserves almost the exact shape of the cone, the increased flowability of the second specimen caused it to flow out. This increase in flow also lead to a visual and tactilely noticeable improvement in fibre dispersion, as a significant decrease in the amount of fibre agglomerations could be observed. This can positively affect the material's tensile properties. Although a decrease in compressive strength was observed, the increased flowability of M4 was considered significant enough to select this mixture over M3.

(a) Flow table specimen using CEM I 52.5 R right after lifting cone (M3)

(b) Flow table specimen using CEM I 52.5 N right after lifting cone (M4)

Figure 3.15: Visual comparison flow table test specimens using different cement types

3.2.4. Packing and Paste Content

To determine the effect packing and paste content had on the flowability and compressive strength of the mixture, four mixtures were compared with varying compositions as can be seen in Table 3.7. For this comparison M4 was the base mixture. Because of the good results in the preliminary study, the mixture by He et al. [80] was used as a reference mixture. Remarkable was the large amount of cement in this mixture, the use of a large amount of silica flour and a very small amount of sand. These characteristic mixture proportions were taken into account in the modification of Mixture M4. Three new mixture designs were created. For all modified mixtures, the paste content was increased compared to that of M4 and the SF content increased. In a previous step in the mixture design it was already proven that using only the finest type of sand the flowability of the mixture was very limited. Therefore, Mixtures M5-1 and M5-2 included the two finest sand fractions similar to the base mixture, opposed to M6 where only the finest sand was used like reported in the mixture by He et al. [80]. Between M5-1 and M5-2, the only difference was the sand content, all other components were kept at the same ratios. In M6, the cement content was lower than in M5-1 and M5-2 and a large amount of only the finest sand was used. In this last mixture, the proportions were chosen such that the PSD curve was particularly close to the A&A curve. The PSD curves of all mixtures are shown in Figure 3.16.

The decrease in paste content between M5-1 and M5-2 resulted in a reduction in flow but also a small increase in mean compressive strength. The PSD for M6 was very close to the A&A curve but the flow diameter was lower than that of the other mixtures. All mixtures had a larger compressive strength than the base mixture. Because of the limited workability of M6, this mixture was not considered further development. Between M5-1 and M5-2 a trade-off had to be made between flowability and compressive strength. Because of the limitations in application using a material with less flowability, M5-1 was selected for further development, despite having a lower compressive strength and slightly higher environmental impact due to the higher cement content.

Table 3.7: Mixtures used to determine the effect of packing and paste content, mixture ratios in kg/m^3

	M4	M5-1	M5-2	M6	He[80]
CEM I 52,5 N	870.0	1119.1	1059.5	955.6	1289
Sibelco M4	-	193.0	182.7	219.7	430
Blast furnace slag	104.4	134.3	127.1	114.7	-
Silica fume	43.8	111.9	105.9	114.7	143
Tap water	204.6	231.2	218.9	197.4	284
Glenium 51	26.6	22.4	21.2	19.1	22
0.125-0.25	707.4	173.6	211.4	716.7	143
0.25-0.5	353.7	322.3	392.5	-	-
fibres	13.7	13.7	13.7	13.7	13.7
Paste content (≤0.125mm) [%]	44.8	72.7	67.6	63.2	92.1
Flow diameter [mm]	16	17.5	16	14.25	-
28-day compr. strength [MPa]	103.7	115.5	122.7	117.7	127.7
STDV compr. strength [MPa]	4.4	6.2	5.1	8.3	1.8

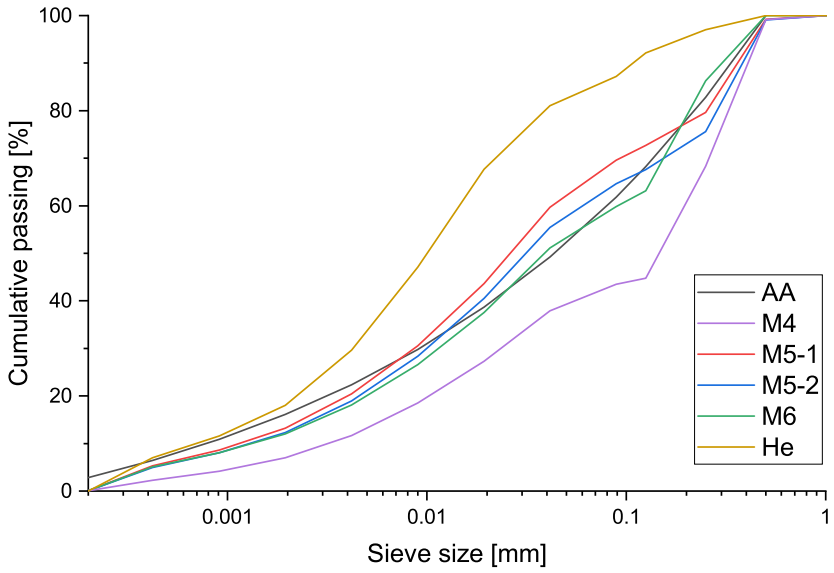

Figure 3.16: PSD curves of mixtures for packing and paste content comparison

3.2.5. Superplasticizer Type and Amount

The two SP types discussed in Section 3.1.2 were compared based on their effect on the flow spread and compressive strength of the mixture. The mixture used for these tests can be seen in Table 3.8. To compare the types and amounts of SP used, the amount of SP was expressed in the ratio of the weight of dry SP material over the total weight of binder in the mixture. The two SP solutions had different dry material contents. The amount of water in the SP used in every mixture was compensated for, meaning that the W/C-ratio was equal in every mixture. For higher SP contents, the water content was lowered by the amount of water in the SP solution. The water and SP contents for all mixtures are shown in Table 3.9. The dry material content is plotted against the resulting diameter from the flow table test in figure 3.17. As to be expected, the flow diameter increased with larger amounts of superplasticizer. A very similar behaviour was visible for both SP types. Because of the limited measurements of the flowability, no standard deviations were calculated.

Table 3.8: Base mixture SP testing

CEM I 52.5N	Sibelco M4	BFS	SF	Water	SP	S 0.125-0.25	S 0.25-0.5	PE fibres
1119.13	192.95	134.30	111.91	variable	variable	173.57	322.34	13.70

Table 3.9: SP and water content mixtures SP testing

	Mix No.	SP content	Dry SP / binder	Water content
Glenium 51	M7-G1	22.38	0.0057	231.21
	M7-G2	25.58	0.0066	229.13
	M7-G3	28.78	0.0074	227.06
	M7-G4	31.98	0.0082	224.98
	M7-G5	35.17	0.0090	222.90
	M7-G6	38.37	0.0098	220.82
SIKA 20HE	M7-S1	19.58	0.0057	234.01
	M7-S2	22.38	0.0066	232.33
	M7-S3	25.18	0.0074	230.65
	M7-S4	27.98	0.0082	228.97
	M7-S5	33.57	0.0098	225.62

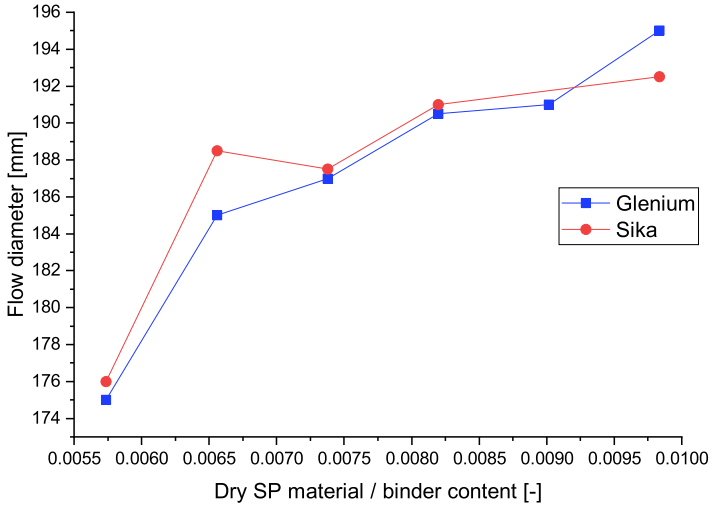

Figure 3.17: Effect of type and amount of SP on the flow diameter

The compressive strength was measured at 7 and 28 days using 40 mm cubes cut from 40×40×160 mm^3 prisms. The influence the amount and type of SP had on the compressive strength can be seen in Figure 3.18. It can be seen directly that the compressive strength was significantly higher when using Glenium 51 over SIKA 20 HE using the same SP contents. Because the flowability was similar for both types, Glenium was preferred over SIKA for this mixture. Only looking at the compressive results for the Glenium mixtures, a slight increase in strength could be seen with an increase in SP content. Besides the flowability and compressive strength, a third attribute now became interesting: bleeding. Increasing the SP content, a limit was met after which a further increase in the SP content leads to bleeding of the concrete mixture. For mixtures with a Glenium content of 0.9% (dry SP/binder) or higher, slight bleeding was visually observed. These mixtures were not considered interesting for the material development. With the increase of SP, the time required for samples to harden increased, but this was not considered a reason to eliminate these mixtures. Because of the increased flowability and compressive strength with higher SP, the mixture with the highest SP content before the bleeding limit was chosen for further development, which is Mixture M7-G4.

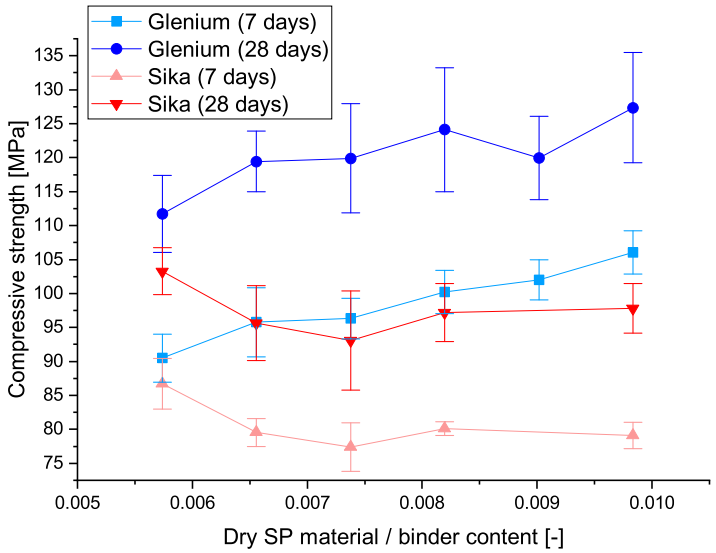

Figure 3.18: Effect of type and amount of SP on the compressive strength at 7 and 28 days

3.2.6. Fibre Type and Quantity

UHMWPE versus Steel Fibres

The different effect steel and (UHMW)PE fibres had on the material's properties were examined using multiple mixtures as presented in Table 3.10. Between M0 and M1, the only difference was the fibre type, steel and PE, which were used in the same volume content for different fibre types. The change to PE fibres directly lead to a decrease in compressive strength and a huge loss in flowability. The drastic decrease in flowability can be explained by the large increase in surface area of the fibres. The lower compressive strength was in agreement with what was discussed in Section 2.2.6, stating the use of PE fibres instead of steel fibres can lead to a reduction in compressive strength.

Because of the poor flowability of M1, this mixture was not used to cast dogbone specimens. After altering the ratios of different sand fractions and lowering the fibre content slightly for an improvement in workability, Mixture M3 was used to cast specimens for direct tensile testing. These results were compared to the tensile results of M0 using steel fibres in Figure 3.19. In this figure, the result of a specimen of the final mixture (M8-F1.4) is also included. This mixture showed strength properties similar to those of M0, but had a significantly larger strain capacity, exhibiting the additional value the use of UHMWPE fibres can offer after the adaptation of the mix design.

Table 3.10: Mixture designs using steel and UHMWPE fibres [kg/m^3] and the corresponding properties

	M0	M1	M3	M8-F1.4
Cement I 52.5 N	-	-	-	1119.1
Cement I 52.5 R	800.4	800.4	800.4	-
Cement I 42.5	69.6	69.6	69.6	-
Sibelco M4	-	-	-	193.0
Blast furnace slag	104.4	104.4	104.4	134.3
Silica fume	43.8	43.8	43.8	111.9
Water	204.6	204.6	204.6	225.0
Superplasticizer	26.6	26.6	26.6	32.0
Sand 0.125-0.25	213.3	213.3	707.4	173.6
Sand 0.25-0.5	318.7	318.7	353.7	322.3
Sand 0.5-1.0	529.1	529.1	-	-
Steel fibres	125	-	-	-
UHMWPE fibres	-	15.6	13.7	13.7
Fibre content [V%]	1.6	1.6	1.4	1.4
Flow diameter [mm]	22.5	12.3	13.5	19.4
28-day compr. strength [MPa]	124.5	116.3	116.6	122.3
STDV compr. strength [MPa]	5.2	4.8	0.7	8.4

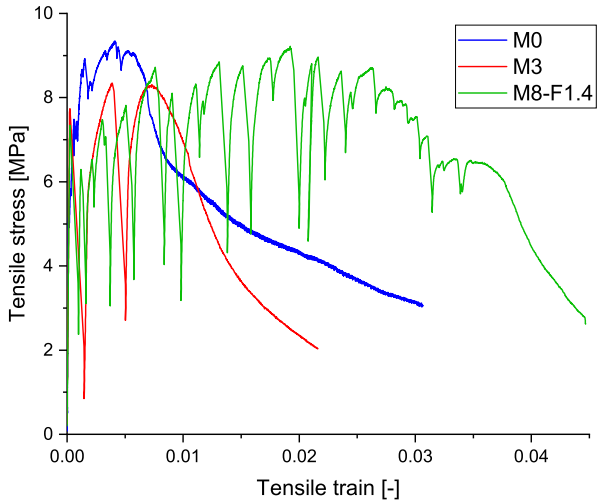

Figure 3.19: Direct tensile results of mixtures including steel or UHMWPE fibres

The Effect of the Amount of UHMWPE Fibres on Compressive Strength and Workability
As discussed in Section 2.2.6, an increasing amount of PE fibres is expected to have a negative effect on the compressive strength of a concrete mixture, in contrast to steel fibres which have a positive effect. The influence of the amount of UHMWPE fibres on the compressive strength was measured twice. Once using an intermediate mixture in the general process of development, where the amount of fibres was lowered and a second time in the last stage of the material development where the tensile behaviour with different fibre contents was tested, in this case with an increase in the amount of fibres compared to the base mixture.

The mixture used for the first investigation of the effect of fibre content on the compressive strength can be seen in Table 3.11. The initial fibre content of 1.4% was lowered to 1.2% and 1.0% to increase the workability and test the accompanied compressive strength. The measured values for flowability and compressive strength are listed in the same table, showing an increase in flowability and a small increase in the average compressive strength at 28 days with the decrease of the fibre content. The

strength increase can be considered insignificant looking at the standard deviations. The outcomes of these tests agreed with the expected behaviour for PE fibre reinforced concretes as discussed in Section 2.2.6.

Table 3.11: Mixtures used for the determination of the effect of fibre content on workability and compressive strength [kg/m^3]

	M6-F1.4	M6-F1.2	M6-F1.0
CEM I 52,5 N	955.6	957.6	959.5
Sibelco M4	219.7	220.1	220.6
Blast furnace slag	114.7	114.9	115.1
Silica fume	114.7	114.9	115.1
Tap water	197.4	197.8	198.2
Glenium 51	19.1	19.2	19.2
Sand 0.125-0.25	716.7	718.2	719.6
fibres	13.7	11.7	9.8
Fibre content [V%]	1.4	1.2	1
Flow diameter [mm]	142.5	160.0	172.5
Compressive strength [MPa]	117.7	119.7	121.3
STDV [MPa]	8.3	9.6	1.3

For the final step in the material development, four mixtures with increasing fibre content were tested for compressive strength, flow and tensile behaviour. All relative ratios other than the fibre content were kept constant. The mixtures used for this are shown in Table 3.12, accompanied by the mean flow diameter and 28 day compressive strength. It can be seen that the flowability clearly decreased with an increase in fibre content, while for the compressive strength a clear relation lacked. The compressive strength was lower for all samples with larger fibre contents than 1.4%, but after a large drop it increased with increasing fibre content. Considering the standard deviations, this increase was not very significant, while the drop in strength associated with the fibre content changing from 1.4% to 1.6% was significant. A possible explanation for inconsistent or unpredictable behaviour can be the extent to which the fibres in the mixture are properly dispersed. If fibres agglomerate in a mixture, these imperfections influence the mechanical properties of the mixture. As the flow diameter is lower for the mixtures with higher fibre contents, the chances of agglomerations occurring increases, leading to lower and inconsistent mechanical properties. Small deviations in mixing procedure or compound properties can thus significantly influence the properties of the material.

Table 3.12: Mixtures used for determination of the effect of fibre quantity [kg/m^3] followed by flow table and compression test results

	M8-F1.4	M8-F1.6	M8-F1.8	M8-F2.0
CEM I 52,5 N	1119.1	1116.8	1114.5	1112.2
Sibelco M4	193.0	192.6	192.2	191.8
Blast furnace slag	134.3	134.0	133.7	133.5
Silica fume	111.9	111.7	111.4	111.2
Tap water	225.0	224.5	224.0	223.6
Glenium 51	32.0	31.9	31.8	31.8
0.125-0.25	173.6	173.2	172.8	172.5
0.25-0.5	322.3	321.7	321.0	320.3
fibres	13.7	15.6	17.6	19.5
Fibre content	1.4	1.6	1.8	2.0
Flow diameter	195.0	178.5	168.5	160.0
Compressive strength [MPa]	122.3	105.5	107.8	113.0
STDV [MPa]	8.4	5.2	3.8	6.0

The Effect of the Amount of UHMWPE Fibres on Tensile Behaviour

Using the mixtures presented in Table 3.12, dogbone samples were cast for direct tensile testing. Due to COVID-19-related circumstances, these tests were executed at 32-36 days of age rather than 28 days. The loads and displacements resulting from the tests were converted to stresses and strains. The results are shown in Figure 3.20. The numbers 1-4 indicate the individual samples tested. Looking closely, it can be noted that some lines had a very abrupt ending even before going into strain softening. This was because of cracks forming outside of or on the edge of the measuring range, leading to unrealistic strain measurements. Therefore, some measurements were cut off early, but from the first part of the measurement some interesting data could still be extracted. Therefore these measurements were still displayed. From these figures, the tensile behaviour for the material can be seen. Every drop in stress indicated the occurrence of a crack in the sample. For most samples, strain hardening could clearly be observed as drops in stress were followed by peaks exceeding the stress values for previous peaks. For every measurement, the stresses and strains at characteristic points were compared and averaged, including the cracking stress, maximum tensile strength and strain at final peak. Table 3.13 shows an overview of these characteristic values. Based on these values, the mixtures using 1.4% and 1.8% fibre showed the best results regarding peak stress and accompanying strain. The cracking strength was highest for the lower fibre contents but came with a significantly higher standard deviation compared to the mixtures using higher fibre contents.

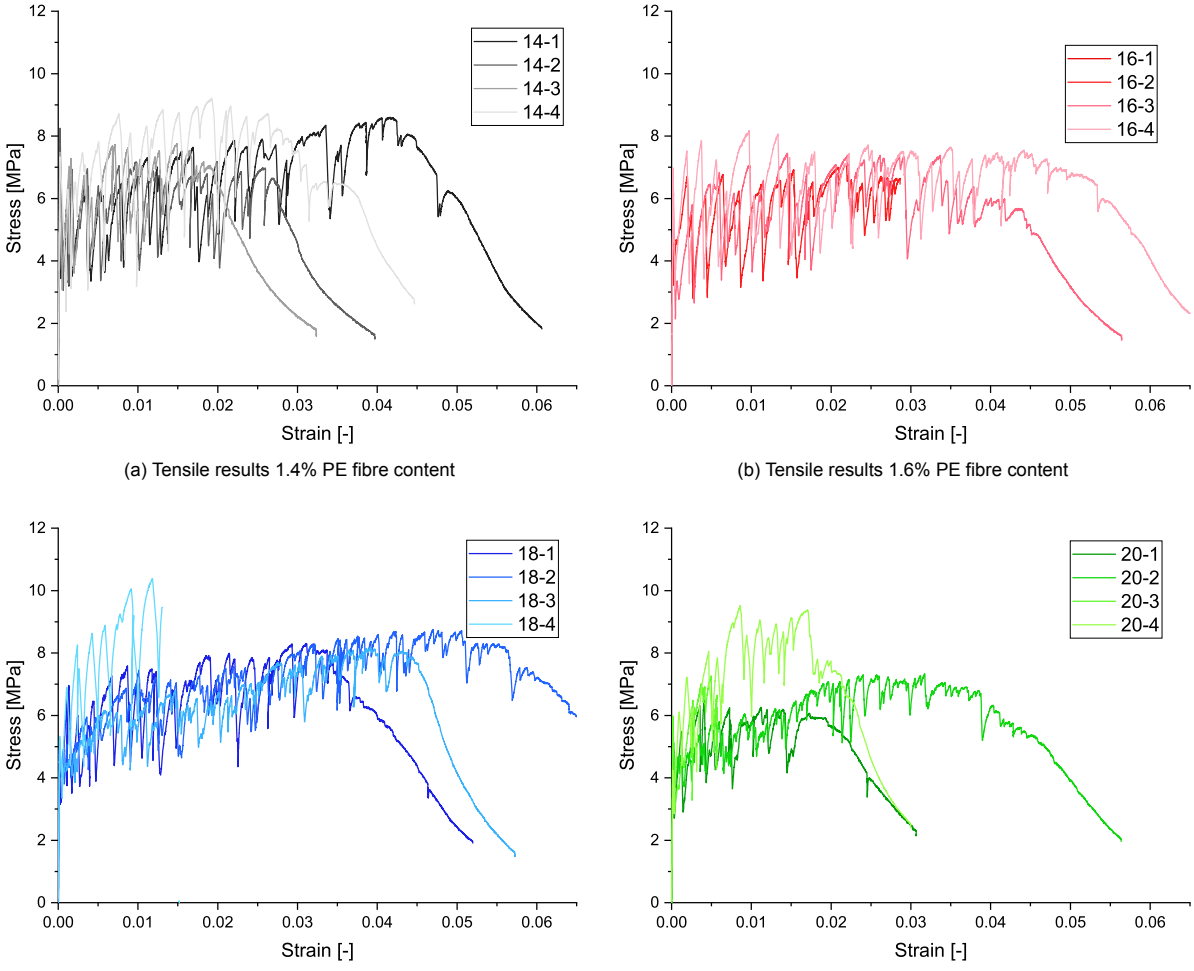

(a) Tensile results 1.4% PE fibre content

(b) Tensile results 1.6% PE fibre content

(c) Tensile results 1.8% PE fibre content

(d) Tensile results 2.0% PE fibre content

Figure 3.20: Tensile stress-strain results of direct tensile testing using different fibre contents

Table 3.13: Characteristic values of tensile testing results

Fibre content [V%]	Cracking strength [MPa]	STDV [Mpa]	Peak strength [MPa]	STDV [Mpa]	Strain at peak strength [-]	Strain at last peak [-]
1.4	6.17	2.00	8.46	0.61	0.0252	0.0325
1.6	6.02	1.27	7.58	0.54	0.0154	0.0489
1.8	4.85	0.60	8.90	1.02	0.0323	0.0471
2.0	4.98	0.64	7.65	1.31	0.0148	0.0269

Figure 3.21 shows the cracking patterns for mixtures using different fibre contents. All samples except for the 1.6%-sample showed evenly distributed cracking. For higher fibre contents, the number of cracks increased and the cracks in the sample appeared smaller compared to lower fibre contents. This could be explained by the increased area of fibre transferring load through the crack. This is in agreement with Section 2.2.6.

(a) 1.4% (b) 1.6% (c) 1.8% (d) 2.0%

Figure 3.21: Final cracking patterns after direct tensile loading, using different fibre contents

Final Mixture Determination
Taking into account the compressive strength and flow diameter as mentioned in Table 3.12, the final mix design was determined. Considering the tensile properties, the mixtures using 1.4% and 1.8% fibres were most appealing. Since good flowability was very important for structural application, a lower fibre content was preferable. The significantly better flowability of the mixture using 1.4% fibres outweighed the slightly reduced strain capacity compared to the mixture using 1.8% fibre. This 1.4% mixture also had a higher compressive strength, reinforcing the decision to select this fibre content for the final mixture.

3.3. Material Properties Final Mixture

After the determination of the final mixture design, extra samples were cast to determine the properties of the material more accurately. Together with previous results from the exact same mixture, the properties can be determined using a larger number of samples, leading to smaller standard deviations.

3.3.1. Compressive Strength

The strength development over time of the final mixture can be seen in Figure 3.22. A 28 day compressive strength just below 120 MPa was reached. With this the goal strength of 120 MPa was nearly reached.

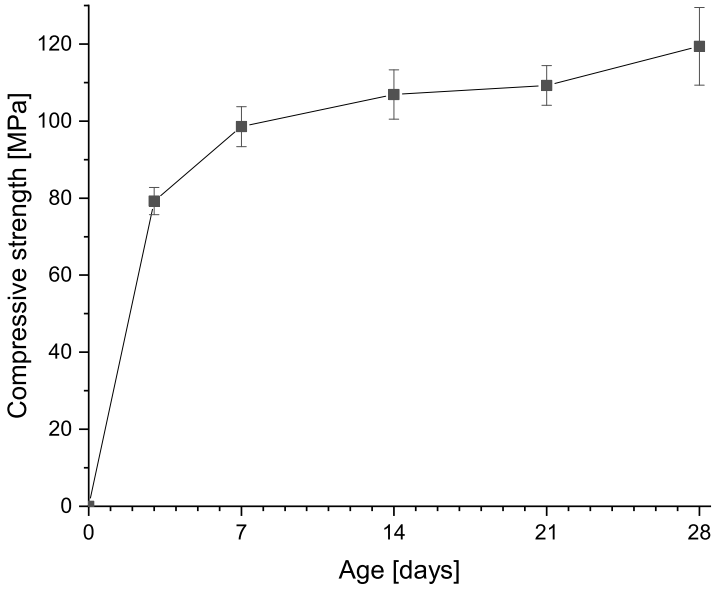

Figure 3.22: Compressive strength development over time

After testing for the modulus of elasticity at 28 days, the 100×100×400 mm^3 specimens were cut into three 100 mm cubes. These were also tested for compression. Many models and experiments have concluded that with the increase of specimen size, the compressive strength decreases and for high strength concretes these differences in strength should be more evident compared to normal strength concrete [119]. Due to the increased homogeneity of the material, an increased specimen size will lead to a decreased variation in compressive strength [120, 121, 122]. With fibre reinforced concrete types, another factor influencing the concrete strength arises: the wall-effect. Due to the frictional restraint of the walls of a mould, the fibres align near the walls when casting, leading to a non-homogeneous fibre orientation [123, 124]. With very small specimen sizes, this wall-effect is of greater influence, as a larger part of the specimen is within a short distance from one of the specimen surfaces. Table 3.14 shows the averaged result of compression strength testing for the 40 mm cubes and 100 mm cubes. The strength of the 100 mm cubes was higher than that of the 40 mm cubes. This indicated that the wall-effect has a stronger influence than the size effect in this case. The influence of the scale effect can however be seen in the standard deviation of the compressive strength. This was lower for the larger specimens, even with a lower number of specimens. This confirmed that the standard deviation reduces with an increasing specimen size.

Table 3.14: Compressive strength of the final mixture using different sample sizes

Cube sample size [mm]	Number of specimens	28 day strength [MPa]	Standard deviation [MPa]
40	15	119.41	10.09
100	6	130.67	5.65

3.3.2. Tensile Response

For the final mixture, eight dogbone specimens were cast for direct tensile testing. Similar to the tensile results in Section 3.2.6, some outcomes were not as reliable due to cracking outside of or at the edge of the measuring length. Four proper results were selected and shown in Figure 3.23. Remarkable were the large drops in stress corresponding to cracks emerging. Compared to SHCC tensile behaviour from literature [40, 125, 126], these drops appeared significantly larger for SH-UHPFRC. This can also be seen in the results for the SH-UHPFRC mixture by He et al. [80], which was used as a reference throughout the mixture development. Also, the large variation in the tensile results stood out. Including the results from M8-F1.4, which equaled the final mixture, a large range of peak strains and stresses could be observed. This

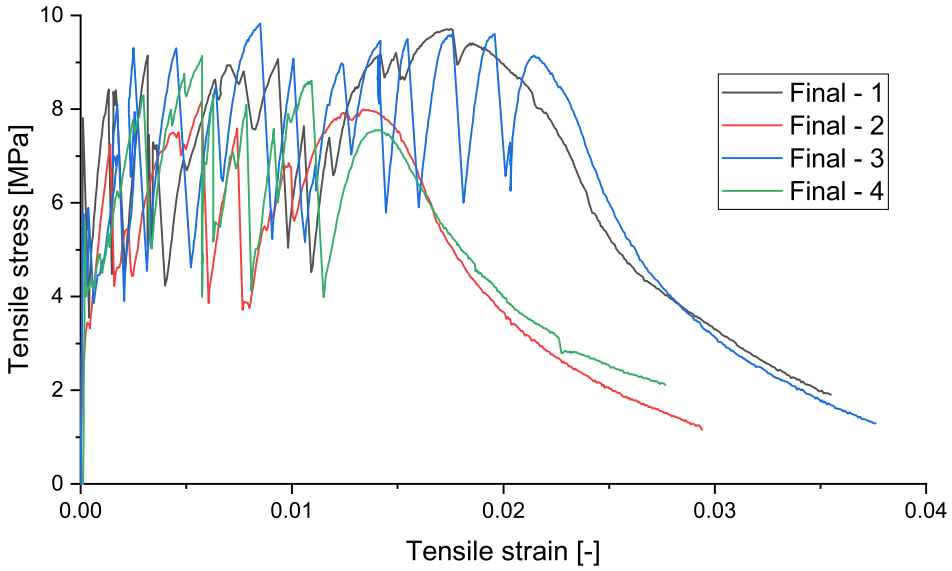

Figure 3.23: Tensile response of samples using the final mixture

Together with results from M8-F1.4 and partly using the aforementioned results where strain measurements were flawed, the average strength values for the mixture were determined. Their characteristic values are summarised in Table 3.15. These values could be used to generally describe the average tensile behaviour. This table shows how the goal tensile strength (7 MPa) and strain capacity (1.5%) were reached with the developed mixture.

Table 3.15: Characteristic values tensile bahviour final mixture

	Strength [MPa]	STDV [MPa]	Strain [%]
First crack	5.91	1.77	0.02
Peak strength	8.92	0.77	1.61
Final peak	7.56	1.20	2.46

DIC

Figure 3.24 shows the DIC results for four specimens. For every specimen DIC images are shown around five set levels of strain: 0.001, 0.005, 0.010, 0.015 and 0.020. The DIC images show the development of cracks with increasing tensile strain. From these images a multiple cracking pattern can be seen. Part of the cracks consisted of multiple cracks, being close enough to each other to appear as one crack at first glance. The number of visible cracks is lower compared to that seen in Figure 3.21a from Section 3.2.6, despite this sample being cast with an identical mixture. The crack spacing was not always constant over the length of the dogbone for all specimens. A possible explanation for this could be imperfections in the sample, such as inhomogeneous fibre dispersion or entrapped air bubbles. After reaching the last peak one of the cracks opened up, leading to a decrease in measured stress and a visible increase in crack width.

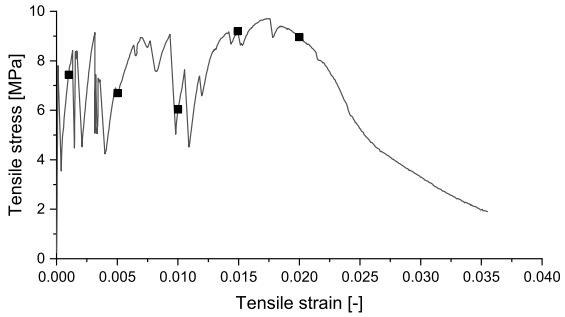

(a) Stress-strain curve final sample 1

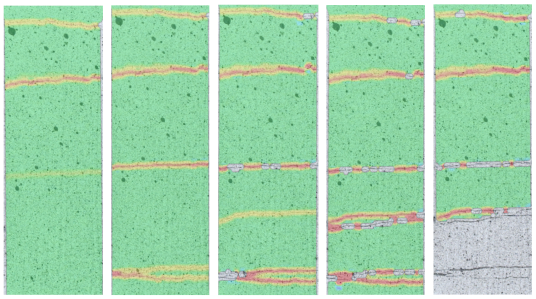

(b) DIC images final sample 1

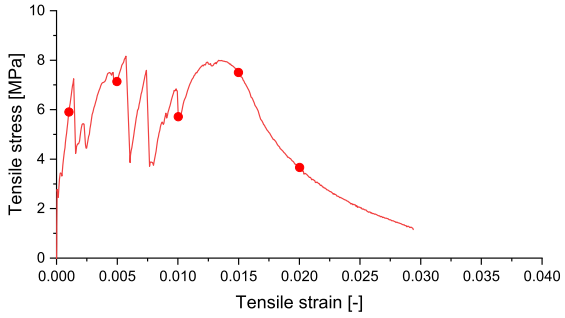

(c) Stress-strain curve final sample 2

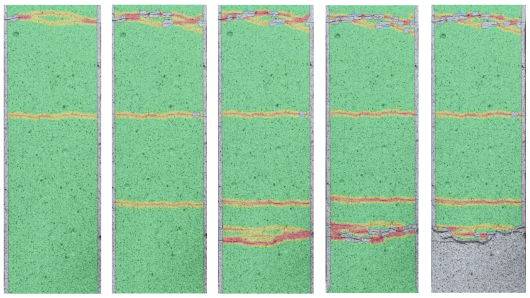

(d) DIC images final sample 2

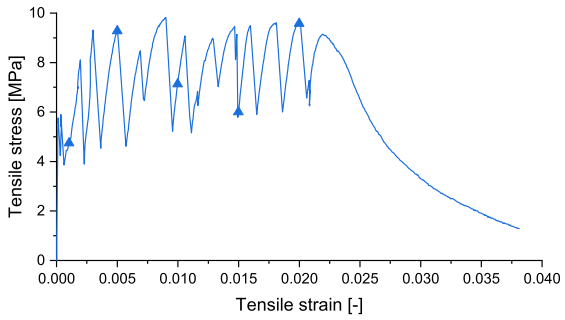

(e) Stress-strain curve final sample 3

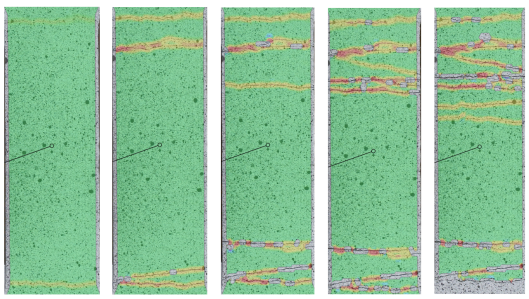

(f) DIC images final sample 3

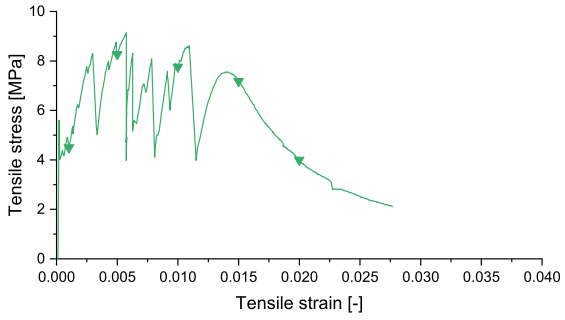

(g) Stress-strain curve final sample 4

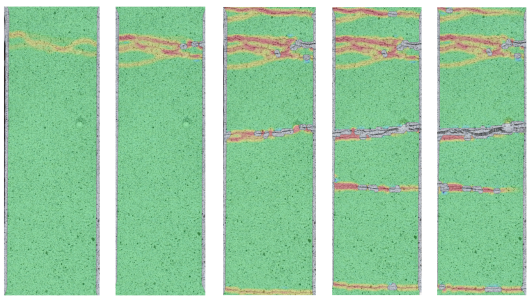

(h) DIC images final sample 4

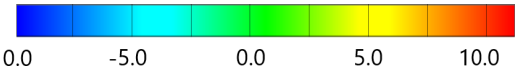

(i) Legend DIC images, strain in vertical direction [%]

Figure 3.24: Stress-strain curves of samples using the final mixtures, accompanied by DIC images corresponding to the load situations as indicated by the symbols in the stress-strain curves.

3.3.3. Flowability

With every casting for mechanical properties, the flowability of the mixture was tested. With an average diameter of 193.1 mm, the flow diameter of the final mixture was lower than that of the original mixture using steel fibres (225 mm). The individual flow measurements are shown in Table 3.16. The mixture was not self compacting and thus required vibration to fill moulds. For the planned application, this is not necessarily an issue as this concerns prefabricated elements rather than in-situ cast elements.

Table 3.16: Flow diameter of the final mixture for multiple tests, all values in mm

D1	D2	AVG
190	195	192.5
190	200	195.0
192	190	191.0
190	197	193.5
192	195	193.5
	Average	193.1
	STDV	1.7

3.3.4. E-modulus

The development of the E-modulus over time is shown in Figure 3.25. In Table 3.17 the E-modulus at 28 days of the final mixture is compared to that of the original mixture. Looking at discussed values in Section 2.3, this was a relatively low E-modulus for an UHPC mixture.

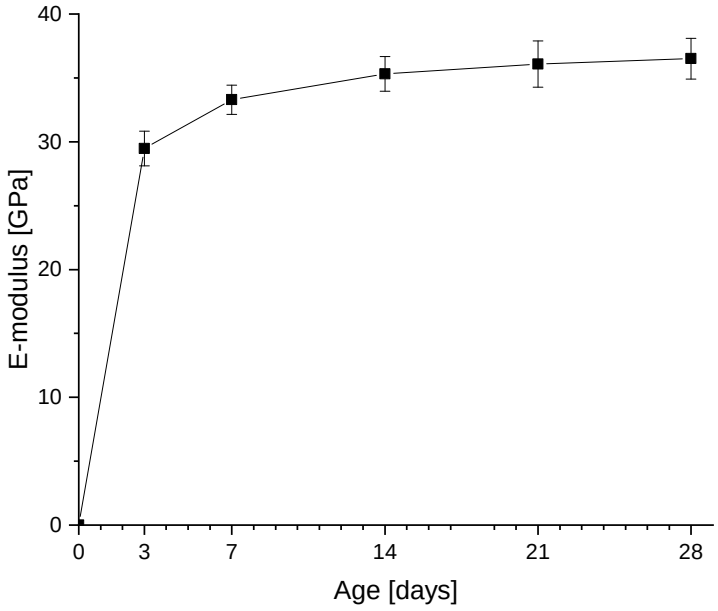

Figure 3.25: E-modulus development over time

Table 3.17: Emod

	E-modulus [GPa]	Standard deviation [GPa]
Original mixture UHPC [115]	45.4	1.0
Final mixture	36.5	1.6

3.3.5. Shrinkage

Both the total and autogenous shrinkage were measured for the final mixture. The drying shrinkage could be determined by subtracting the autogenous shrinkage from the total shrinkage. Figure 3.26a shows the weight loss of the samples used for shrinkage determination. From this plot, it can be clearly seen that the wrapped specimens barely lost any weight. Because no moisture could evaporate, no drying shrinkage occurred. The unwrapped specimens showed a large decrease in weight over the first days, indicating a large amount of water evaporating. This slowly stabilized after around 7 days, similar to the strength development of the material. After a few weeks the weight of the samples increased slightly. Figure 3.26b shows how the change in length of the specimens changed over time. After a quick decrease in length in the first days, the trend became more flat. Despite the curve flattening over time, the length change did not stabilise before 90 days of age. Compared to the total shrinkage of a NC mixture (400-600 microstrains), an average total shrinkage just below 700 microstrains is considerably large. The difference between the average of the curves representing the total shrinkage and the autogenous shrinkage represents the drying shrinkage. Using an average value the drying shrinkage was determined to be 12.5% of the total shrinkage at 90 days. This confirms the expectation that the drying shrinkage should be limited, as stated in Section 2.3.4. Considering application, this large amount of autogenous shrinkage could cause early-age cracking and must therefore be examined further.

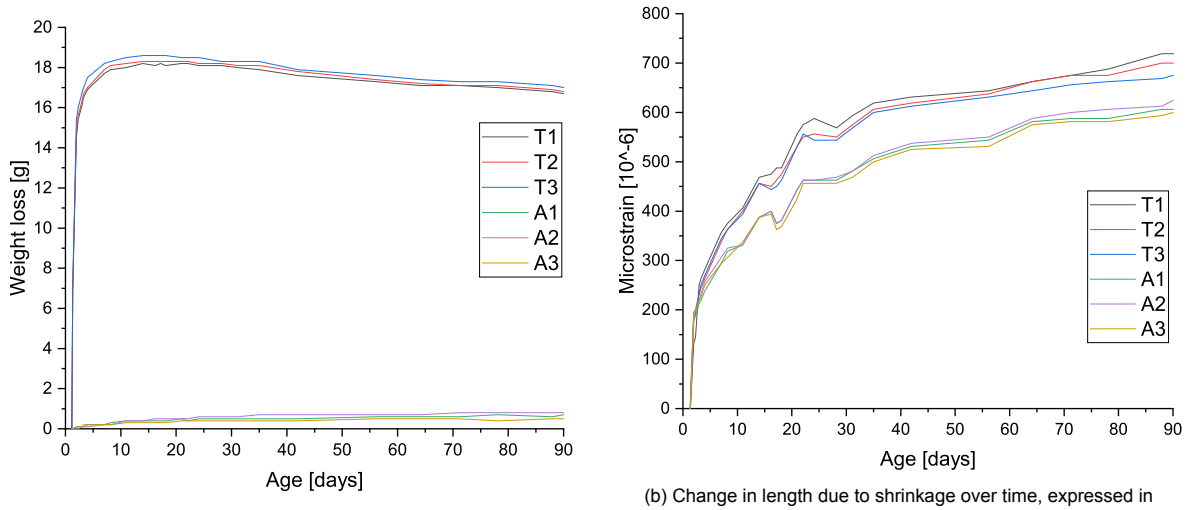

(a) Weight loss due to shrinkage over time

(b) Change in length due to shrinkage over time, expressed in microstrain

Figure 3.26: Total (T) and autogenous (A) shrinkage

The samples used for shrinkage measurements were cured in a climate room at 20 °C and 50% RH. This was different from the other samples. To determine the influence of this different curing regime, six 40 mm cubes cured in these conditions were tested for compressive strength. The difference in compressive strength of these samples and those cured in a moisture room is shown in table 3.18. The moisture cured samples had a higher average compressive strength. This noticeable effect curing conditions have on the developed material, must be taken into account for applications.

Table 3.18: The effect of curing regime on the compressive strength of the final mixture

Curing	Compressive strength [MPa]	Standard deviation [MPa]
20°C, 50% RH	102.06	6.86
22°C, 99% RH	119.41	10.09

3.3.6. Setting Time

Using the measurements from the vicat device, the initial and final setting time of the mixture were determined. Figure 3.27 shows the measurements of the needle penetration depth over time. The time at which the penetration depth reaches 36.5 mm and 2.5 mm were recorded as the initial and final setting time respectively. Table 3.19 shows these setting times and the average initial and final setting time.

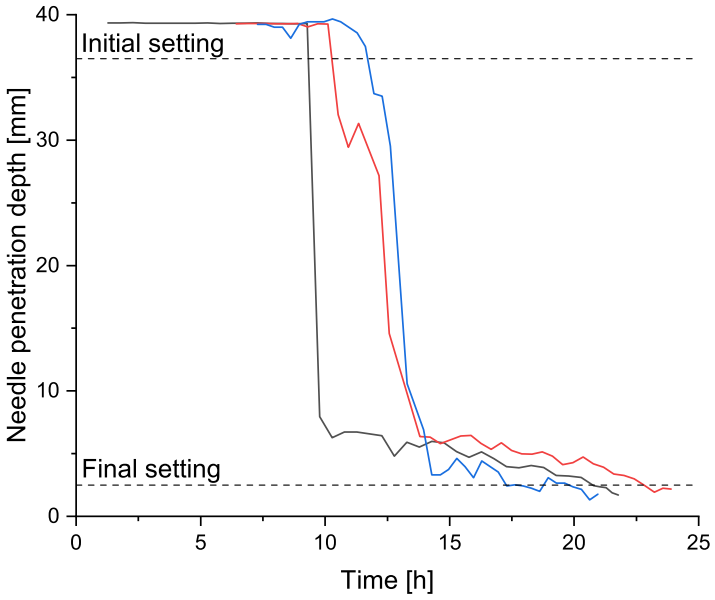

Figure 3.27: Vicat measurements for final mixture, showing the needle penetration depth over time

Table 3.19: Measured initial and final setting time [h]

	Initial	Final
Measurement 1	9.78	20.78
Measurement 2	10.27	22.82
Measurement 3	11.62	20.29
AVG	10.56	21.29
STDV	0.95	1.34

3.4. Discussion

A large number of several tests was executed for the material development of SH-UHPFRC. For each test only a limited amount of specimens was used, leading to relatively high standard deviation. The execution of the mixing procedure could have had an influence on the properties of the mixtures. Especially for the mixtures with limited workability, small deviations in procedure could have affected the material properties. The same procedure for mixing, casting and curing was applied for all specimens. The effect of changing anything in this procedure has not been investigated.

Compared to steel fibres, using PE fibres lead to a drastic decrease in workability because of the significantly higher surface area. Especially in a mixture with a low w/b-ratio like (SH-)UHPFRC, the surface area of material components could play a significant role. Because of this more adaptions to the mixture were required to improve the workability without sacrificing the mechanical properties of the material. To improve the workability, the use of a large amount of SP was necessary. This affected the setting time of the concrete. This makes the developed material less suitable for repair applications that would require a rapid strength development. For strengthening applications, an increased setting time is acceptable as this often concerns prefab elements.

The use of higher amounts of fibres lead to a negligible difference in compressive strength, while significantly reducing the workability of the mixture. The cracking pattern showed a large amount of narrow cracks, showing an increase in fibre content enhances the multiple cracking behaviour of SH-UHPFRC. In the stress-strain curves of the direct tensile tests differences between mixtures with different fibre contents were limited. Direct tensile testing was done twice for the same mixture. The studying of the cracking patterns lead to different observations for both measurements. For the first batch of tested specimen (M8-F1.4), the pictures taken showed many small cracks over the specimen. The second batch (final mixture testing), was analysed using DIC. These results showed fewer cracks over the full length of the measuring area compared to the earlier samples. The mixtures used were identical, the

age at which the samples were tested was not. The difference in age could be a reason for the different cracking behaviour. Further research could be executed on the effect of age on the tensile behaviour of SH-UHPFRC.

The SH-UHPRFC mixture was developed for strengthening applications of RC elements. To fulfill this purpose, an additional optimization study should be done. Using a wider range of varying parameters, the material's properties could be further improved. Aim for an optimization study could be to achieve a higher flowability and ability for self compaction. The developed material showed large drops in stress with every crack occurring in the direct tensile test. This could be a result of improper proportions of fibre strength, concrete strength and bond between fibre and matrix. A study on the optimization of the interaction between fibre and matrix for this material could give insights in how to optimize the use of the UHMWPE fibres. Some properties of SH-UHPFRC have not been studied in this research, as this was not within the scope, but can be important for strengthening applications. This includes the effect of larger scale, environmental influences, dynamic loading and long term testing.

4

Numerical Study of a Shear-Deficient RC Beam Strengthened with SH-UHPFRC

To determine the effects the developed material can have when applied as a strengthening material, numerical models were made using ATENA software. In these FEM (Finite Element Method) models, the shear capacity of a normal reinforced concrete beam was compared to a hybrid beam that had been strengthened with a layer of SH-UHPFRC on each side. The expectation was that this would largely increase the shear capacity of the element as discussed in Section 2.4.2. To determine solely the effect of increased strain capacity of the strengthening material, additional material models were used and the results were compared. The material characteristics as found in the material research in Chapter 3 were used as input values for the modelling of the SH-UHPFRC.

4.1. Model Dimensions and Simulation Strategy

In the PhD study this thesis contributes to, a series of experiments was conducted using shear-deficient beams strengthened with UHPFRC laminates. These were tested using a three point bending test. In this thesis, a numerical model was used to determine the shear capacity using SH-UHPFRC laminates. The beam dimensions are shown in Figures 4.1 and 4.2. To ensure no singularities occurred in the model at the loading point and supports, steel plates were used to distribute the forces over the beam more equally. No shear reinforcement was used in the reference beam to ensure the beam would fail in shear.

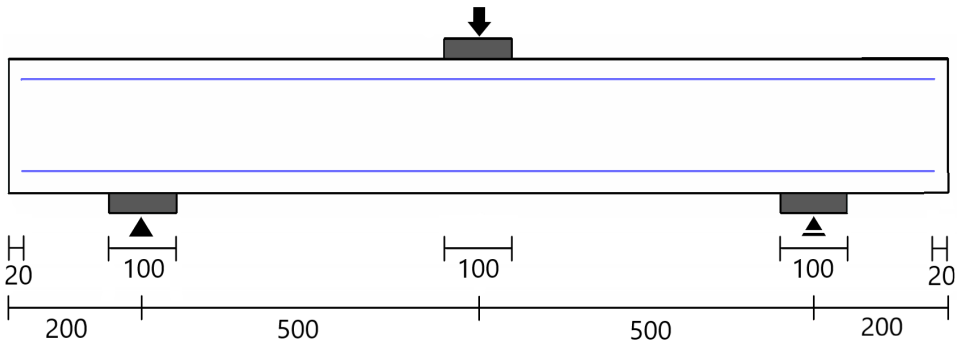

Figure 4.1: Longitudinal dimensions for the modelled beam. Dimensions in mm

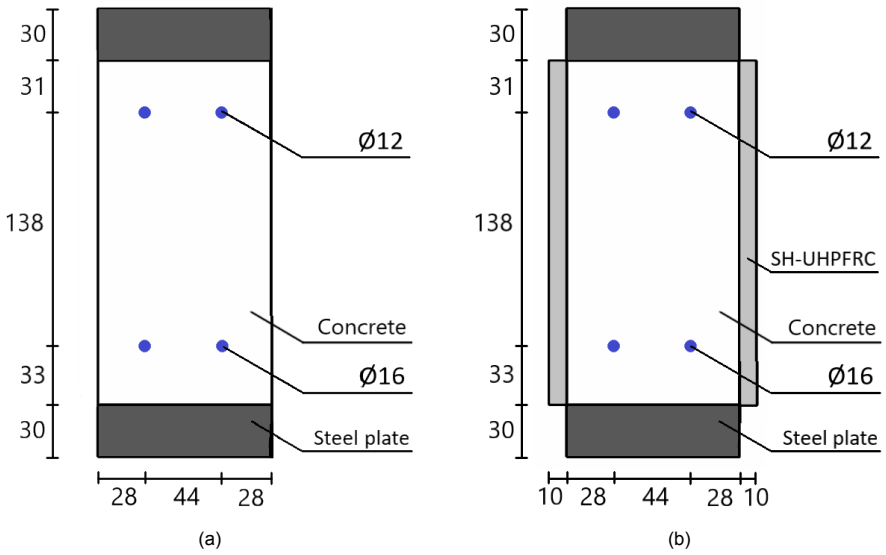

Figure 4.2: Transverse dimensions for reference beam (a) and strengthened beam (b). Dimensions in mm

Four distinct materials were used in the numerical simulation: steel, reinforcement, concrete and a strengthening material (SH-UHPFRC). The steel for the support plates was modelled using a linear elastic isotropic material with an E-modulus of 210 GPa. For the reinforcement, a bilinear stress-strain relation was used. In Table 4.1 the material properties used as input are summed up, Figure 4.3 shows the bilinear stress-strain relation visually. For both the reinforcement bars and the steel plates, a perfect connection to the concrete was assumed. The bond between NC and SH-UHPFRC is assumed to be perfect, indicating the effect of delamination is not included in this research (see Section 2.4.3).

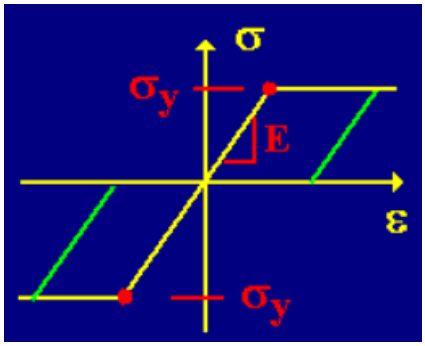

Figure 4.3: Modelled stress-strain relationship for steel reinforcement

Table 4.1: Material input properties of steel reinforcement

	Value	Unit
E-modulus E	200	GPa
Yield strength σ_y	550	MPa
Bar diameter	12/16	mm

For the concrete beam, a non-linear fracture plastic model was used. This model assumed non-linear behaviour before the maximum compressive strength was reached, including a hardening regime in this part of the stress-strain relation. The fracture-plastic constitutive model combined the models for tensile and compressive behaviour, combining plastic and fracturing behaviour. Besides the possibility to alter the compressive and tensile model separately, this material model also included the ability to handle physical phenomenon of crack closure [105]. This model was based on smeared cracking rather than discrete cracking, meaning cracks were smeared over continuum elements instead of cracks appearing as discontinuities *between* elements, which requires more prior knowledge of the cracking behaviour [106]. The constitutive model for the NC is shown in Figure 4.4, the material parameters are summarized in Table 4.2. The maximum aggregate size was also included, as aggregate interlock in shear was considered in the material model.

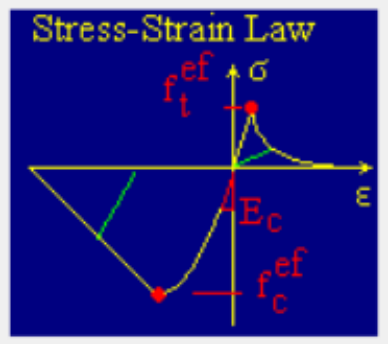

Figure 4.4: Modelled stress-strain relation NC

Table 4.2: Material input NC

	Value	Unit
E-modulus E	28.9	GPa
Compressive strength f_c	24.8	MPa
Tensile strength f_t	2.24	MPa
Maximum aggregate size	0.016	m

The strengthening material was modelled similar to the NC except it allowed for a user-defined tensile behaviour amongst other additional options. This enabled the inclusion of strain hardening and softening, which were necessary to define the strengthening material. Figure 4.5 shows the stress-strain relation used for the strengthening material in tension, in compression this was similar to that in Figure 4.4. The input for these relations is listed in Table 4.3. The tensile function was varied for different strengthening materials as is described in Sections 4.3 and 4.4. The localized plastic and fracture strain had to be included for these user defined material inputs. The localized fracture strain depended on the tensile function used in the material input, the localized plastic strain was equal for all strengthening materials as an identical compressive behaviour was assumed.

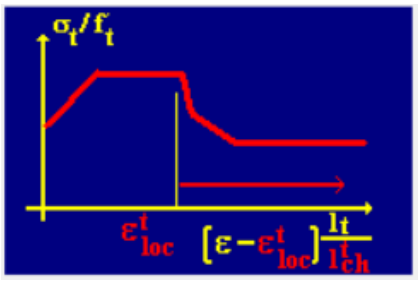

Figure 4.5: Input tensile stress-strain relation strengthening material

Table 4.3: Material input strengthening material

	Value	Unit
E-modulus E	36.15	GPa
Compressive strength f_c	101.5	MPa
Localized plastic strain $\epsilon_{pl,loc}$	-2.78 E-3	-
Tensile strength f_t	5.91	MPa
Localized fracture strain $\epsilon_{f,loc}$	varying	-

The mesh size was determined following three criteria, as proposed by Arif [106]: Non-Linear Finite Element Analysis (NLFEA) guidelines [127], a criterion based on beam height [128] and the thickness of the thinnest element in the model. The NLFEA guidelines [127] state that the maximum mesh size equals the minimum of three values based on the length (l), height (h) and width (b) of a concrete beam element. A research on the modeling of shear behaviour found an improvement in results after a further reduction of the maximum allowable mesh size based on the beam height [128]. The last criterion used for the determination of the mesh size concerns the dimensions of the modelled construction. The smallest element dimension is considered as a maximum mesh size. For the beam in this research, the thickness of the strengthening laminates was the smallest dimension. An overview of all criteria can be seen in Table 4.4. Finally, a mesh size of 10 mm was chosen for the numerical analysis. This was used for the entire model, ensuring compatibility between the individual elements. The Newton-Raphson method was used as a solution method. This method approximates a function by straight lines following the slope of the function at a reference point. By selecting the options to update the stiffness of the curve with every iteration, the Modified Newton-Raphson was chosen.

Table 4.4: Compressive strength of the final mixture using different sample sizes

	NLFEA guidelines[127]			Putter [128]	Smallest dimension
Criterion	$\frac{l}{50}$	$\frac{h}{6}$	$\frac{b}{6}$	$\frac{h}{20}$	min $\{h, b, l\}$
Maximum mesh size [mm]	20.0	16.7	33.3	10.0	10.0

4.2. Validation of Reference Beam

To validate the FEM model, a comparison between a physical experiment and a numerical result was made. The load-deflection curves of the experimental and numerical (FEM) outcome are shown in Figure 4.6. This shows that the first peak strength for the simulation (64.0 kN) was higher compared to that of the experiment (54.9 kN). The deflection at which this load drop occurred was equal for the model and the physical experiment. The peak strength in the simulation was very close to the second and highest peak of the experimental outcome (59.8 kN). The post-peak behaviour of the modelled beam showed a lower deflection capacity compared to that of the physical beam. The experiment also lead to an increase in strength after the first peak, where in the FEM model the load does not reach this initial peak load a second time. The initial slope of the curve representing the FEM was steeper, implying a larger bending resistance. Possible explanations for these deviations are material imperfections, environmental influences during curing or shrinkage. These physical effects can influence an experiment but are not included in FEM modelling.

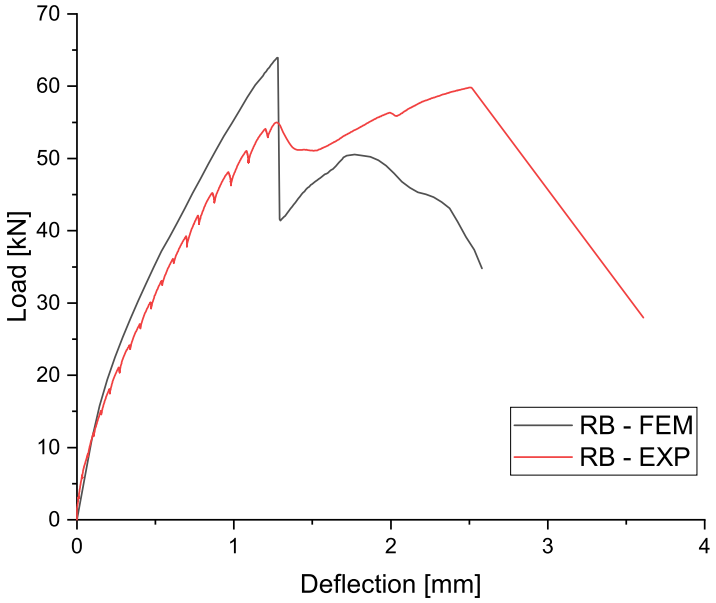

Figure 4.6: Load-deflection curves of the experimental and numerical RB for three point bending test

The cracking pattern of the experimental result was recorded using DIC and these images were used to measure the strain of the RC beam. The results of this are shown in Figure 4.7a. Figure 4.7b shows the principal strain (iso-areas) and cracks (lines) in the result of the numerical analysis. A similar cracking pattern was observed showing flexural cracks at the bottom of the beam and more severe cracks between the supports and the point of load application, indicating shear failure. The pattern in the numerical outcome was nearly symmetrical, opposed to the experimental outcome where the main shear failure was visible on one side of the beam. This was to be predicted, as in a physical experiment small imperfections in material, element symmetry or experimental set up influence the test outcome, which is not the case in a perfectly symmetrical numerical model.

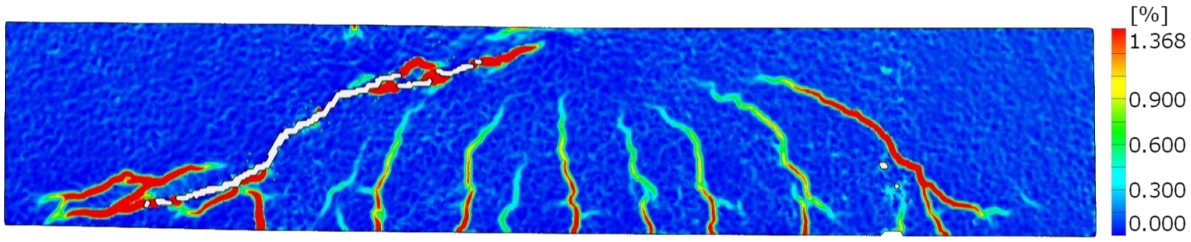

(a) DIC results of three point bending experiment showing strain [%] after shear failure

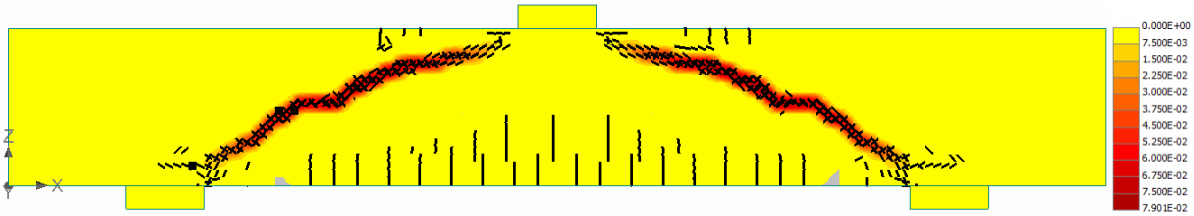

(b) ATENA model results showing principal strain[-] and indicating cracks using black lines, minimum visible crack width 0.01 mm

Figure 4.7: Comparison of the cracking pattern between experimental result (a) and numerical result (b)

4.3. Shear Strengthening using SH-UHPFRC

4.3.1. Material Input SH-UHPFRC

The material developed in Chapter 3 was meant to be used as a strengthening material for shear-deficient beams. This material was simulated in ATENA using a simplified tensile function consisting of four linear segments, as can be seen in Figure 4.8. This function was based on the experimental outcomes as were found during the material development using direct tensile tests (Section 3.23). After reaching the cracking strength, the strength is increased further with increasing strain until the peak strength. Since in experimental outcomes the peak strength often not coincided with the final peak, the stress does not directly go down after reaching the peak strength in the simplified stress-strain curve. The third segment represents the additional peaks existing before the curve goes down without any further occurrence of new peaks. Despite the downward slope in experimental outcomes showing asymptotic behaviour, a linear segment was used to model the strength decrease in the material input.

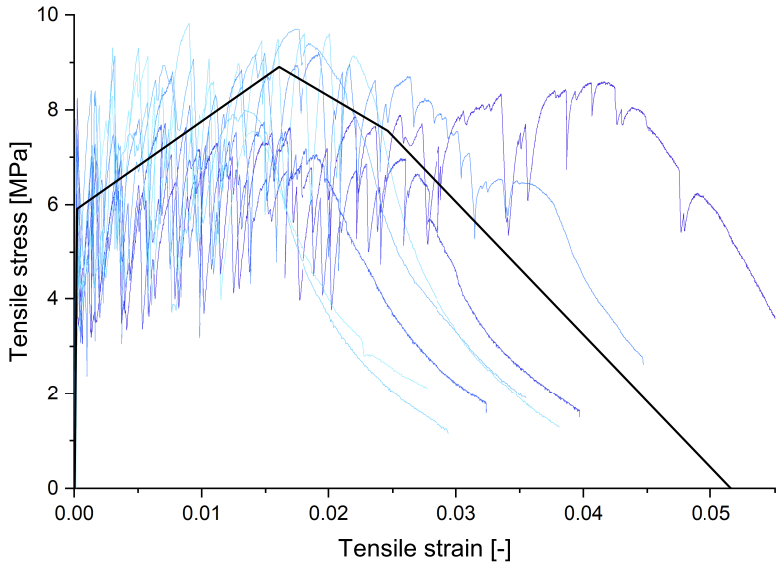

Figure 4.8: Material input for SH-UHPFRC based on experimental outcomes

4.3.2. Numerical Results

Figure 4.9 shows the load-deflection curve for the modelled reference beam and the strengthened beam. The strengthened beam improved the peak load and the ductility of the reference beam by 78% (Table 4.5). The initial slope of the strengthened beam is higher than that of the reference beam. This can be explained by the increased width of the beam, leading to a larger moment of inertia, and the superior material properties of SH-UHPFRC, including a higher E-modulus. This improves the bending resistance of the beam. After the peak load was reached, the strengthened beam sustained the peak load for a certain increase in deflection. However, for the reference beam a sudden drop of load was observed after arriving at the peak load. Figure 4.9 also shows the maximum crack width development. For the reference beam, the crack width suddenly increased after reaching the peak load, after which it continues to increase rapidly. For the strengthened beam a jump in maximum crack width was also visible at the deflection corresponding to the peak load. This jump was significantly smaller, suggesting the SH-UHPPFRC laminates not only increased the peak strength and limited the strength loss at failure but also decreased the width of immediate crack growth. The maximum crack width as stated in NEN-EN 1992-1-1 equals 0.3 mm, based on non-prestressed elements and assuming a possibly harsh environment. For the reference beam this maximum was exceeded directly after failure, reaching a crack width of 0.5 mm. For the strengthened beam this requirement was fulfilled slightly longer after cracking, as the maximum allowable crack width was exceeded at nearly 2.5 mm deflection.

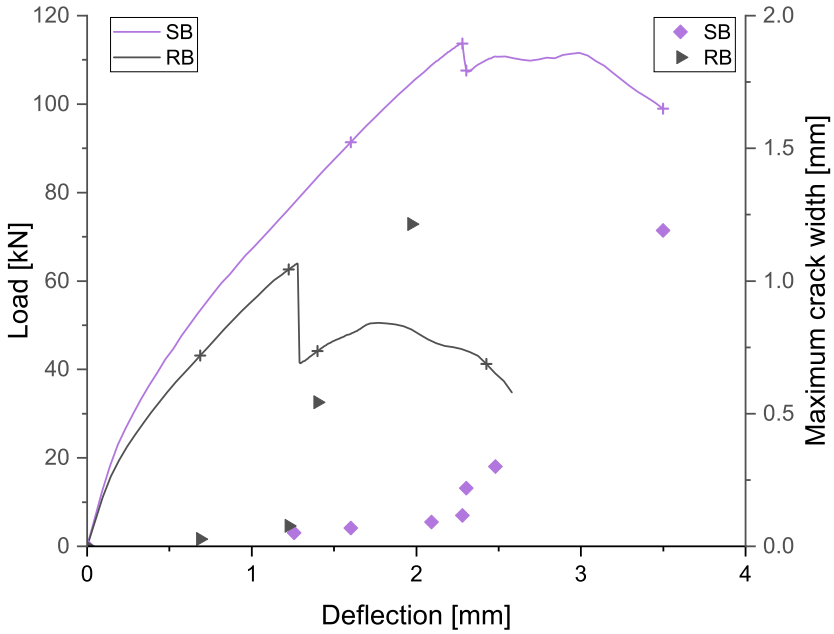

Figure 4.9: Load-deflection curve of the reference beam (RB) versus the strengthened beam (SB) including crack width development. Characteristic points indicated by +

Table 4.5: Peak load of reference beam and beam strengthened using SH-UHPFRC

	Load [kN]	Deflection [mm]
Reference beam	63.9	1.3
Strengthened beam	113.7	2.3
Improvement [%]	77.9	78.1

Figure 4.10 shows the crack pattern development of the reference and strengthened beam at characteristic points, indicated by + in Figure 4.9. For the reference beam flexural cracks started forming at early loading (Figure 4.10a). Before reaching the peak load some inclined cracks became visible (Figure 4.10c). Immediately after the peak load (Figure 4.10e) a clear shear crack is visible, accompanied

by a significant increase in maximum crack width (Figure 4.9). After this the shear cracks widened further and the crack elongated further towards the steel plates. For the strengthened beam the global cracking behaviour was similar to that of the reference beam, only at a higher level of load and deflection. For the strengthened beam flexural cracks were developing at the value of deflection where the reference beam had already attained its peak strength (Figure 4.10b). Similarly these cracks developed to inclined cracks and after the peak load shear cracks became visible (Figures 4.10d, 4.10f, 4.10h). Besides the difference in load capacity and ductility, the cracking pattern shows an additional effect of strengthening the reference beam using SH-UHPFRC. Compared to the reference beam the strengthened beam showed a larger number of cracks. The multiple cracking behaviour of the SH-UHPFRC lead to a large number of small cracks opposed to fewer large cracks as seen in the reference beam.

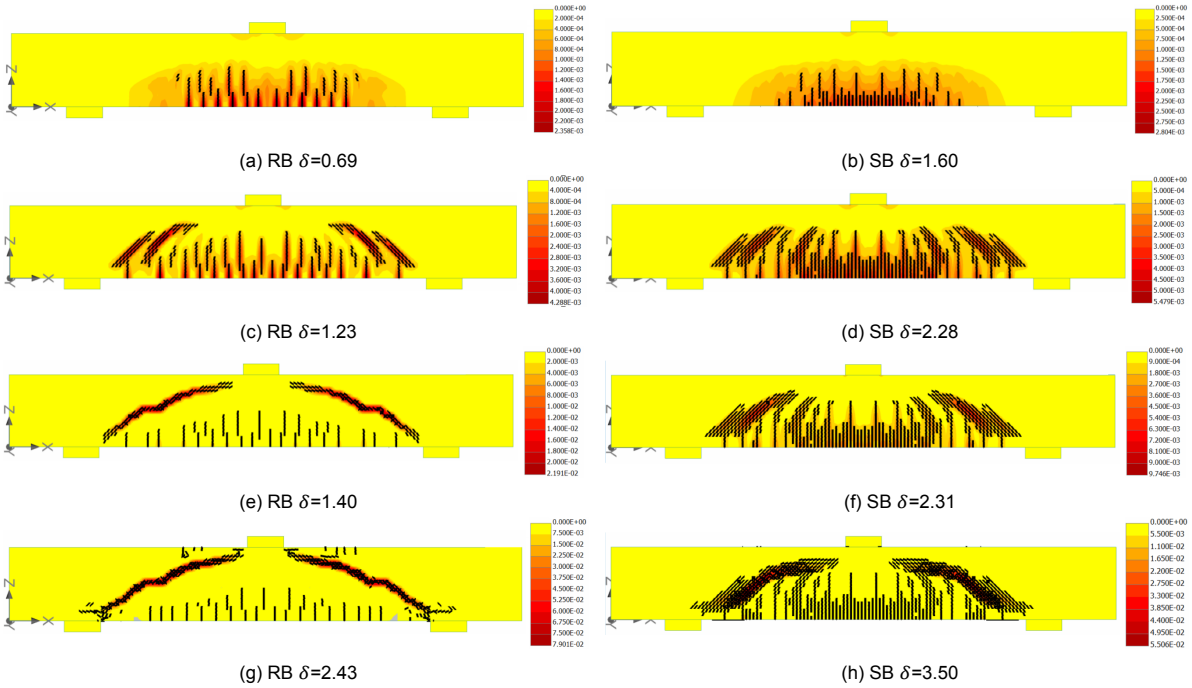

(a) RB δ=0.69 (b) SB δ=1.60

(c) RB δ=1.23 (d) SB δ=2.28

(e) RB δ=1.40 (f) SB δ=2.31

(g) RB δ=2.43 (h) SB δ=3.50

Figure 4.10: Crack pattern development reference beam versus strengthened beam with principal strain in ISO areas. Deflection δ in mm, minimum visible crack width 0.01 mm.

4.4. Parametric Study

To determine the effect of an increased tensile strain capacity, multiple material models were generated and used for strengthening materials in the FEM model. Using these materials to strengthen the reference beam in all these analyses, the effect was determined by inspecting the load-deflection curves, crack patterns and the development of crack widths.

4.4.1. Material Inputs

For the material inputs, the material properties of the developed SH-UHPFRC were used as a starting point. All properties except the tensile function and localized fracture strain were kept constant. The cracking strength was also equal for all material models. Apart from the simplified tensile function for SH-UHPFRC, four more models were generated. The tensile function for each of these can be seen in Figure 4.11. Models 1-3 were used to determine the effect of purely increasing the strain capacity. These materials were modelled to have no increase in stress after reaching the cracking strength. After the first crack, the models each had a different level of continuing strain increase: 0%, 1% and 3%. This was followed by a stress decrease retaining the same downward slope as the SH-UHPFRC curve. The localized fracture strain equals the final strain value before the onset of the stress decrease.

Model 4 was included in this research to establish the influence of increasing the peak strength of the model without changing the final strain capacity of the material compared to Model 3. Important to

note is that this change in peak strength was accompanied by other changes in the tensile function. Because of the increase in strength, the second branch in the stress-strain relation had a different slope (E-modulus) compared to Material Model 3. The localized fracture strain changed as well, as this now equaled the strain at peak stress, resulting in a lower value. This increased the length of the strain softening range.

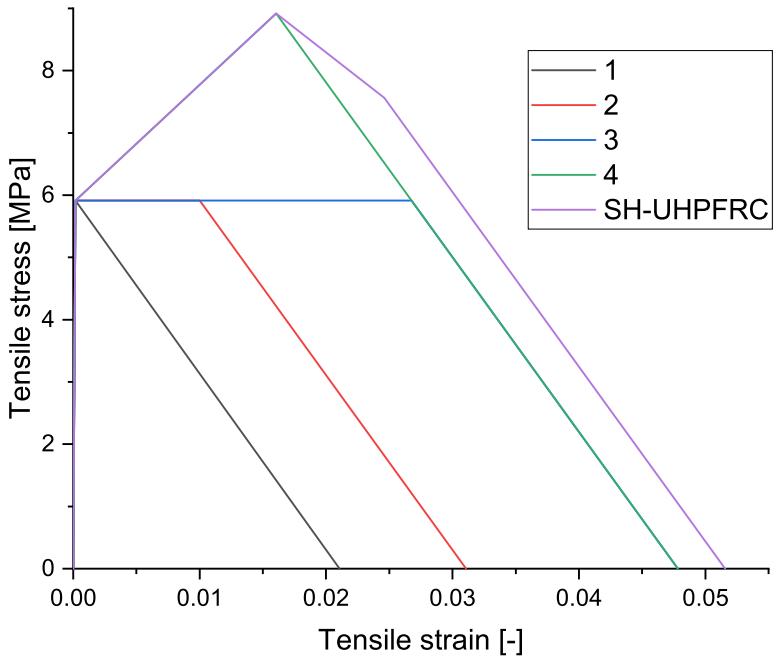

Figure 4.11: Tensile behaviour for different material models used in parametric study

4.4.2. Numerical Results

Figure 4.12 shows the load-deflection curve and crack width development of the beams strengthened using Material Models 1, 2 and 3. By only increasing the strain of these materials, no significant difference in peak strain was observed. On the contrary, the post peak behaviour showed a more distinct variation between the three strengthening materials. For the material models with longer strain capacity, the post-peak load capacity remained higher than that of the material without. For Material Model 1, the load after reaching peak strength immediately dropped down. For Models 2 and 3 a smaller drop in load is visible, after which a relatively high load could be retained with increasing deflection. Figure 4.12 also shows a relation between the increase in strain capacity of the strengthening material and the crack width development. For a material with increased strain capacity the slope of the crack development is smaller. For Model 1 the allowable crack width limit (≤0.3 mm) is exceeded with the drop in load capacity. For Models 2 and 3 a limited additional deflection is possible before exceeding the maximum allowable crack width.

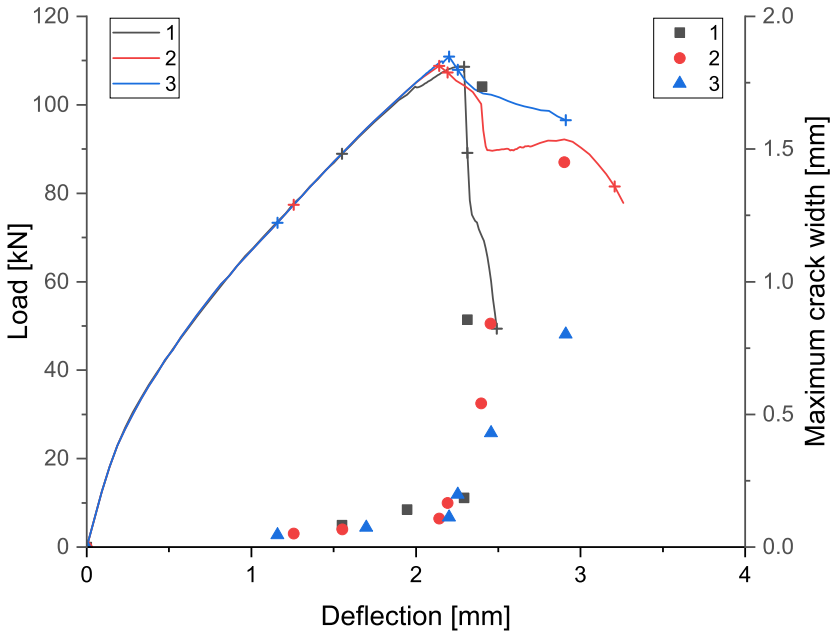

Figure 4.12: Load-deflection curve of Material Models 1-3 including crack width development. Characteristic points indicated by +

The crack pattern development of Models 1 and 2 is displayed in Figure 4.13, for Model 3 this can be seen in Figure 4.15. The displacements at which these images were taken are indicated in Figure 4.12 with +. These images show, similar to those in Section 4.3, four characteristic stages in the loading behaviour. Firstly, pure flexural bending could be seen from the vertical cracks at the bottom of the beam. This phase was followed by an increase in shear accompanied by an increase in diagonal cracks. Shear failure occurred and after this one or two cracks opened up, leading to a decrease in bearing capacity. Remarkable is that, opposed to the results from Section 4.3, these images show a non-symmetric cracking pattern. Using a fully symmetric model this was not to be expected. Compared to Model 1, Models 2 and 3 showed a significantly larger amount of cracks. The increase in strain capacity in the material model appeared to result in a higher number of small cracks, rather than fewer cracks with a larger crack width. Comparing the shape of the shear crack at and after the peak load, a more inclined angle could be seen with an increase in the strain capacity. The slope became more curved (like an S-shape) for Models 2 and 3.

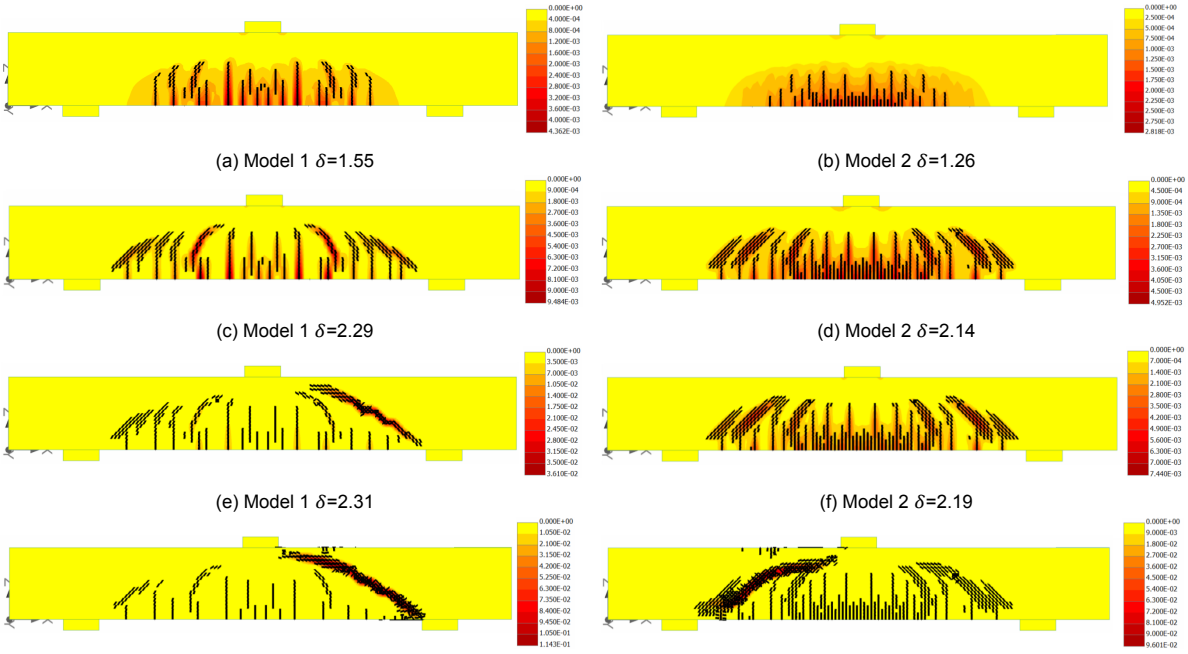

(a) Model 1 δ=1.55 (b) Model 2 δ=1.26

(c) Model 1 δ=2.29 (d) Model 2 δ=2.14

(e) Model 1 δ=2.31 (f) Model 2 δ=2.19

(g) Model 1 δ=2.49 (h) Model 2 δ=3.21

Figure 4.13: Crack pattern development of beam strengthened with materials using Material Models 1 and 2, with principal strain in ISO areas. Deflection δ in mm, minimum visible crack width 0.01 mm.

Figure 4.14 shows the load-deflection curve and crack width development for beams strengthened with Material Models 3 and 4. Despite an increase in peak strength in Model 4 over Model 3, the peak in the load-deflection curve remained very similar. For Model 4 the figure shows a longer displacement over which the peak strength could be sustained. In the development of maximum crack width could be seen that the slope of the crack development over increasing deflection reduced with the increase in peak strength.

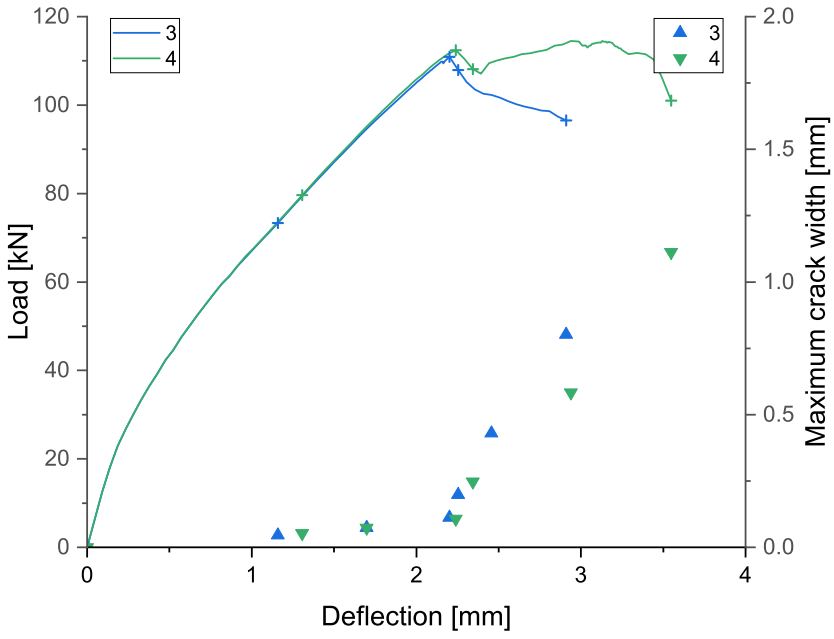

Figure 4.14: Load-deflection curve of Material Models 3 and 4 including crack width development. Characteristic points indicated by +

The crack development of Models 3 and 4 can be compared using Figure 4.15. The global behaviour the two sets of images is similar, showing comparable results for equal deflection. For model 4 a slight increase of the number of cracks was visible compared to that of Model 3.

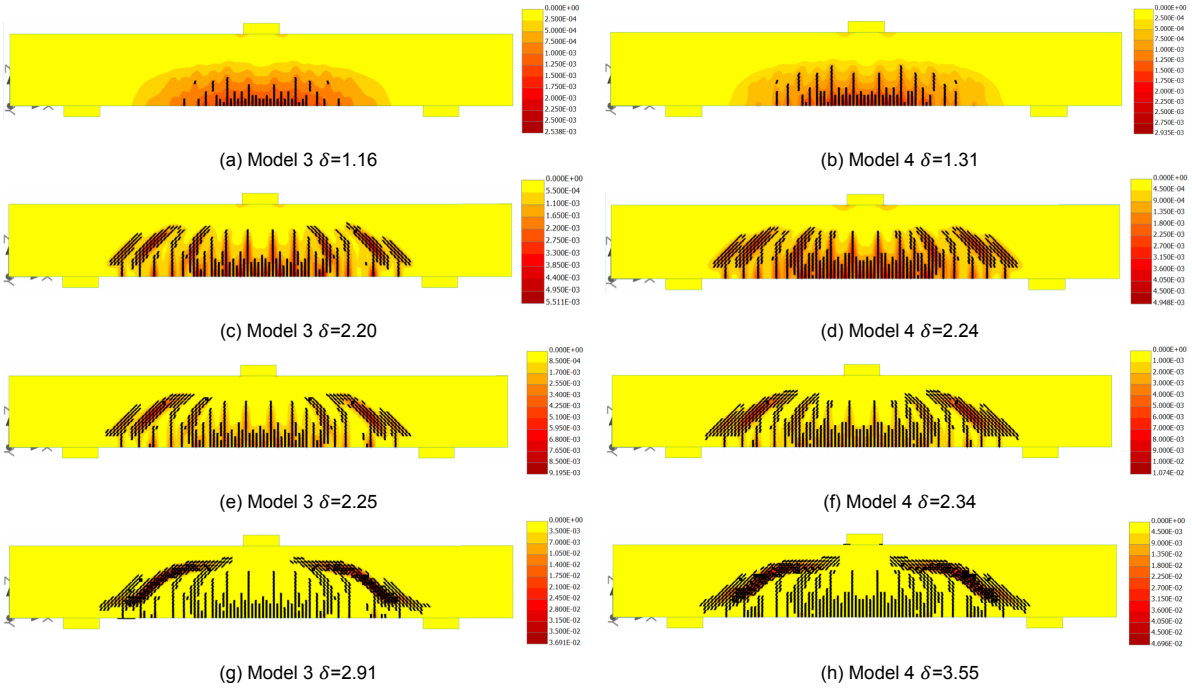

(a) Model 3 δ=1.16 (b) Model 4 δ=1.31

(c) Model 3 δ=2.20 (d) Model 4 δ=2.24

(e) Model 3 δ=2.25 (f) Model 4 δ=2.34

(g) Model 3 δ=2.91 (h) Model 4 δ=3.55

Figure 4.15: Crack pattern development of beam strengthened with materials using Material Models 3 and 4, with principal strain in ISO areas. Deflection δ in mm, minimum visible crack width 0.01 mm.

4.5. Discussion

The advantages of using SH-UHPFRC to strengthen a shear-deficient RC beam were shown. The use of 10 mm thick laminates lead to a significant increase in shear capacity and ductility. From the cracking pattern of the strengthened beam it was visible multiple small cracks developed, increasing in width after reaching the peak strength. The RC beam showed an abrupt failure with an immediate increase in crack width, exceeding the maximum as presented in standards. The peak load could be sustained for a longer increase in deflection by the strengthened beam compared to the RC beam, showing a more ductile post-peak behaviour. Because of the fibres in SH-UHPFRC bridging emerging cracks, loads could still be transferred after the capacity of the concrete matrix was reached. In RC beams this is only possible at the reinforcement bars while for SH-UHPFRC the whole strengthening laminate can contribute to this, resulting in larger deflection range in which the beam could bear high loads. Besides the increase in mechanical properties, the crack width was also reduced by using the strengthening laminates, contributing to an increased durability.

From the parameter study, it became clear that an increase in strain capacity does not directly lead to a significant increase in the shear capacity nor the ductility of the strengthened beam. The development of the cracking pattern showed an increase in the number of cracks with an increasing strain capacity of the strengthening material. The maximum crack width is also limited with an increase in the strain capacity of the strengthening material. The increase in peak strength lead to a similar result, indicating both parameters could affect the strengthening ability of the material. The multiple cracking behaviour of SH-UHPFRC limited the further development of cracks, resulting in an increased number of small cracks rather than a limited number of wider cracks. Despite the load capacity and ductility of the beam barely increasing with the increase of strain capacity of the strengthening material, this increased strain capacity lead to an increase of the extend to which the deflection could be increased while sustaining the peak load. Similar results were found by Shin et al. [129]. They used Ductile Fiber Reinforced Cementitious Composite to strengthen the tension zone in a beam subjected to bending.

In this research different levels of strain strain capacity were examined with varying peak stresses and strain hardening slopes. They concluded the first cracking strength mainly influences the peak load of the strengthened beam, while the post peak behaviour is influenced by the peak strength and strain hardening slope of the strengthening material [129]. These conclusions match the outcomes of this research. For further research the influence of the cracking strength of the strengthening material on the mechanical behaviour of the beam could be investigated.

Only a limited amount of variations in the material model was explored in this research. Only the tensile behaviour of the material was varied in strain capacity and peak strain. Other attributes of the strengthening material like a difference in peak strength, different E-modulus or varying compressive strength could be of significant influence on the behaviour of a beam strengthened using this material. Also the extend in which material parameters were examined was limited. This could be a possible explanation for all results being close. More research could be done using a larger range of values for strain capacity and strengths, possibly leading to more distinct results. The cracking behaviour of SH-UHPFRC could be studied in more detail and used in the material model of the strengthening material. This aspect of the material input was not included in this research.

To resemble practical application purposes, additional model parameters could be included. The connection between the RC beam and the strengthening laminates was modelled as a perfect bond. This parameter could be varied to resemble practice, as delamination can lead to brittle failure of structural elements [130]. The use of shear reinforcement was not included in this research. In practice this type of reinforcement is present in many structural elements. Research could be done on the efficiency of shear reinforcement versus shear strengthening using SH-UHPFRC, based on capacity, durability and costs. The combination of using shear reinforcement and strengthening laminates could also be investigated.

5

Environmental Impact Comparison

In this chapter, the environmental impact of the developed mixture is evaluated. As described in Section 2.5, the environmental impact is generally significantly higher for UHPC-like materials compared to conventional concrete mixtures. In the following sections, the environmental impact per volume was determined for multiple types of concrete. As this comparison does not consider the different mechanical properties, the calculated impact per volume was used to make a performance based comparison using the numerical results from Chapter 4.

5.1. Method

5.1.1. Rekentool Groen Beton

The CUR ”Rekentool Groen Beton” (calculation tool for green concrete) was used to determine the environmental impact of concrete mixtures and prefabricated elements. The tool determines the environmental impact in eleven environmental impact categories. Table 5.1 shows these categories. A database provides the amounts of emissions per category for construction materials. These impact factors represent the amount of emission per kilogram construction material, expressed in the unit corresponding to the concerned impact category. Table 5.1 also shows the shadow costs associated with every category. This is used to combine all impacts into one value by multiplying the quantity of emission by the shadow costs per unit and summing this value for every impact category. This Environmental Cost Indicator (ECI) allows for a straightforward comparison between materials or elements. Equation 5.1 shows this calculation using a formula.

$$ECI_{mix} = \sum_{i,j} mass_i \times impact\ factor_{i,j} \times shadow\ cost_j \tag{5.1}$$

where $i =$ material component and $j =$ impact category

Table 5.1: Environmental impact categories included in the CUR calculation tool

LCI category	Abbreviation	Unit	Shadow costs per unit [€]
Abiotic depletion, non-fuel	ADP nf	[kg Sb eq]	0.16
Abiotic depletion, fuel	ADP f	[kg Sb eq]	0.16
Global warming potential	GWP	[kg CO2 eq]	0.05
Ozone layer depletion	ODP	[kg CFC-11 eq]	30.00
Oxidation	POCP	[kg C2H4 eq]	2.00
Acidification	AP	[kg SO2 eq]	4.00
Eutrophication	EP	[kg PO4 eq]	9.00
Human toxicity	HT	[kg 1,4-DB eq]	0.09
Freshwater aquatic ecotoxicity	FAETP	[kg 1,4-DB eq]	0.03
Marine aquatic ecotoxicity	MAETP	[kg 1,4-DB eq]	0.0001
Terrestrial ecotoxicity	TETP	[kg 1,4-DB eq]	0.06

The calculations were based on the used material components only. The analysis did not include the maintenance during the life span of a construction, nor the demolition at end of life. These aspects can be considered, but no quantitative value was attached.

5.1.2. Material Input

The calculation tool comes with a database containing all commonly used materials for concrete. Almost all materials used in the developed mixture can be found in this database. For the M4 silica powder used in the developed material, the database did not provide a similar material. Because this is a siliceous material, it could be compared to sand for this study. This assumption neglects the processing required to create M4 powder, but this was estimated to be of minor influence for the ECI calculations.

UHMWPE is a not a commonly used construction material and was not available in any environmental database. For PE fibres, also no data was available in the tool's database. For this reason, PP fibres were used in calculations. To validate this assumption, a literature study comparing the environmental impact of PP and PE was done. Several researches showed a highly similar CO_2-emission (GWP) for both materials [131, 132, 133]. Harding et al. [134] (citing work by Boustead [135]) discussed the environmental impact of high density PE (HDPE), low density PE (LDPE), PP and one other polymer product. This comparison showed a similar or lower impact for HDPE/LDPE for most LCA categories. Only in HT and POCP, the impact of PP is lower. Tabone et al. [136] made a similar comparison. PE and PP scored similarly in every impact category, PP having slightly lower values in most categories. Alsabri and Al-Ghamdi [137] concluded PP to be better in terms of LCA compared to PE, aside from PP having a 5% larger CO_2-emission. Although some contradicting statements were found in literature, the general trend observed was that the differences between PP and PE are limited. Looking at the GWP, the differences were usually about 5% and can be in either direction. For this reason, the LCA values for PP from the tool's database were considered adequate as an estimation for PE.

5.2. Material Comparison

5.2.1. Material Impact per Cubic Meter

Table 5.2 shows all mixtures compared in this section. In addition to the developed SH-UHPFRC mixture, three other mixtures were compared based on their ECI value. The NC mixture is identical to the NC used in the numerical analysis in Chapter 4. Reinforcement was not taken into account in this section, as this has no set ratio compared to the mixture's components. The UHPFRC mixture [115] was the starting point of the material development. Additionally, this comparison included a SHCC mixture developed at TU Delft [138]. Similar to SH-UHFRC, this mixture has strain hardening properties and contains synthetic fibres.

The PVA fibres used in the SHCC mixture were not included in the database of the calculation tool. Van den Heede et al. [139] discussed the environmental impact difference between PP and PVA in multiple

impact categories. Since PVA has a higher impact in all categories, using PP as an estimate value could lead to an underestimated environmental impact. In this paper, the inventory of the environmental impacts would lead to PVA having a total ECI value seven times higher compared to PP for equal weight. Because of the difference in detail for the inventory, this comparison is not perfectly fair, yet it gives a clear indication that PVA fibres have a significantly higher environmental impact than PP fibres, which must be considered when evaluating the calculation outcomes.

Table 5.2: Mixtures for comparison based on environmental impact, quantities in kg/m^3. *The amount of M4 silica powder is incorporated in the amount of sand in ECI calculations.

	NC	SH-UHPFRC	UHPFRC [115]	SHCC [138]
CEM I	260.0	1119.1	870.0	-
CEM III	-	-	-	790.0
SF	-	111.9	43.8	-
M4*	-	193.0	-	-
GGBFS	-	134.3	104.4	-
LP	-	-	-	790
Sand	847.4	495.9	1061.1	-
Gravel	1123.3	-	-	-
Water	156.0	225.0	204.6	410.0
SP	0.26	31.98	26.60	2.13
Steel fibre	-	-	125.0	-
Synthetic fibre	-	13.7 (UHMWPE)	-	26.0 (PVA)

The ECI was calculated as discussed in Section 5.1.1. The ECI values are shown in Table 5.3. From this, a significant difference can be seen between the NC and the high performance mixtures. Figure 5.1 shows the ECI per category for all materials. From these figures it becomes clear that a higher cement content had a vast influence on the environmental impact, as this contributed most in many categories. In the SH-UHPFRC and UHPFRC, the amount of SP was significantly larger and this can be seen in the GWP and AP categories. The steel fibres in UHPFRC resulted in this material having the highest ECI score. Compared to the PE fibres in SH-UHPFRC, the steel fibres in UHPFRC contributed to a significantly higher impact. To emphasize this difference, the relative impact of PE fibres compared to steel was calculated, which can be seen in Figure 5.2. This figure shows the impact per category for steel and PE fibres for equal volumes. Due to the large difference in density between steel fibres (7850 kg/m^3) and PE fibres (975 kg/m^3), a comparison based on equal weight could lead to misleading contrasts. Considering an equal volume, steel fibres scored higher in every impact category.

Table 5.3: ECI values for all considered mixtures in Euros per cubic meter €/m^3

NC	SH-UHPFRC	UHPFRC [115]	SHCC [138]
16.23	74.17	80.36	26.41

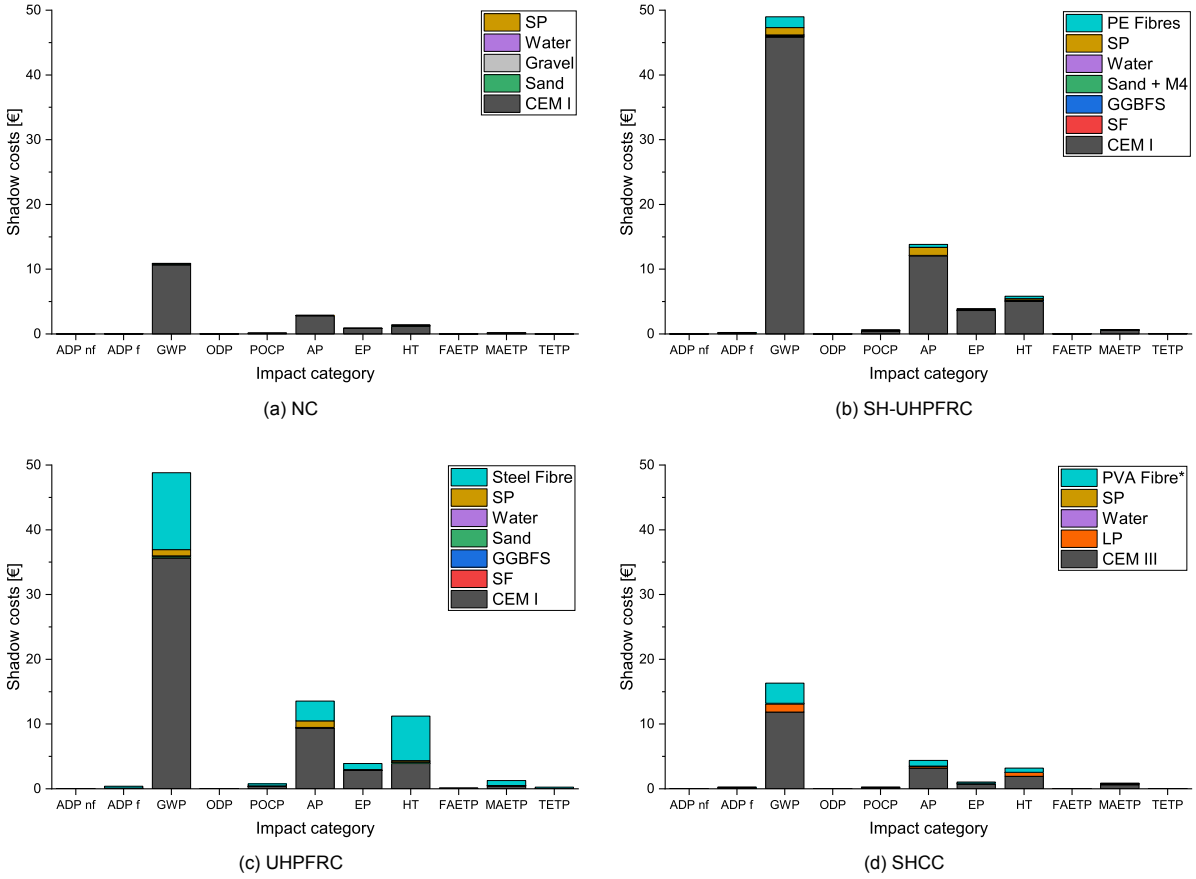

(a) NC (b) SH-UHPFRC

(c) UHPFRC (d) SHCC

Figure 5.1: Environmental impact per category for one cubic meter of different materials, expressed in €.

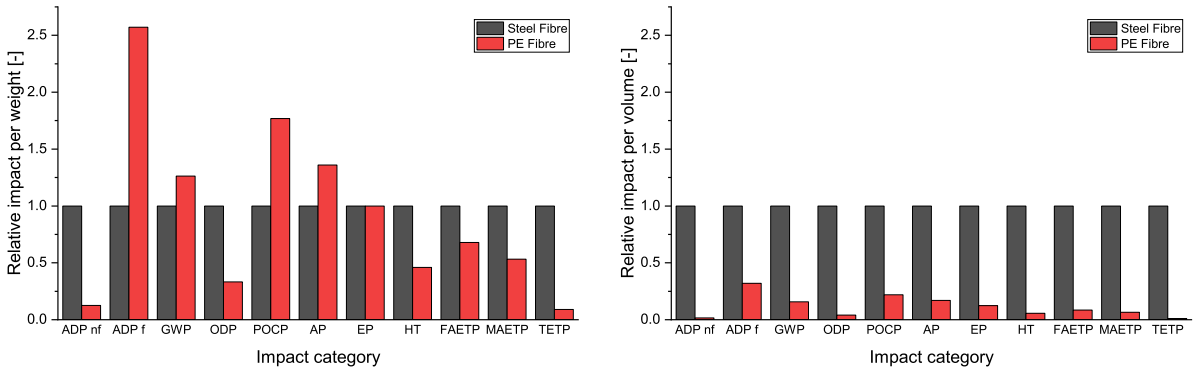

(a) Comparison based on weight (b) Comparison based on volume

Figure 5.2: Relative environmental impact of PE fibres compared to steel fibres based on weight and volume

5.2.2. Comparison Including Structural Performance

To make a performance based comparison, an ECI calculation was done for the strengthened beam as discussed in Chapter 4. This beam was compared to the reference beam. Only longitudinal reinforcement was included. Stirrups were excluded from these calculations, as these were also not included in the numerical analysis. An overview of the volumes of each material used in the two beams is shown in Table 5.4. These volumes were used to determine the total ECI value for the element, which can also be found in the table. From this table, it becomes clear that the reinforcement contributed most to the total environmental impact. Figure 5.3 shows the impact of the element components per impact category.

Table 5.4: ECI values for reference and strengthened beam including material volumes

	Reference beam		Strengthened beam	
	Volume [m3]	ECI [€]	Volume [m3]	ECI [€]
NC	2.71E-02	0.44	2.71E-02	0.44
Reinforcement	8.55E-04	1.09	8.55E-04	1.09
SH-UHPFRC	-	-	5.60E-03	0.42
Total ECI		1.54		1.95

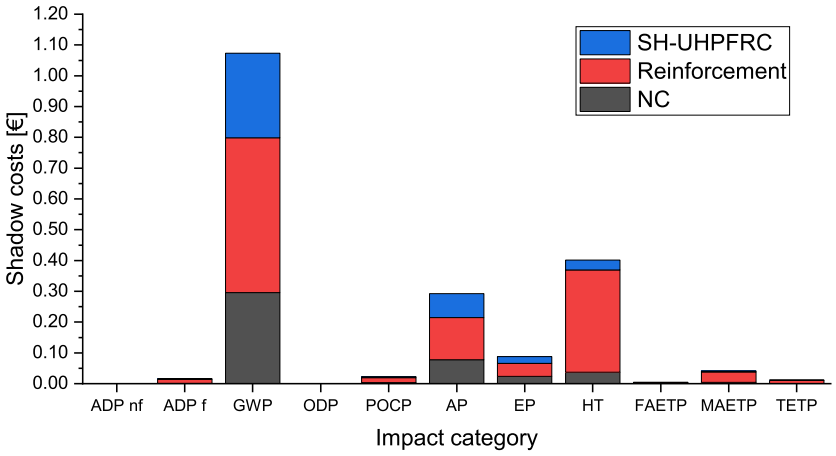

Figure 5.3: ECI for materials used in strengthened beam per impact category

The use of SH-UHPFRC laminates lead to in increase in ECI of 26.6%. In Section 4.3, the increase in shear capacity and ductility was discussed, which can be weighed against the increase in environmental impact. To enable a fair comparison, beams with similar mechanical properties should be studied. A comparison was made between the strengthened beam using SH-UHPFRC and a RC beam with increased thickness, such that the shear capacity of the beam equals that of the strengthened beam. No other design parameters are varied. Using the equation for the shear capacity of a reinforced concrete beam from NEN-EN 1992-1-1 (Equation 5.2), the relation between the width of this beam (b) and the shear capacity was determined (Equation 5.3). The shear capacity of the beam increased with 78%, resulting in an increase in beam width of 137%.

$$
\begin{aligned}
V_{Rd,c} &= C_{Rd,c} k (100 \rho_l f_{ck})^{1/3} bd \\
\text{where } V_{Rd,c} &= \text{ Shear capacity;} \\
C_{Rd,c} &= \text{ constant;} \\
k &= \sqrt{200/d} \leq 2.0 \text{ coefficient, } d \text{ in mm;} \\
\rho_l &= A_s/bd \text{ longitudinal reinforcement ratio;} \\
f_{ck} &= \text{ characteristic compressive strength;} \\
b &= \text{ beam width;} \\
d &= \text{ effective cross section height}
\end{aligned}
\tag{5.2}
$$

$$
V_{Rd,c} \sim b^{2/3} \tag{5.3}
$$

Using the calculated beam width, the volume of the concrete was recalculated to calculate the new ECI value for the widened beam, as shown in Table 5.5. This table also includes the calculated ECI values for both beams. Figure 5.4 shows these ratios in ECI values visually. The large increase in concrete

volume required to acquire the same increase in shear capacity, lead to a significant increase in the ECI value of the beam element. Despite the SH-UHPFRC having a much higher ECI value per volume, the increased performance could not be matched by increasing the width of the RC beam using only NC without surpassing the ECI value of the strengthened beam. This demonstrates the supremacy of strengthening using SH-UHPFRC over using NC to strengthen a shear-deficient structural element.

Table 5.5: ECI values for widened RC beam and SH-UHPFRC-strengthened beam including material volumes

	Beam with increased width		Strengthened beam	
	Volume [m3]	ECI [€]	Volume [m3]	ECI [€]
NC	6.56E-02	1.07	2.71E-02	0.44
Reinforcement	8.55E-04	1.09	8.55E-04	1.09
SH-UHPFRC	-	-	5.60E-03	0.42
Total ECI		2.16		1.95

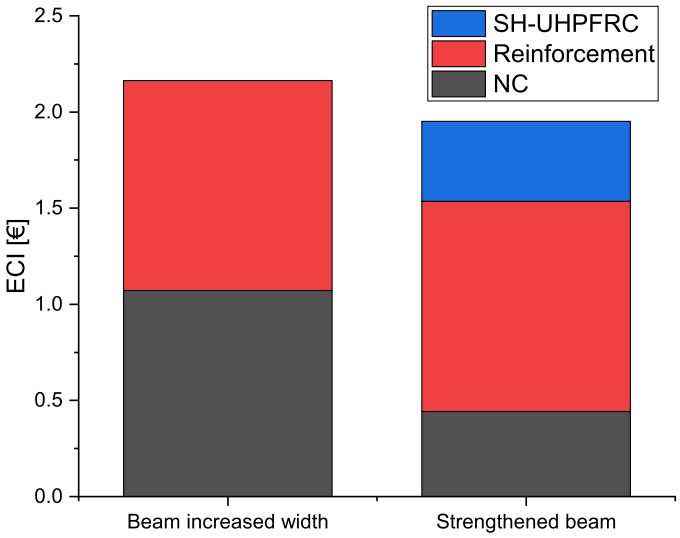

Figure 5.4: ECI for materials used in the widened beam and the strengthened beam

5.3. Discussion

The ECI calculations done in this thesis give an estimation of the environmental impact for the developed mixture compared to other types of concrete. In this calculation some assumptions were made. Not all materials used in the different mixtures were available in the database provided with the CUR calculation tool. Assuming these missing materials to have an impact similar to materials available in the database, could lead to deviations. Especially the assumption for synthetic fibres could have had a significant influence on the resulting ECI. As not much data was available on the environmental impact of the production of these specific fibres, a rough assumption had to be made. For PE fibres, the use of PP fibres appeared to be a proper estimation. For UHMWPE fibres, no data was found on the CO_2-emission or other environmental impact. Because of this, no validation of the assumption using PP fibres was possible.

For the SH-UHPFRC, UHPFRC and SHCC fibres were included in the ECI calculation. These fibres had a significant contribution to the total environmental impact of the material. Opposed to fibre reinforcement, reinforcement bars were not included in the material comparison. This caused NC to have an advantage over the other mixtures, as this mixture did not contain any type of reinforcement in the mixture itself. For a fair comparison based on mixture per volume, an average reinforcement ratio could be assumed for each mixture.

The calculated width of the widened beam did not give a realistic beam design. A beam with a width larger than the height of the beam, without using shear reinforcement and additional longitudinal reinforcement would not be used in practice. The calculated additional volume of concrete merely indicated the superiority of the additional shear resistance contributed by the SH-UHPFRC.

All calculations done in this chapter have been based purely on the environmental impact caused by the production of the material components used. The transport of materials, production of the concrete and waste disposal were not included in this analysis. In a full life cycle analysis these phases would be included, as well as the phase of use and maintenance. The comparison of elements was only based on the ECI value and the shear capacity of the beam. Other mechanical properties as well as the durability were not included. Considering the exceptional mechanical properties and crack width control of SH-UHPRFC, this would be advantageous when compared to NC. The increased durability of UHPC-like mixtures can increase the service life of structural elements and lead to a lower requirement of maintenance. In a full life cycle analysis, these factors could partly compensate for the higher ECI value of the SH-UHPFRC mixture. A full life cycle analysis could provide a more elaborate analysis of the environmental impact of strengthening structural elements using SH-UHPFRC. Including all phases of a structural element's life cycle and considering the higher life span of SH-UHPFRC could show the true benefits of using this strengthening material.

6

Conclusions and Recommendations

6.1. Conclusions

A SH-UHPFRC mixture was developed, having an average compressive strength of about 120 MPa, a tensile strength of 8.9 kN and a strain capacity over 2.0%. This was done using a large amount of cement, only fine fillers and a low water content. Using a low w/b-ratio, only fine materials and thin UHMWPE fibres, assuring a proper level of flowability required some additional changes in the mixture design. The use of a larger amount of SP and replacing fine cement by normally graded cement were key in achieving an acceptable flowability level. With the use of higher contents of UHMWPE fibre, the flowability of the mixture decreased. The compressive strength was barely affected by a change in the fibre content. The cracking pattern of specimens used for direct tensile testing showed a slight increase of narrow cracks for higher fibre contents, opposed to a lower number of wider cracks. Despite this visible effect, the increase in fibre content did not result in a significant effect on the strength of the material nor the strain capacity, within the range of fibre contents used. Compared to steel fibres, the use of UHMWPE fibres caused a significant decrease in the flowability of the mixture. The compressive strength was lower for mixtures containing UHMWPE fibres compared to those including steel fibres.

Using a FEM model of a RC beam strengthened with SH-UHPFRC laminates on the sides, subjected to a three-point bending test, the contribution of SH-UHPFRC strengthening to the shear capacity was estimated. Compared to the reference beam without any strengthening, both the shear capacity and the ductility of the strengthened beam were increased by 78%. The cracking behaviour changed significantly because of the strengthening material. The use of the laminates lead to a large number of narrow cracks, opposed to the limited number of large cracks in the RC beam. The crack width development was slower for the strengthened beam, leading to a higher durability. A parametric study was used to determine the effect of an increased strain capacity in the strengthening material on the structural behaviour of the strengthened beam. Within the considered range of strain capacity, no clear effect was observed on the shear capacity nor the ductility of the beam. The maximum cracking width of the element became smaller with increasing shear capacity and the observed number of cracks increased. A similar result was visible for an increase in peak strength, showing a more ductile behaviour without a clear improvement in the shear capacity. The results indicated that the peak strength and strain capacity of the strengthening material might only have affected the post peak behaviour of the strengthened beam, while the cracking strength of the strengthening material influenced the peak load and ductility of the strengthened beam.

The environmental impact of the developed SH-UHPFRC mixture was weighed against the environmental impact of NC, UHPFRC and SHCC. The high cement content of UHPFRC and SH-UHPFRC lead to these materials having the highest environmental impact per volume. The PE fibres and the large amount of SP in the mixture contributed significantly to the environmental impact of the material, despite being much less significant than the contribution of cement to the environmental impact. Compared to steel fibres, PE fibres have a lower impact considering equal volumes. To consider the

environmental effect of using SH-UHPFRC in strengthening applications, a comparison was made between a RC beam and a RC beam strengthened with SH-UHPFRC. The strengthened beam had a 26.6% higher impact compared to the reference beam without strengthening. The shear capacity of the beam was increased by 78% by adding the SH-UHPFRC laminates. To enable a fair comparison, the width of the RC beam is increased to result in a beam with equal shear capacity compared to the strengthened beam. This resulted in a higher environmental impact for the RC beam, showing how SH-UHPFRC can lead to a lower environmental impact with equal performance. This comparison did not consider the enhanced durability due to crack limitation and increased life span of the strengthened element.

6.2. Recommendations

The use of SH-UHPFRC for strengthening applications seems promising, but further research and optimisation for this material is important. Improvement of the flowability is necessary to be able to construct thin strengthening elements. A material optimization study could be done focusing on improving the flowability without negatively affecting the mechanical properties of the mixture. To fully utilize the UHMWPE fibers' properties, the fibre-matrix interaction could be investigated and enhanced. Also, the effect of increasing age on the tensile behaviour of the mixture could be studied, comparing both mechanical properties and cracking behaviour. Further determination of the material properties could be beneficial for the modelling and application of SH-UHPFRC. A material research including more specific material properties and high numbers of specimen could lead to more reliable results. Additional to further material level research, the behaviour of the material should be studied for environmental impacts, long term effects and size effect to assemble a complete overview of all material characteristics to use for application.

For the modelling of the strengthened beam only the tensile response was varied in this research. Using a wider range of parameters with a larger range of values could give a more complete view of the effect each parameter has on the mechanical response of the element. The use of a higher cracking strength or a larger range of strain capacities could possibly lead to more distinct differences in beam capacity. Adaptions to bond strength between NC and SH-UHPFRC could be implemented to better resemble structural elements in practice. Experimental tests could be executed to determine the relation between bond stress and slip, which functions as input for the interface elements.

A full life cycle analysis for a structural element strengthened with SH-UHPFRC could demonstrate the value of the developed material. Considering the long life span and superior durability properties of SH-UHPFRC, this analysis could prove the use of this material to be beneficial considering the environmental impact, on top of the improved mechanical performance.

Bibliography

[1] Michael Schmidt and Ekkehard Fehling. “Ultra-High-Performance Concrete: Research, Development and Application in Europe”. In: *ACI Special Publication* 228 (Jan. 2005).

[2] M.A. Bajaber and I.Y. Hakeem. “UHPC evolution, development, and utilization in construction: a review”. In: *Journal of Materials Research and Technology* 10 (2021), pp. 1058–1074. ISSN: 2238-7854.

[3] Shamsad Ahmad, Ibrahim Hakeem, and Mohammed Maslehuddin. “Development of an optimum mixture of ultra-high performance concrete”. In: *European Journal of Environmental and Civil Engineering* 20.9 (2016), pp. 1106–1126.

[4] Joost C. Walraven. “High performance fiber reinforced concrete: progress in knowledge and desgin codes”. In: *Materials and Structures* 42 (2009), pp. 1247–1260.

[5] Yen Lei Voo, Stephen J Foster, and Chen Cheong Voo. “Ultrahigh-performance concrete segmental bridge technology: Toward sustainable bridge construction”. In: *Journal of Bridge Engineering* 20.8 (2015), B5014001.

[6] Yitao Huang et al. “Strengthening of concrete structures with ultra high performance fiber reinforced concrete (UHPFRC): A critical review”. In: *Construction and Building Materials* 336 (2022), p. 127398.

[7] Eugen Brühwiler. “Rehabilitation of concrete bridges using Ultra-High Performance Fibre Reinforced Concrete (UHPFRC)”. In: *Proceedings of 3rd International Symposium on Life-cycle civil Engineering*. Vol. 1. CONF. CRC Press/Balkema. 2012, pp. 1934–1941.

[8] Yixin Chen, Jing Yu, and Christopher K.Y. Leung. “Use of high strength Strain-Hardening Cementitious Composites for flexural repair of concrete structures with significant steel corrosion”. In: *Construction and Building Materials* 167 (2018), pp. 325–337. ISSN: 0950-0618.

[9] Antoine E Naaman. “Tensile strain-hardening FRC composites: Historical evolution since the 1960”. In: *Advances in construction materials 2007*. Springer, 2007, pp. 181–202.

[10] Viktor Mechtcherine. “Novel cement-based composites for the strengthening and repair of concrete structures”. In: *Construction and building materials* 41 (2013), pp. 365–373.

[11] Antoine E Naaman. “High performance fiber reinforced cement composites”. In: *Naaman AE. High-performance construction materials: science and applications. Singapore: World Scientific Publishing* (2008), pp. 91–153.

[12] David R Lan Kar. “Properties, applications: Slurry infiltrated fiber concrete (SIFCON)”. In: *Concrete International* 6.12 (1984), pp. 44–47.

[13] Ziad Bayasi and Jack Zeng. “Flexural behavior of slurry infiltrated mat concrete (SIMCON)”. In: *Journal of materials in civil engineering* 9.4 (1997), pp. 194–199.

[14] Onkar Mishra and SP Singh. “An overview of microstructural and material properties of ultra-high-performance concrete”. In: *Journal of Sustainable Cement-Based Materials* 8.2 (2019), pp. 97–143.

[15] Benjamin Allen Graybeal. “Characterization of the behavior of ultra-high performance concrete”. PhD thesis. 2005.

[16] Kay Wille, Sherif El-Tawil, and Antoine E Naaman. “Properties of strain hardening ultra high performance fiber reinforced concrete (UHP-FRC) under direct tensile loading”. In: *Cement and Concrete Composites* 48 (2014), pp. 53–66.

[17] Kay Wille et al. “Ultra-high performance concrete and fiber reinforced concrete: achieving strength and ductility without heat curing”. In: *Materials and structures* 45.3 (2012), pp. 309–324.

[18] Kay Wille, Antoine E Naaman, and Gustavo J Parra-Montesinos. “Ultra-High Performance Concrete with Compressive Strength Exceeding 150 MPa (22 ksi): A Simpler Way.” In: *ACI materials journal* 108.1 (2011).

[19] Songlin Yang and Bo Diao. “Influence of curing regime on the ductility of ultra-high performance fiber reinforced concrete (UHPFRC)”. In: *ICCTP 2009: Critical Issues In Transportation Systems Planning, Development, and Management*. 2009, pp. 1–7.

[20] Benjamin Graybeal and Jussara Tanesi. “Durability of an ultrahigh-performance concrete”. In: *Journal of materials in civil engineering* 19.10 (2007), pp. 848–854.

[21] Kay Wille, Dong Joo Kim, and Antoine E Naaman. “Strain-hardening UHP-FRC with low fiber contents”. In: *Materials and structures* 44.3 (2011), pp. 583–598.

[22] Minoru Kunieda and Keitetsu Rokugo. “Recent progress on HPFRCC in Japan”. In: *Journal of Advanced Concrete Technology* 4.1 (2006), pp. 19–33.

[23] Iurie Curosu, Viktor Mechtcherine, and Oliver Millon. “Effect of fiber properties and matrix composition on the tensile behavior of strain-hardening cement-based composites (SHCCs) subject to impact loading”. In: *Cement and Concrete Research* 82 (2016), pp. 23–35.

[24] Gideon PAG van Zijl et al. “Durability of strain-hardening cement-based composites (SHCC)”. In: *Materials and structures* 45.10 (2012), pp. 1447–1463.

[25] Lisa Matthys. “Design tool voor UHPC-elementen”. MA thesis. KU Leuven, 2020.

[26] Pierre Richard and Marcel Cheyrezy. “Composition of reactive powder concretes”. In: *Cement and concrete research* 25.7 (1995), pp. 1501–1511.

[27] Dale P Bentz et al. “Effects of cement particle size distribution on performance properties of Portland cement-based materials”. In: *Cement and concrete research* 29.10 (1999), pp. 1663–1671.

[28] Ali Mardani-Aghabaglou, Burak Felekoğlu, and Kambiz Ramyar. “Effect of cement C 3 A content on properties of cementitious systems containing high-range water-reducing admixture”. In: *Journal of Materials in Civil Engineering* 29.8 (2017), p. 04017066.

[29] E Hanna et al. “Rheological Behavior of Portland cement in the Presence of a Super Plasticizer”. In: *Special Publication* 119 (1989), pp. 171–188.

[30] Youzhu Lin et al. “Effect of silica fumes on fluidity of UHPC: Experiments, influence mechanism and evaluation methods”. In: *Construction and Building Materials* 210 (2019), pp. 451–460.

[31] Jeff Kaimao Weng, BW Langan, and MA Ward. “Pozzolanic reaction in Portland cement, silica fume, and fly ash mixtures”. In: *Canadian journal of civil engineering* 24.5 (1997), pp. 754–760.

[32] L Senff et al. “Effect of nano-SiO2 and nano-TiO2 addition on the rheological behavior and the hardened properties of cement mortars”. In: *Materials Science and Engineering: A* 532 (2012), pp. 354–361.

[33] Jung Jun Park et al. “Influence of the ingredients on the compressive strength of UHPC as a fundamental study to optimize the mixing proportion”. In: *Proceedings of the second international symposium on ultra high performance concrete*. Kassel Germany. 2008, pp. 105–112.

[34] François de Larrard and Thierry Sedran. “Optimization of ultra-high-performance concrete by the use of a packing model”. In: *Cement and concrete research* 24.6 (1994), pp. 997–1009.

[35] M.I. Khan, Galal Fares, and Shehab Mourad. “Optimized fresh and hardened properties of strain hardening cementitious composites: Effect of mineral admixtures, cementitious composition, size, and type of aggregates”. In: *Journal of Materials in Civil Engineering* 29.10 (2017), p. 04017178.

[36] Caijun Shi et al. “A review on ultra high performance concrete: Part I. Raw materials and mixture design”. In: *Construction and Building Materials* 101 (2015), pp. 741–751.

[37] Kay Wille and Christopher Boisvert-Cotulio. “Material efficiency in the design of ultra-high performance concrete”. In: *Construction and Building Materials* 86 (2015), pp. 33–43.

[38] R Yu, PHJH Spiesz, and HJH Brouwers. “Development of an eco-friendly Ultra-High Performance Concrete (UHPC) with efficient cement and mineral admixtures uses”. In: *Cement and Concrete Composites* 55 (2015), pp. 383–394.

[39] Ravi Ranade et al. “Composite Properties of High-Strength, High-Ductility Concrete.” In: *ACI Materials Journal* 110.4 (2013).

[40] Kequan Yu et al. “A strain-hardening cementitious composites with the tensile capacity up to 8%”. In: *Construction and Building Materials* 137 (2017), pp. 410–419.

[41] R Shionaga et al. “OPTIMIZATION OF TENSILE STRAIN-HARDENING CEMENTITIOUS COMPOSITES FOR TENSILE STRAIN CAPACITY”. In: *3rd International RILEM Conference on Strain Hardening Cementitious Composites*. 2014, p. 79.

[42] Iurie Curosu et al. “Tensile behavior of high-strength strain-hardening cement-based composites (HS-SHCC) made with high-performance polyethylene, aramid and PBO fibers”. In: *Cement and Concrete Research* 98 (2017), pp. 71–81.

[43] Iurie Curosu, A Ashraf, and Viktor Mechtcherine. “Behaviour of Strain-Hardening Cement-Based Composites (SHCC) Subjected to Impact Loading”. In: *Proceedings of the 3rd International RILEM Conference on Strain Hardening Cementitious Composites SHCC3, Dordrecht, Netherlands, RILEM SARL Publications*. 2014, pp. 121–128.

[44] Juan Yang et al. “Mechanical properties and durability of ultra-high performance concrete incorporating coarse aggregate”. In: *Key Engineering Materials*. Vol. 629. Trans Tech Publ. 2015, pp. 96–103.

[45] Jing Yu and Christopher KY Leung. “Strength improvement of strain-hardening cementitious composites with ultrahigh-volume fly ash”. In: *Journal of Materials in Civil Engineering* 29.9 (2017), p. 05017003.

[46] Shwan H Said and Hashim Abdul Razak. “The effect of synthetic polyethylene fiber on the strain hardening behavior of engineered cementitious composite (ECC)”. In: *Materials & Design* 86 (2015), pp. 447–457.

[47] Kamal Henri Khayat et al. “Rheological properties of ultra-high-performance concrete—An overview”. In: *Cement and Concrete Research* 124 (2019), p. 105828.

[48] Nicolas Roussel. *Understanding the rheology of concrete*. Elsevier, 2011.

[49] Pierre Rossi. “Ultra-high performance fibre reinforced concretes (UHPFRC): an overview”. In: *Fifth RILEM Symposium on Fibre-Reinforced Concretes (FRC)*. 2000, pp. 87–100.

[50] Jian-Guo Dai, Bo-Tao Huang, and Surendra P Shah. “Recent Advances in Strain-Hardening UHPC with Synthetic Fibers”. In: *Journal of Composites Science* 5.10 (2021), p. 283.

[51] Ke-Quan Yu et al. “Development of ultra-high performance engineered cementitious composites using polyethylene (PE) fibers”. In: *Construction and Building Materials* 158 (2018), pp. 217–227.

[52] K Kobayashi and R Cho. “Flexural characteristics of steel fibre and polyethylene fibre hybrid-reinforced concrete”. In: *Composites* 13.2 (1982), pp. 164–168.

[53] Alessandro P Fantilli, Hirozo Mihashi, and Paolo Vallini. “Multiple cracking and strain hardening in fiber-reinforced concrete under uniaxial tension”. In: *Cement and Concrete Research* 39.12 (2009), pp. 1217–1229.

[54] Tetsuo Kanamoto, Edward S Sherman, and Roger S Porter. “Extrusion of polyethylene single crystals”. In: *Polymer Journal* 11.6 (1979), pp. 497–502.

[55] Ronald F Zollo. “Fiber-reinforced concrete: an overview after 30 years of development”. In: *Cement and concrete composites* 19.2 (1997), pp. 107–122.

[56] Victor C Li and Tetsushi Kanda. “Innovations forum: engineered cementitious composites for structural applications”. In: *Journal of Materials in Civil Engineering* 10.2 (1998), pp. 66–69.

[57] Shuai Zhou et al. “Review of cementitious composites containing polyethylene fibers as repairing materials”. In: *Polymers* 12.11 (2020), p. 2624.

[58] Ye Li, En-Hua Yang, and Kang Hai Tan. “Flexural behavior of ultra-high performance hybrid fiber reinforced concrete at the ambient and elevated temperature”. In: *Construction and Building Materials* 250 (2020), p. 118487.

[59] Kittinun Sirijaroonchai, Sherif El-Tawil, and Gustavo Parra-Montesinos. “Behavior of high performance fiber reinforced cement composites under multi-axial compressive loading”. In: *Cement and Concrete Composites* 32.1 (2010), pp. 62–72.

[60] Ekkehard Fehling et al. *Ultra-high performance concrete UHPC: Fundamentals, design, examples*. John Wiley & Sons, 2015.

[61] M Iqbal Khan, Galal Fares, and Shehab Mourad. “Optimized fresh and hardened properties of strain hardening cementitious composites: Effect of mineral admixtures, cementitious composition, size, and type of aggregates”. In: *Journal of Materials in Civil Engineering* 29.10 (2017), p. 04017178.

[62] Ali A Ramezanianpour et al. “Influence of various amounts of limestone powder on performance of Portland limestone cement concretes”. In: *Cement and Concrete Composites* 31.10 (2009), pp. 715–720.

[63] Wei Huang et al. “Effect of cement substitution by limestone on the hydration and microstructural development of ultra-high performance concrete (UHPC)”. In: *Cement and Concrete Composites* 77 (2017), pp. 86–101.

[64] Alaa M Rashad and Sayieda R Zeedan. “A preliminary study of blended pastes of cement and quartz powder under the effect of elevated temperature”. In: *Construction and building materials* 29 (2012), pp. 672–681.

[65] T Stovall, Francois De Larrard, and M Buil. “Linear packing density model of grain mixtures”. In: *Powder technology* 48.1 (1986), pp. 1–12.

[66] Melvin Mooney. “The viscosity of a concentrated suspension of spherical particles”. In: *Journal of colloid science* 6.2 (1951), pp. 162–170.

[67] René Feret. “Sur la compacité des mortiers hydrauliques”. In: *Ann. Pntas et Chaussees, Mem Doc* 4 (1892), pp. 5–164.

[68] William B Fuller and Sanford E Thompson. “The laws of proportioning concrete”. In: *Transactions of the American Society of Civil Engineers* 59.2 (1907), pp. 67–143.

[69] AHM Andreasen. “Über die Beziehung zwischen Kornabstufung und Zwischenraum in Produkten aus losen Körnern (mit einigen Experimenten)”. In: *Kolloid-Zeitschrift* 50.3 (1930), pp. 217–228.

[70] James E Funk and Dennis R Dinger. “Derivation of the Dinger-Funk particle size distribution equation”. In: *Predictive Process Control of Crowded Particulate Suspensions*. Springer, 1994, pp. 75–83.

[71] Libya Ahmed Sbia et al. “Production methods for reliable construction of ultra-high-performance concrete (UHPC) structures”. In: *Materials and Structures* 50.1 (2017), pp. 1–19.

[72] Ketan A. Ragalwar et al. “Influence of Distribution Modulus of Particle Size Distribution on Rheological and Mechanical Properties of Ultra-High-Strength SHCC Matrix”. In: *Strain-Hardening Cement-Based Composites*. Ed. by Viktor Mechtcherine, Volker Slowik, and Petr Kabele. Dordrecht: Springer Netherlands, 2018, pp. 221–229.

[73] Arun R Arunothayan et al. “Development of 3D-printable ultra-high performance fiber-reinforced concrete for digital construction”. In: *Construction and Building Materials* 257 (2020), p. 119546.

[74] Weina Meng, Mahdi Valipour, and Kamal Henri Khayat. “Optimization and performance of cost-effective ultra-high performance concrete”. In: *Materials and structures* 50.1 (2017), pp. 1–16.

[75] Ketan Ragalwar et al. “Significance of the particle size distribution modulus for strain-hardening-ultra-high performance concrete (SH-UHPC) matrix design”. In: *Construction and Building Materials* 234 (2020), p. 117423.

[76] Ekkehard Fehling et al. “Ultra high performance concrete (UHPC)”. In: *Proceedings of the Second International Symposium on Ultra High Performance Concrete*. Wiley Online Library. 2008.

[77] Mohamadreza Shafieifar, Mahsa Farzad, and Atorod Azizinamini. “Experimental and numerical study on mechanical properties of Ultra High Performance Concrete (UHPC)”. In: *Construction and Building Materials* 156 (2017), pp. 402–411.

[78] R.K. Tai. “Upscaling of Strain-Hardening Cementitious Composites”. MA thesis. TU Delft, 2015.

[79] Arnon Bentur and Sidney Mindess. *Fibre reinforced cementitious composites*. Crc Press, 2006.

[80] Shan He et al. “Strain hardening ultra-high performance concrete (SHUHPC) incorporating CNF-coated polyethylene fibers”. In: *Cement and concrete research* 98 (2017), pp. 50–60.

[81] Zhen Zheng et al. “Surface modification of ultrahigh-molecular-weight polyethylene fibers”. In: *Journal of Polymer Science Part B: Polymer Physics* 42.3 (2004), pp. 463–472.

[82] Hwai-Chung Wu and Victor C Li. “Fiber/cement interface tailoring with plasma treatment”. In: *Cement and Concrete Composites* 21.3 (1999), pp. 205–212.

[83] Katrin Habel, Emmanuel Denarié, and Eugen Brühwiler. “Time dependent behavior of elements combining ultra-high performance fiber reinforced concretes (UHPFRC) and reinforced concrete”. In: *Materials and structures* 39.5 (2006), pp. 557–569.

[84] Xue Ouyang et al. “Experimental investigation and prediction of elastic modulus of ultra-high performance concrete (UHPC) based on its composition”. In: *Cement and Concrete Research* 138 (2020), p. 106241.

[85] Ali Alsalman et al. “Evaluation of modulus of elasticity of ultra-high performance concrete”. In: *Construction and Building Materials* 153 (2017), pp. 918–928.

[86] Kyungtaek Koh et al. “Shrinkage properties of ultra-high performance concrete (UHPC)”. In: *Advanced Science Letters* 4.3 (2011), pp. 948–952.

[87] Linmei Wu et al. “Autogenous shrinkage of high performance concrete: A review”. In: *Construction and Building Materials* 149 (2017), pp. 62–75.

[88] Dale P Bentz and Ole Mejlhede Jensen. “Mitigation strategies for autogenous shrinkage cracking”. In: *Cement and Concrete Composites* 26.6 (2004), pp. 677–685.

[89] Surendra P Shah, W Jason Weiss, and Wei Yang. “Shrinkage Cracking–Can It Be Prevented?” In: *Concrete International* 20.4 (1998), pp. 51–55.

[90] Bassam A Tayeh et al. “Mechanical and permeability properties of the interface between normal concrete substrate and ultra high performance fiber concrete overlay”. In: *Construction and building materials* 36 (2012), pp. 538–548.

[91] Alireza Valikhani et al. “Experimental evaluation of concrete-to-UHPC bond strength with correlation to surface roughness for repair application”. In: *Construction and Building Materials* 238 (2020), p. 117753.

[92] Mo Li and Victor C Li. “Behavior of ecc/concrete layered repair system under drying shrinkage conditions/das verhalten eines geschichteten instandsetzungssystems aus ecc und beton unter der einwirkung von trocknungsschwinden”. In: *Restoration of Buildings and Monuments* 12.2 (2006), pp. 143–160.

[93] M Lukovic. “Influence of interface and strain hardening cementitious composite (SHCC) properties on the performance of concrete repairs”. In: (2016).

[94] Abul K Azad and Ibrahim Y Hakeem. “Flexural behavior of hybrid concrete beams reinforced with ultra-high performance concrete bars”. In: *Construction and Building Materials* 49 (2013), pp. 128–133.

[95] Abul K Azad and Ibrahim Y Hakeem. “Flexural behavior of hybrid hollow-core slab built with ultra high performance concrete faces”. In: *Materials and Structures* 49.9 (2016), pp. 3801–3813.

[96] Sriram Aaleti and Sri Sritharan. “Quantifying bonding characteristics between UHPC and normal-strength concrete for bridge deck application”. In: *Journal of Bridge Engineering* 24.6 (2019), p. 04019041.

[97] Hasan Murat Tanarslan et al. “Shear strengthening of RC beams with externally bonded UHPFRC laminates”. In: *Composite Structures* 262 (2021), p. 113611.

[98] Mohammed A Sakr et al. “Shear strengthening of reinforced concrete beams using prefabricated ultra-high performance fiber reinforced concrete plates: Experimental and numerical investigation”. In: *Structural Concrete* 20.3 (2019), pp. 1137–1153.

[99] AP Lampropoulos et al. “Strengthening of reinforced concrete beams using ultra high performance fibre reinforced concrete (UHPFRC)”. In: *Engineering Structures* 106 (2016), pp. 370–384.

[100] Cheng Chen, Haiyang Cai, and Lijuan Cheng. “Shear strengthening of corroded RC beams using UHPC–FRP composites”. In: *Journal of Bridge Engineering* 26.1 (2021), p. 04020111.

[101] Abd El-Hakim Khalil et al. “Behavior of RC beams strengthened with strain hardening cementitious composites (SHCC) subjected to monotonic and repeated loads”. In: *Engineering Structures* 140 (2017), pp. 151–163.

[102] Mohamed Hussein, Minoru Kunieda, and Hikaru Nakamura. “Strength and ductility of RC beams strengthened with steel-reinforced strain hardening cementitious composites”. In: *Cement and Concrete Composites* 34.9 (2012), pp. 1061–1066.

[103] Jiaying Wei et al. “Shear strengthening of reinforced concrete beams with high strength strain-hardening cementitious composites (HS-SHCC)”. In: *Materials and Structures* 53.4 (2020), pp. 1–15.

[104] Tamen Ueda and Jianguo Dai. “Interface bond between FRP sheets and concrete substrates: properties, numerical modeling and roles in member behaviour”. In: *Progress in Structural Engineering and Materials* 7.1 (2005), pp. 27–43.

[105] Libor Jendele Vladimír Červenka and Jan Červenka. *ATENA Program Documentation, Part 1: Theory*. Červenka Consulting s.r.o. Prague, 2020, pp. 44–60.

[106] Ajlal Arif. “Numerical Study of Shear Strengthening of Reinforced Concrete Beams using Strain-Hardening Cementitious Composites”. MA thesis. TU Delft, 2020.

[107] Evi Aprianti. “A huge number of artificial waste material can be supplementary cementitious material (SCM) for concrete production–a review part II”. In: *Journal of cleaner production* 142 (2017), pp. 4178–4194.

[108] Harald S Müller, Michael Haist, and Michael Vogel. “Assessment of the sustainability potential of concrete and concrete structures considering their environmental impact, performance and lifetime”. In: *Construction and Building Materials* 67 (2014), pp. 321–337.

[109] VG Papadakis and S Tsimas. “Supplementary cementing materials in concrete: Part I: efficiency and design”. In: *Cement and concrete research* 32.10 (2002), pp. 1525–1532.

[110] S Samad and A Shah. “Role of binary cement including Supplementary Cementitious Material (SCM), in production of environmentally sustainable concrete: A critical review”. In: *International journal of Sustainable built environment* 6.2 (2017), pp. 663–674.

[111] Thorsten Stengel and Peter Schießl. “Sustainable construction with UHPC–from life cycle inventory data collection to environmental impact assessment”. In: *Proceedings of the 2nd international symposium on ultra high performance concrete. Kassel University Press, Kassel*. 2008, pp. 461–468.

[112] Pei Yan et al. “Experimental research on ductility enhancement of ultra-high performance concrete incorporation with basalt fibre, polypropylene fibre and glass fibre”. In: *Construction and Building Materials* 279 (2021), p. 122489.

[113] Amir Hajiesmaeili and Emmanuel Denarié. “Next generation UHPFRC for sustainable structural applications”. In: *DSCS 2018: 2nd International Workshop on Durability and Sustainability of Concrete Structures*. CONF. 2018.

[114] Amir Hajiesmaeili et al. “Life cycle analysis of strengthening existing RC structures with R-PE-UHPFRC”. In: *Sustainability* 11.24 (2019), p. 6923.

[115] Nikhil Awasthy. “Development of Mechanical Properties of Concrete with Time - Experimental and Numerical Study”. MA thesis. TU Delft, 2019.

[116] *Master®Glenium 51 con. 35% NL*. SPL EN 934-2 : T3.1/T3.2. Master Builders Solutions Nederland B.V. Apr. 2021.

[117] *PRODUCT DATA SHEET Sika® ViscoCrete®-20 HE*. 021301011000000037. Sika Group. Sept. 2018.

[118] *Ultra High Molecular Weight Polyethylene Fiber from DSM Dyneema*. DSM Dyneema®.

[119] Abdalla Talaat et al. “Factors affecting the results of concrete compression testing: A review”. In: *Ain Shams Engineering Journal* 12.1 (2021), pp. 205–221.

[120] JJ Tucker. “Effect of Dimensions of Specimens upon the Precision of Strength Date”. In: *Proceedings of the ASTM*. Vol. 45. 1945, pp. 952–959.

[121] Jishan Xu and Xixi He. “Size effect on the strength of a concrete member”. In: *Engineering Fracture Mechanics* 35.4-5 (1990), pp. 687–695.

[122] Jin-Keun Kim and Seong-Tae Yi. “Application of size effect to compressive strength of concrete members”. In: *Sadhana* 27.4 (2002), pp. 467–484.

[123] MG Alberti, A Enfedaque, and JC Gálvez. “A review on the assessment and prediction of the orientation and distribution of fibres for concrete”. In: *Composites Part B: Engineering* 151 (2018), pp. 274–290.

[124] Patrick Stähli and Jan GM Van Mier. “Manufacturing, fibre anisotropy and fracture of hybrid fibre concrete”. In: *Engineering fracture mechanics* 74.1-2 (2007), pp. 223–242.

[125] K Rokugo et al. “Direct tensile behavior and size effect of strain-hardening fiber-reinforced cement-based composites (SHCC)”. In: *6th International Conference on Fracture Mechanics of Concrete and Concrete Structures*. 2007.

[126] Eduardo B Pereira, Gregor Fischer, and Joaquim AO Barros. “Direct assessment of tensile stress-crack opening behavior of Strain Hardening Cementitious Composites (SHCC)”. In: *Cement and concrete Research* 42.6 (2012), pp. 834–846.

[127] Max AN Hendriks, Ane de Boer, and Beatrice Belletti. “Guidelines for nonlinear finite element analysis of concrete structures”. In: *Rijkswaterstaat Centre for Infrastructure, Report RTD* 1016.1 (2017), p. 2017.

[128] Arjen de Putter. “Towards a uniform and optimal approach for safe NLFEA of reinforced concrete beams: Quantification of the accuracy of multiple solution strategies using a large number of samples”. MA thesis. TU Delft, 2020.

[129] SK Shin, JJH Kim, and Yun Mook Lim. “Investigation of the strengthening effect of DFRCC applied to plain concrete beams”. In: *Cement and Concrete Composites* 29.6 (2007), pp. 465–473.

[130] Alessandro Cabboi et al. “Static and dynamic testing of delamination in hybrid SHCC/concrete beams”. In: *Composite Structures* 281 (2022), p. 114961.

[131] Wieland Hoppe, Nils Thonemann, and Stefan Bringezu. “Life cycle assessment of carbon dioxide–based production of methane and methanol and derived polymers”. In: *Journal of Industrial Ecology* 22.2 (2018), pp. 327–340.

[132] Nobuhiko Narita, Masayuki Sagisaka, and Atsushi Inaba. “Life cycle inventory analysis of CO2 emissions manufacturing commodity plastics in Japan”. In: *The International Journal of Life Cycle Assessment* 7.5 (2002), pp. 277–282.

[133] Mariam Al-Ma’adeed et al. “Life Cycle Assessment of Particulate Recycled Low Density Polyethylene and Recycled Polypropylene Reinforced with Talc and Fiberglass”. In: *Composite Science and Technology*. Vol. 471. Key Engineering Materials. Trans Tech Publications Ltd, June 2011, pp. 999–1004.

[134] K.G. Harding et al. “Environmental analysis of plastic production processes: Comparing petroleum-based polypropylene and polyethylene with biologically-based poly-β-hydroxybutyric acid using life cycle analysis”. In: *Journal of Biotechnology* 130.1 (2007), pp. 57–66.

[135] I Boustead. “Ecoprofiles of plastics and related intermediates”. In: *Association of Plastics Manufacturers in Europe, Brussels, Belgium* (1999).

[136] Michaelangelo D. Tabone et al. “Sustainability Metrics: Life Cycle Assessment and Green Design in Polymers”. In: *Environmental Science & Technology* 44.21 (2010), pp. 8264–8269.

[137] Amzan Alsabri and Sami G. Al-Ghamdi. “Carbon footprint and embodied energy of PVC, PE, and PP piping: Perspective on environmental performance”. In: *Energy Reports* 6 (2020). The 7th International Conference on Energy and Environment Research—“Driving Energy and Environment in 2020 Towards A Sustainable Future”, pp. 364–370.

[138] Mladena Luković et al. “Strain Hardening Cementitious Composite (SHCC) for crack width control in reinforced concrete beams”. In: *Heron* 64.1/2 (2019), p. 181.

[139] Philip Van den Heede et al. “Cradle-to-gate life cycle assessment of self-healing engineered cementitious composite with in-house developed (semi-) synthetic superabsorbent polymers”. In: *Cement and Concrete Composites* 94 (2018), pp. 166–180.